# LOS ALAMOS SCIENTIFIC LABORATORY

## OF THE UNIVERSITY OF CALIFORNIA

LOS ALAMOS, NEW MEXICO

CONTRACT W-7405-ENG.36 WITH THE
U.S. ATOMIC ENERGY COMMISSION

ERRATA

LA-1693

| Page No. | Location of Change | From | To |
|---|---|---|---|
| 20 | line 12 | $E/E$ | $E/\dot{E}$ |
| 43 | equation (17) | This should read $A = \frac{1}{2\sqrt{2}} \left(\frac{m}{2\pi kT}\right)^3$ | |
| 43 | equation (18) | $\frac{\pi}{2}$ | $\frac{\pi}{4}$ |
| 103 | equation (17) | $\frac{\pi}{2}$ | $\frac{\pi}{4}$ |
| 105 | equation (19) | The exponential should be $e^{-\mu v^2/2kT}$ | |
| 108 | line 10 | (33) | (22) |
| 131 | Fig. 7 | The ordinate should be $2\beta_1$. | |

LOS ALAMOS SCIENTIFIC LABORATORY
of the
UNIVERSITY OF CALIFORNIA

Report written:
July 1, 1954
Report distributed:

LA-1693

# THE STRUCTURE OF A SHOCK FRONT IN ARGON

Work done by:
John W. Bond, Jr.

Report written by:
John W. Bond, Jr.



PHYSICS

CONTENTS

CONTENTS (Continued)

## ABSTRACT

If a one-dimensional shock wave travels through argon, the translational degrees of freedom of the atoms are immediately excited and reach translational equilibrium within two collision lengths. If the shock velocity is sufficiently high, energy will be transferred from the translational degrees of freedom to those of electronic excitation and ionization until complete thermal equilibrium exists. The region between the first disturbance in front of the shock and the point at which thermal equilibrium is first realized is the shock front.

A method of computing the equilibrium conditions, which was first applied by Bethe to air, has been used for the argon equilibrium reaction, $A = A^+ + e$, where only singly-ionized argon atoms have been considered. The corresponding partition functions for density ratios from 2 to 20 and temperatures from $7500^\circ$ to $26{,}000^\circ$ are tabulated. Applying the standard shock relations, the equilibrium conditions behind the shock front have been computed for shock velocities between $3 \cdot 10^5$ and $9 \cdot 10^5$ cm/sec for two fore-pressures, viz., $p_1 = 1.0$ and 59.38 cm Hg.

The non-equilibrium region which exists between the front of the shock and the equilibrium region has been treated by considering the individual atomic interactions that take place. From the point where translational equilibrium is first reached to a point where there is a sufficient number of electrons for ionizing collisions between electrons and atoms to be of importance, ionizing reactions between argon atoms predominate. Then the reaction $e + A = 2e + A^+$ takes over only to be

dampened by recombination between electrons and ions until the gas has been completely equilibriated. Pressure, density, temperature and degree of ionization have been computed across the shock front for various shock velocities and presented in graphical form. Thus the width of the shock front and, consequently, the relaxation time for ionization are given as functions of shock velocity.

Various theories for the recombination of electrons and ions have been discussed and it is shown that Kramers' classical theory of radiative recombination is incorrect but that a quantum theory gives the right order of magnitude result. Three-body recombination coefficients have been computed by a method of microscopic reversibility.

LIST OF FIGURES

LIST OF FIGURES (Continued)

LIST OF FIGURES (Continued)

LIST OF FIGURES (Continued)

LIST OF TABLES

# INTRODUCTION

A shock wave travelling through an atmosphere of argon gas may conveniently be described in the following way. In front of the shock wave is the undisturbed atmosphere in equilibrium. Upon being struck by the shock, a violent disturbance occurs, which soon however settles down to a new condition of statistical equilibrium behind the shock. Connection between the two regions of equilibrium is uniquely determined by the Rankine-Hugoniot or shock relations (Ref 46).

Disturbance of the statistical equilibrium takes place in the following way. As a shock wave passes through the gas, the translational degrees of freedom of the atoms are excited. The distance required to achieve translational equilibrium has been investigated theoretically (Ref 44, 45, 46, 48, 60, 63, 64, 65, 66) and in the limit of strong shocks is of the order of two collision lengths. This seems to have received satisfactory experimental verification (Ref 61, 62). Because the distance is so short it does not concern us in this report. If the temperature of the translational degrees of freedom is sufficiently high, transfer of energy to other degrees of freedom takes place until complete thermal equilibrium is reached. The region in which this transfer of energy takes place is referred to as the non-equilibrium region. We then define the shock front to be all the region between the undisturbed atmosphere in front of the shock wave and the point behind the front of the shock wave at which thermal equilibrium is first essentially achieved.

It is the purpose of this study to determine quantitatively the conditions and extent of the shock front for shock velocities high enough so that there is some degree of ionization and low enough so that the number of doubly ionized argon atoms is negligible. The reasons for choosing argon as the gaseous medium are, first, because it is a monatomic gas hence molecular degrees of freedom such as rotation, vibration, and dissociation do not need to be considered, and second, because more experimental data pertaining to shocks are available for argon than for most other gases.

Measurements have been made by various investigators on the detailed structure of argon shocks of the following quantities: material velocity, shock width, spectral distribution, luminosity, electrical conductivity, and potential distribution. In addition there are measurements of many overall phenomena of the shock including reflection, refraction, and diffraction of shock waves as they impinge on or pass through various media, how much energy is lost to a shock front in air as it passes through a cloud containing water droplets (e.g., fog), and how much energy is lost to a shock front by radiation. A detailed theoretical knowledge of the structure of a shock front is desirable in order to obtain an interpretation for some of the physical measurements made as well as to predict others. Also, we wish to test the validity of approximating the shock front by a physical discontinuity, as is usually done. It is essentially for these reasons that this report is written.

In Part I we consider the equilibrium region which is a plasma consisting of neutral argon atoms in various states of excitation, singly charged argon ions, and electrons. The equation of state for such a plasma is derived and it is shown how the component concentrations behind the shock may be computed.

In Part II we discuss the various atomic interactions that take place in the non-equilibrium region of the shock front. We evaluate the reactions that contribute to the production of electrons using the available experimental cross-sections. Once a sufficient number of electrons has been produced recombination of electrons and ions occurs until a balance between the production and recombination of electrons has been reached. Several recombination processes take place, none of which have been experimentally determined for the temperature and density conditions that prevail in a shock front of the strength we will consider. Hence theoretical relations for the recombination processes are derived.

The theory of Parts I and II is applied to a few special cases in Part III. Equilibrium calculations have been made for shock velocities between $3 \cdot 10^5$ and $9 \cdot 10^5$ cm per sec and for initial or fore-pressures of 1.0 cm Hg and 59.38 cm Hg, the latter corresponding to atmospheric conditions at Los Alamos. Processes contributing to the production of electrons in a shock front are evaluated numerically for temperatures between about $8000^\circ$ and $35000^\circ$. Recombination processes, depending on both density and temperature, are also evaluated. Finally, conditions

in the non-equilibrium region have been computed for an initial pressure of 59.38 cm Hg and shock velocities of 5.0, 5.5, and $6.0 \cdot 10^5$ cm per sec.

The important contributions of this report are the following. Partition functions for argon have been computed and tabulated for temperatures from $7500^\circ$ to $26000^\circ$ and for density ratios from 2 to 20. The equilibrium constant K for the reaction $A \rightleftharpoons A^+ + e$ for the above range of density and temperature and with an initial pressure of 59.38 cm Hg is tabulated. For an initial pressure of h cm Hg the corresponding equilibrium constant is obtained by multiplying the tabulated K by 59.38/h. An approximate method by which the energy per particle and the component concentrations may be conveniently obtained from the equilibrium constant is presented in Part III. The values thus obtained agree well with the more exact method given in Part I.

The quantitative calculations on the shock front show, not only the true profile, but that the shock front is of such an extent and the conditions such as pressure, temperature, and density of such magnitude that for many of the physical applications mentioned previously the shock front should not be treated as a discontinuity. In addition, from the degree of ionization one can predict the spectral distribution and luminosity and possibly compute the conductivity.

Perhaps the most significant theoretical contribution of this report is the derivation of the recombination coefficient. It is shown that Kramers' classical theory of radiative recombination gives

a value that is too large by a factor of about $10^5$, but that a quantum theory evaluation is of the correct order of magnitude. Also since the usual theories of three-body recombination are not applicable to our case, we separately evaluated this coefficient by using the principle of microscopic reversibility applied to the equilibrium state.

## PART I: THE EQUILIBRIUM REGION BEHIND THE SHOCK FRONT

### 1. Introduction.

The general hydrodynamic features of a shock are determined by the properties of the equilibrium regions in front of and behind the shock front. The conditions in front of the shock are completely known, of course. However, behind the shock front in argon we have a plasma consisting of argon atoms in various states of excitation, argon ions, and electrons. Despite the fact that such a plasma has received considerable attention, particularly at low pressures and temperatures (Ref 1, 2, 56, 57, 58, 59), knowledge of this state is far from being satisfactory. This is especially true at the high pressures and temperatures behind a shock front.

In Part I, therefore, we calculate the equilibrium equation of state and the thermodynamic functions of the argon plasma. There are available several methods for determining the equation of state of a gas. We have used here the Saha equation and evaluated the partition functions by a method suggested by Bethe (Ref.67). The reason for using Bethe's method is that it is simple and well adapted for high speed computing machines. In this calculation, as indeed throughout this report, it will be assumed that the number of doubly ionized argons is negligible although, occasionally, brief reference will be made to interactions involving $A^{++}$.

### 2. Equilibrium Conditions.

Consider a plasma state behind the shock front in complete thermal equilibrium. We wish to calculate the concentrations of the three com-

ponents, A, $A^+$, and electrons, as functions of density and temperature. Let the concentration $[A]$ be defined as the ratio of the number of neutral argon atoms to the original number before ionization takes place. Similarly $[A^+]$ is the ratio of the number of singly charged argon ions to the original number of argon atoms and $[\mathcal{El}]$ is the corresponding concentration for electrons, where, at all times

$$[\mathcal{El}] = [A^+] \quad .$$

The equilibrium reaction is

$$A = A^+ + \mathcal{El}$$

so that

$$[A] + [A^+] = 1 \tag{1}$$

If g is the average number of particles into which an argon atom splits at temperature T, then

$$g = [A] + 2[A^+] \tag{2}$$

where the factor of 2 is due to the presence of one electron for each ion.

Assume the perfect gas equation of state to hold,

$$p = g\rho \frac{R}{M} T, \tag{3}$$

where R is the gas constant per mol and M is the original molecular weight.

If E is the internal energy per gram, the quantity $\beta$ is defined by

$$E = (\beta - 1) \frac{p}{\rho} \quad . \tag{4}$$

Then from the relation

$$E = \frac{p}{(\gamma-1)\rho} , \tag{5}$$

$\gamma$ is given by

$$\gamma = \frac{\beta}{\beta - 1} . \tag{6}$$

For a perfect gas $\gamma$ is equal to the ratio of specific heats, although, in general, particularly for a solid, this is not true.

Following Bethe we define a quantity $\epsilon$ from the enthalpy i, i.e.,

$$i = E + \frac{p}{\rho} = \frac{R}{M} T\epsilon = \beta \frac{p}{\rho} . \tag{7}$$

From (3) and (7),

$$E = (\epsilon - g) \frac{R}{M} T = \left(\frac{\epsilon}{g} - 1\right) g \frac{R}{M} T ,$$

or

$$\beta = \frac{\epsilon}{g} . \tag{8}$$

The quantities $\beta$ and $\epsilon$ have been defined for computational purposes. We can define a parameter analogous to $\beta$ separately for atoms, ions, and electrons. This parameter $\beta(q_i)$ will include the energy of translation and electronic excitation, hence for each species

$$\beta(q_i) - 1 = \frac{E(q_i)}{kT} \tag{9}$$

where $E(q_i)$ is the internal energy per particle and where $q_i$ stands for a particular particle which, in our case may be an argon atom, A, an argon ion, $A^+$, or an electron, $\mathcal{E}\ell$ ; i.e.,

$$\beta(A)-1 = \frac{E(A)}{kT} ,$$

$$\beta(A^+)-1 = \frac{E(A^+)}{kT} ,$$

$$\beta(\mathcal{E}\ell)-1 = \frac{E(\mathcal{E}\ell)}{kT} .$$

If $n, n^+$ and $n_e$ are the number of neutral atoms, the number of ions, and the number of electrons per $cm^3$ then the internal energy per gram is

$$E = \frac{nE(A) + n^+\left\{E(A^+) + I\right\} + n_e E(\mathcal{E}\ell)}{\rho} .$$

Substitute the following quantities in E,

$$\rho = m(n+n^+), \quad [A] = \frac{n}{n+n^+} , \quad \left[A^+\right] = \frac{n^+}{n+n^+} , \quad \left[\mathcal{E}\ell\right] = \frac{n_e}{n+n^+} .$$

Then

$$E = [A]\frac{E(A)}{m} + \left[A^+\right]\frac{\left\{E(A^+)+I\right\}}{m} + \left[\mathcal{E}\ell\right]\frac{E(\mathcal{E}\ell)}{m} .$$

If we now substitute this into (7) using (3) we have

$$[A]\frac{E(A)}{m} + \left[A^+\right]\frac{\left\{E(A^+)+I\right\}}{m} + \left[\mathcal{E}\ell\right]\frac{E(\mathcal{E}\ell)}{m} + g\frac{R}{M}T = \epsilon\frac{R}{M}T.$$

We now divide through by $RT/M = kT/m$ obtaining

$$[A]\frac{E(A)}{kT} + \left[A^+\right]\frac{\left\{E(A^+)+I\right\}}{kT} + \left[\mathcal{E}\ell\right]\frac{E(\mathcal{E}\ell)}{kT} + g = \epsilon .$$

Using (2), (9), and the fact that $\left[\mathcal{E}\ell\right] = \left[A^+\right]$ we finally have

$$\epsilon = \beta(A)\,[A] + \beta(A^+)\,[A^+] + \frac{I(A)}{kT}\,[A^+] + \beta(\mathcal{E}\ell)\,[\mathcal{E}\ell]$$

where I(A) is the ionization energy for argon and $\beta(A)$ means $\beta$ for neutral argon and includes the energy of translation and excitation. $\beta(A^+)$ is similarly defined for singly ionized argon. Since, for a free particle the energy is 3/2 kT, from (9), we have

$$\beta(\mathcal{E}\ell) = 2.5,$$

hence

$$\epsilon = \beta(A)\,[A] + [A^+]\left\{\beta(A^+) + \frac{I(A)}{kT} + 2.5\right\}. \tag{10}$$

The equilibrium constant for the argon interaction is

$$K = \frac{[A^+]\,[\mathcal{E}\ell]}{[A]} \tag{11}$$

or, if $x = [A^+]$,

$$K = \frac{x^2}{1-x}\ . \tag{12}$$

3. The Partition Functions.

Once the equilibrium conditions have been defined, then, for an ionizing reaction the Saha equation may be used to write the equilibrium constant in terms of the partition functions. The Saha equation for the argon equilibrium reaction may be written

$$K = \left(\frac{2\pi k\mu}{h^2 N_o}\right)^{3/2} \cdot \frac{1}{n_1} \cdot \frac{T^{3/2}}{\gamma}\ \frac{Z_n(A^+)\cdot Z(\mathcal{E}\ell)\cdot e^{-I/kT}}{Z(A)}\ , \tag{13}$$

where $\mu$ is the reduced mass, i.e.,

$$\mu = \frac{m^+ m_e}{m} \quad , \qquad m = m^+ + m_e \tag{14}$$

and

$n_1$ = number of argon atoms in one $cm^3$ of the undisturbed gas in front of the shock

$\eta$ = density ratio = $\rho_4/\rho_1$

$\rho_1$ = density of the undisturbed gas (cf Fig. 1, Part II)

$\rho_4$ = density in the equilibrium region behind the shock

k = Boltzmann's const

h = Planck's const

$N_o$ = Avogadro's number

T = temperature in degrees absolute

I = first ionization potential of argon

$Z(A^+)$ = internal partition function for the argon ion

$Z(A)$ = internal partition function for the neutral argon atom

$Z(\xi\ell)$ = internal partition function for the electron.

The density ratio $\eta$ is used in (13) in place of the corresponding pressure ratio $\xi$ because $\eta$ varies between 1 and about 10 across the shock front whereas $\xi$ may become very large and, in fact, is set equal to $\infty$ in the strong shock approximation.

The internal partition functions are defined by

$$Z = \sum_n g_n \, e^{-E_n/kT} \tag{15}$$

where n corresponds to a state of the system with energy $E_n$ and sta-

tistical weight $g_n$ (the energy of the ground state is arbitrarily set equal to zero). The internal partition function of the electrons reduces simply to the degeneracy 2. Hence, if

$$f = f(T,\eta) = \left(\frac{2\pi k\mu}{h^2 N_o}\right)^{3/2} \cdot \frac{1}{n_1} \cdot \frac{T^{3/2}}{\eta} , \tag{16}$$

then

$$K = 2f \frac{Z(A^+)\cdot e^{-I/kT}}{Z(A)} . \tag{17}$$

At high temperatures the higher excited states of the atom become numerous and may contribute appreciably to the partition function. The summing over these higher states could become quite laborious but even worse would be the overlapping of the higher quantum states of neighboring atoms. Therefore, a cut-off must be made. This cut-off successively eliminates the high quantum states of the atom as the density is increased. The corresponding process is termed pressure ionization.

The radius of a hydrogen-like electron orbit is

$$a_n = a_o n^2 \tag{18}$$

where $a_o$ is the first Bohr radius and n is the principal quantum number. We now assume all electron orbits to be suppressed whose radius $a_n$ exceeds half the average distance between atoms. Let this half-distance be $r_o$; then, if L is the number of atoms per $cm^3$ in front of the shock,

$$\frac{4\pi}{3} r_o^3 = \frac{1}{L\eta}$$

or

$$r_o = \left(\frac{3}{4\pi L \eta}\right)^{1/3} .$$

From (18), the limiting value of n is

$$n = \left(\frac{r_o}{a_o}\right)^{1/2} = \frac{1}{a_o^{1/2}} \left(\frac{3}{4\pi L \eta}\right)^{1/6}$$

$$n_\eta = D \cdot \eta^{-1/6} \ , \ D = \text{const} = \frac{1}{a_o^{1/2}} \left(\frac{3}{4\pi L}\right)^{1/6} . \qquad (19)$$

As $n_\eta$ is non-integer, g is reduced proportionately in the following way: For $n \geq n_\eta + \frac{1}{2}$ the state will be completely cut off and for $n \leq n_\eta - \frac{1}{2}$ the state will be fully counted in the partition function. In between these values of n the multiplicity is adjusted according to the formula

$$g_{\text{effective}} = g_n \left\{ \frac{(n_\eta + 1/2) - n}{(n_\eta + 1/2) - (n_\eta - 1/2)} \right\} = g_n \, (n_\eta + 1/2 - n) \qquad (20)$$

Hence, the internal partition function of the atom depends not only on the temperature but to a small extent on the density, i.e.,

$$Z = Z(T, \eta).$$

The effect of the above approximation is discussed in Ref 69 where it is pointed out that the partition function of the free electrons is underestimated, since their potential energy is neglected. Also, the integration over phase space is not carried out properly. While it is difficult to estimate the size of the error, it can not be large since theory and experiment are in good agreement (cf Part III, section 3). In addition, the above theory agrees with more precise calculations made at Los Alamos.

The contribution to the partition function from the low states is easy to obtain because of their small number. However, the contributions from the higher states which have one electron excited to $n \geq 4$ is a different matter both because of the great number available and because of the cut-off that must be made. Hence the partition function for the neutral atom may be written as

$$Z = Z_{low} + Z_{high} \tag{21}$$

where $Z_{low}$ is summed over the low states ($n = 3$) as in (15).

The ground state of argon is a $(3p)^6\ ^1S_o$ level with a multiplicity of one and an energy by convention equal to zero. There is also a level from the configuration $(3p)^5(3d)$, observed spectroscopically, which has a relatively high energy, viz, 113000 $cm^{-1}$ or 162,500 degrees. This level has a multiplicity 60. Levels with two excited electrons have such high energies as to be unimportant in the partition function. Using these levels the evaluation of $Z_{low}$ is shown in the following table: (cf Table IV, Part III)

Table I

(A I at $T = 25000^o$)

| State | $g_n$ | $E_n(cm^{-1})$ | $E_n$ (degrees) | $g_n e^{-E_n/kT}$ |
|---|---|---|---|---|
| $3p^6\ ^1S$ | 1 | 0 | 0 | 1 |
| $3p^5d$ | 60 | 113,000 | 162,500 | .0902 |

From this table it is seen that $Z_{low} = 1.0902$ when $T = 25000^o$.

We now evaluate $Z_{high}$ by the following approximation: Consider a highly excited atom as an ion with an electron moving around the ion in a large orbit. The spectrum will be alkali-like and the energy $E_{n\ell}$, of a state of principal quantum number n and orbital quantum number $\ell$, will be

$$E_{n\ell} = I + E_{ion} - E'_{n\ell} \tag{22}$$

where

$E_{ion}$ = excitation energy of the ion ($\geq 0$)

$E'_{n\ell}$ = binding energy of the electron.

If (22) is substituted in (15) $Z_{high}$ becomes

$$Z_{high} = Z_{ion} \cdot e^{-I/kT} \cdot z_{high} \cdot \tag{23}$$

$Z_{ion}$ is determined similarly to $Z_{low}$ although the low states are more numerous for A II than for A I. $z_{high}$ is the partition function for the (one electron) high excited states of the neutral argon atom, neglecting the multiplicity of the core configuration (which is included of course in $Z_{ion}$). It is given by

$$z_{high} = \sum g_{n\ell}(\eta)\, e^{+E'_{n\ell}/kT} \tag{24}$$

where $g_{n\ell}(\eta)$ is the adjusted multiplicity, eq. (20). As shown by (22) $E'_{n\ell}$ corresponds to a positive binding energy which is subtracted from the energy of the ion, i.e.,

$$E'_{n\ell} = I - E_n$$

where $E_n$ is the excitation energy. The high excited states of the ion

have not been included because their contribution to the partition function is negligible in the temperature range with which we are concerned.

4. The Energy Content.

Knowing the partition function it is possible to obtain the various other thermodynamic functions. The energy content is of particular interest because of its importance in determining the shock conditions (section 5).

The average energy per particle in units of kT is

$$\mathcal{B}(q_i)-1 = \frac{3}{2} + \frac{\sum g_n \frac{E_n}{kT} e^{-E_n/kT}}{Z} \qquad (25)$$

where 3/2 represents the translational energy, $E_n$ the internal energy per particle for the remaining degrees of freedom and Z is the corresponding partition function.

Let

$$W = \sum g_n \frac{E_n}{kT} e^{-E_n/kT} \qquad (26)$$

then

$$\mathcal{B} = \frac{5}{2} + \frac{W}{Z} \quad . \qquad (27)$$

W may be evaluated in the same way as Z, i.e.,

$$W = W_{low} + W_{high} \qquad (28)$$

where $W_{low}$ is given by (26) but summed over just the low states. $W_{high}$ is obtained by substituting (22) in (26):

$$W_{high} = \frac{I}{kT} Z_{high} + e^{\frac{-I}{kT}} (W_{ion}\, z_{high} - w_{high}\, Z_{ion}) \tag{29}$$

where

$$W_{ion} = \sum g_n \frac{E_{ion}}{kT}\ e^{\frac{-E_{ion}}{kT}} \tag{30}$$

and

$$w_{high} = \sum g_{n\ell} (\eta) \frac{E'_{n\ell}}{kT} e^{+\frac{E'_{n\ell}}{kT}} \tag{31}$$

and $Z_{high}$, $Z_{ion}$, $z_{high}$ are determined according to (23) and (24).

Equation (25) follows from the formula for the internal energy per mol $E_i$, i.e.,

$$E_i = RT^2 \frac{d}{dT} \ln Z_i \ . \tag{32}$$

Other quantities of interest in shock propagation may be similarly determined. If $F_i$ is the free energy per mol, $S_i$ the entropy, and $C_i$ the heat capacity per mol, then

$$F_i = - RT \ln Z_i \tag{33}$$

$$S_i = R \frac{d}{dT} (T \ln Z_i) \tag{34}$$

$$C_i = R \frac{d}{dT} T^2 \frac{d}{dT} \ln Z_i = \frac{dE_i}{dT} \ . \tag{35}$$

In equations (32) to (35) only the contributions from the internal degrees of freedom are included.

## 5. The Shock Front without Heat Conduction or Viscosity.

In sections 2 to 4 we have shown how component concentrations and energy content may be calculated in a gas which is in a state of complete thermal equilibrium. If we now specify this equilibrium state to be that which exists behind a shock front, then the density and temperature are determined by the conservation equations, the equation of state, the shock velocity, and the initial conditions. In this section we assume that heat conductivity and viscosity can be neglected which is perfectly valid if the conditions are those of equilibrium (cf section 6).

The procedure for calculating $\beta$ for atoms and ions is given in section 4 and that for calculating $\epsilon$ and g in section 2. Then, from (8), the value of $\beta$ for the gaseous mixture is given by

$$\beta = \frac{\epsilon}{g} . \tag{36}$$

Consider a one-dimensional shock for which the shock equations may be written:

Conservation of mass:

$$\rho v = m = \text{const} \tag{37}$$

where $\rho$ is the density and v the velocity with respect to the shock front, i.e.,

$$v = u - U, \tag{38}$$

u being material velocity and U the shock velocity.

Conservation of momentum:

$$p + mv = mV, \quad V = \text{const} \tag{39}$$

Conservation of energy:

$$\beta \frac{p}{\rho} + \frac{1}{2} v^2 = \frac{1}{2} C^2, \quad C = \text{const.} \tag{40}$$

The equation of state is given by (3), i.e.,

$$p = g \frac{R}{M} \rho T . \tag{41}$$

If we substitute (37) and (41) into (39) and (40) and divide through by $\rho_1^2$ we obtain

$$g\eta^2 \frac{R}{M} T - \frac{m}{\rho_1} V\eta + \left(\frac{m}{\rho_1}\right)^2 = 0$$

$$\beta g \frac{R}{M} \eta^2 T - \frac{1}{2} C^2 \eta^2 + \frac{1}{2} \left(\frac{m}{\rho_1}\right)^2 = 0.$$

We take the variable parameter, aside from the initial conditions, to be the shock velocity U. This is because it is the most accurately measured quantity in shock experiments. Also, in producing shock waves by high explosives, one method is to detonate a stick of high explosive in a gas chamber. In this case the detonation velocity and the shock velocity in the gas will be equal and detonation velocities are well known.

The last two equations are re-written as

$$g \eta^2 \frac{R}{M} T - UV\eta + U^2 = 0 \tag{42}$$

$$\beta g \frac{R}{M} \eta^2 T - \frac{1}{2} C^2 \eta^2 + \frac{1}{2} U^2 = 0 \tag{43}$$

The constants V and C are determined from the conditions in front of the shock. Then, for a given value of U, and if $\beta(\eta,T)$ and $g(\eta,T)$ are known, the quantities $\eta$, T, $\xi$ and u may be uniquely determined in the shock front and behind the shock front.

In the above equation radiation has been neglected but a brief consideration shows that this is probably a good approximation for the range of shock strengths* we are considering. For example, if $\xi = 500$, $\eta = 7$, and $\gamma = 4/3$ which is about right for T = 20,000 degr and $U = 6.10^5$ cm/sec, then the energy density for internal degrees of freedom is $10^{11}$ ergs per gram. However, if we assume black-body radiation, the radiation density is only about $10^5$ ergs per gram.

Assuming about 0.1 of the argon atoms are either excited or ionized (cf Part III, Table IV) and an average wave-length for emitted radiation of $2 \cdot 10^{-5}$ cm, we obtain a rate of radiation of about $10^{15}$ ergs per gm per sec (see eq (28), Part II). If we compare this with the internal energy, viz, $10^{11}$ ergs per gm we see that the relaxation time, E/E, for radiation loss is of the order of 100 $\mu$secs. It may be seen from Fig 17, Part III, that this relaxation time is much longer than times of interest in the shock front. (As will be shown in Part III, times of interest are of the order of magnitude of $10^{-8}$ sec, which is also about the lifetime of a radiative transition.) Even the total shock width involves a time considerably less than the above relaxation time.

---

*Shock strength is defined here as the pressure ratio $\xi = p_4/p_1$ where $p_4$ is the equilibrium pressure and $p_1$ is the fore-pressure.

## 6. The Shock Front with Heat Conduction and Viscosity.

We have shown in section 5 how the equilibrium conditions behind a shock front may be determined; however thermal conductivity and viscosity have been omitted from the equations. In this section we will include these terms and briefly consider how the equations could then be treated.

In the temperature range of interest here ($5000^{\circ}$ to $30{,}000^{\circ}$) values of the heat conductivity K or the viscosity $\mu$ are not well known. But it has been indicated, eq (35), how the specific heat and, eq (6), $\gamma$ may be determined. According to Chapman and Cowling (Ref 70) the quantity

$$f_1 = \frac{K}{\mu C_v} \tag{44}$$

is reasonably constant with temperature if $\gamma$ is constant (see, also, Ref 71). It is doubtful that such a relation is valid if ionization is involved, i.e., if $\gamma$ varies. However, if we knew the specific heat at constant volume $C_v$ the ratio $\frac{K}{\mu}$ could, in principle, be obtained.

If heat conduction and viscosity are included in the conservation equations, (37) to (40), they may be written (Ref 63)

$$\rho v = m = \text{const} \tag{45}$$

$$mv + (p-\sigma) = mV = \text{const} \tag{46}$$

$$m\left(\frac{v^2}{2} + E\right) + v(p-\sigma) - H = \frac{1}{2} mC^2 = \text{const.} \tag{47}$$

The equation of state is, again,

$$p = g \frac{R}{M} \rho T \ . \tag{48}$$

Assuming a $\gamma$-law and using (48), eq (47) becomes

$$m \left[ \frac{v^2}{2} + (\beta - 1)\, g \frac{RT}{M} \right] + v(p - \sigma) - H = \frac{1}{2} mC^2 . \tag{49}$$

$\sigma$ is the ordinary stress term due to viscosity and - H is the heat flow intensity, i.e.,

$$H = K \frac{dT}{dx} , \qquad \sigma = \frac{4}{3} \mu \frac{dv}{dx} \tag{50}$$

Putting the relation for $\sigma$ into (46) and using (48) and (45) we get

$$\frac{4}{3} \frac{\mu}{m} \frac{dv}{dx} = v + \frac{gRT}{Mv} - V \ . \tag{51}$$

Substituting (46) into (49) and using the relation for H, (50):

$$\frac{K}{m} \frac{dT}{dx} = vV - \frac{1}{2} C^2 - \frac{v^2}{2} + (\beta - 1) \frac{gRT}{M} \tag{52}$$

Dividing (52) by (51):

$$\frac{dT}{dv} = \frac{4\mu}{3K} \frac{vV - \frac{v^2}{2} - \frac{1}{2} C^2 + (\beta - 1) \frac{gRT}{M}}{v + \frac{gRT}{Mv} - V} \tag{53}$$

Let

$$h(v,T) = v + \frac{gRT}{Mv} - V \ , \tag{54}$$

$$j(v,T) = \frac{4\mu}{3K} \left[ vV - \frac{v^2}{2} - \frac{1}{2} C^2 + (\beta - 1) \frac{gRT}{M} \right] ,$$

or using,

$$\beta - 1 = \frac{1}{\gamma - 1} \quad ,$$

$$j(v,T) = \frac{4}{3} P_r \left[ M \frac{(\gamma-1)}{gR} \left( vV - \frac{v^2}{2} - \frac{1}{2} C^2 \right) + \frac{T}{\gamma} \right] \tag{55}$$

where $P_r$ is a modified Prandtl's number (Ref 63), which is g times the usual Prandtl's number,

$$P_r = \frac{\gamma g R}{(\gamma-1)M} \frac{\mu}{K} \tag{56}$$

If h = 0, conservation of momentum is obtained and j = 0 gives conservation of energy.

Letting

$$v^2 = z, \qquad 2vdv = dz;$$

then (53) becomes, with (54), (55),

$$\frac{dT}{dz} = \frac{2}{3} P_r \frac{\left[ \alpha(V\sqrt{z} - \frac{z}{2} - \frac{1}{2} C^2) + \frac{T}{\gamma} \right]}{z + \frac{gRT}{M} - V\sqrt{z}} = \frac{k_1}{k_2} \tag{57}$$

where

$$\alpha = \frac{(\gamma-1)M}{\gamma g R}$$

$$k_1 = \frac{2}{3} P_r \left[ \alpha(V\sqrt{z} - \frac{z}{2} - \frac{1}{2} C^2) + \frac{T}{\gamma} \right]$$

and

$$k_2 = z + \frac{gR}{M} T - V\sqrt{z}$$

Equation (57) has a singularity whenever the numerator and the denominator on the right-hand side go to zero simultaneously. The curve of $k_2 = 0$ in the z,T-plane intersects the z-axis at $z = 0$ and at $z = V^2$ and has its maximum value of T at $z = V^2/4$. It is concave toward the z-axis. Since $V^2$ is always greater than or equal to z, the curve of $k_1 = 0$ in the z,T-plane has a negative derivative and is convex toward the z-axis. It intersects the T-axis at

$$T = \frac{\gamma-1}{gR} \frac{C^2}{2}$$

and has a minimum at $z = V^2$, intersecting the $k_2$-curve in the two points $(z_1, T_1)$ and $(z_4, T_4)$ where $z_1 > z_4$, $T_1 < T_4$ (cf Fig. 1). The shock width is then the distance between points 1 and 4.

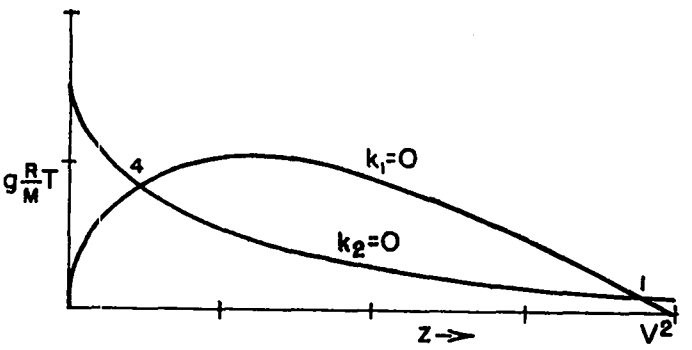


Fig. 1

From $k_1 = k_2 = 0$,

$$z\left(\frac{\gamma+1}{2}\right) - \gamma V\sqrt{z} + (\gamma-1)\frac{C^2}{2} = 0$$

or

$$\sqrt{z} = \frac{\gamma V \pm \sqrt{\gamma^2 V^2 - (\gamma^2-1)c^2}}{\gamma+1} \tag{58}$$

This shows that z is a sensitive function of $\gamma$ which, in turn, depends on say z and T. A method for determining $\gamma$ has been discussed previously.

Also, for $k_1 = k_2 = 0$

$$T = \frac{M}{gR}(V\sqrt{z}-z) = \alpha\left(\frac{c^2}{2} - \frac{z}{2}\right) \tag{59}$$

One may obtain the integral curves for (57) by using the method of isoclines. Writing (57) as

$$\frac{dT}{dz} = \frac{2P_r}{3\gamma gR}\,\frac{T-T_a}{T-T_b} \tag{60}$$

where

$$T_a = \gamma\alpha\left(\frac{z}{2} - V\sqrt{z} + \frac{c^2}{2}\right) \tag{61}$$

$$T_b = \frac{M}{gR}\,(V\sqrt{z}-z)\,. \tag{62}$$

$\gamma$ and g vary across the shock front staying, for our temperature range, between 1 and 2. As the temperature increases $\gamma$ decreases and g increases their product remaining approximately constant.

Let

$$G = \frac{2P_r}{3\gamma gR} = \frac{2}{3}\,\frac{\mu/K}{(\gamma-1)} \tag{63}$$

then (60) becomes

$$\frac{dT}{dz} = G\lambda, \qquad \lambda = \frac{T_\lambda - T_a}{T_\lambda - T_b}, \qquad T_\lambda = \frac{T_a - T_b}{1-\lambda} \tag{64}$$

The isocline for dT/dz is a curve of constant $\lambda$. If $\lambda = \infty$, $T_\lambda = T_b$ and if $\lambda = 0$, $T_\lambda = T_a$. If $\lambda = 1$, $T_a = T_b$ and we obtain (58) where the plus sign corresponds to $z_1$ and the minus sign to $z_4$. Using additional values for $\lambda$ it may be seen that point 1 is a nodal point and point 4 is a saddle point, i.e., an infinite number of integral curves pass through point 1 and a finite number (viz., 2) through point 4. If $\lambda = (\gamma-1)$ we obtain the second equation of (59), i.e.,

$$T_\lambda = \frac{(\gamma-1)M}{\gamma g R}\left(\frac{c^2}{2} - \frac{z}{2}\right) \tag{65}$$

which is a straight line connecting the points 1 and 4.

If these results are applied to the region in which complete thermal equilibrium exists then, since dT/dz = 0 here, equations (58) and (59) may be used to calculate the equilibrium conditions. Fortunately, the viscosity and heat conductivity drop out for dT/dz = 0 and the method of section 5 may be used to compute the equilibrium conditions behind the shock front.

- - - - - - - - - -

Application of the theory given in sections 2 to 5 is made in Part III. The partition functions and equilibrium constants for a wide range of densities and temperatures have been computed and are tabulated in Table IV of Part III. Equilibrium conditions behind the shock front

for U between $3 \cdot 10^5$ and $9 \cdot 10^5$ cm/sec and for $p_1$ = 1.0 and 59.38 cm Hg have been calculated and are presented in both graphical and tabular form.

## PART II: THE NON-EQUILIBRIUM REGION

### 1. Introduction.

In Part I it has been shown how the conditions in the region behind the shock where thermal equilibrium is assumed to be established may be completely determined. We now wish to look at the non-equilibrium portion of the shock, i.e., the part between the undisturbed gas in front of the shock and the equilibriated region behind the shock.

Although a true thermodynamic temperature does not exist in this region, the velocity distribution of the neutral atoms, the ions, and the electrons is at each point close to maxwellian. We may therefore introduce a local "temperature" which is characteristic of this distribution. The use of such a temperature is probably valid, since the high density and pressure involved cause a maxwellian distribution to be very quickly established.

Let us divide the shock front in the following way. Region 1 is the undisturbed part in front of the shock. Region 4 is the part behind the shock in which complete thermal equilibrium is assumed to be achieved and for which the conditions have been previously calculated. In region 2 we assume only elastic collisions and a width of about two

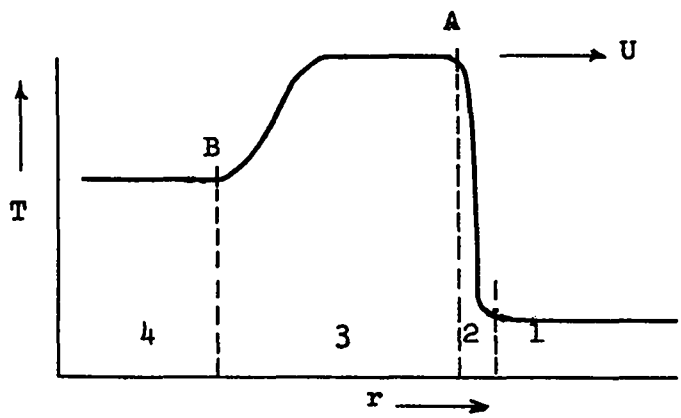


Fig. 1

mean free paths, as it has been shown that equilibrium between translational degrees of freedom is established in about two collisions for strong shocks (Ref 44, 45, 46). Because of the small extent of region 2 and because its thickness does seem to be known reasonably well, we will not consider it further. We will be concerned only with region 3 in the following. This is the region in which excitation and ionization of the argon atoms takes place and we wish to calculate how long it takes to go from point A to point B (Fig. 1), i.e., from where there is complete equilibrium between translational degrees of freedom only, to where there is complete equilibrium between all degrees of freedom.

To obtain the conditions at point A we use the shock equations with the assumption, however, that the internal degrees of freedom are not excited. We therefore use a constant $\gamma$, viz., $\gamma = 5/3$ for argon. The temperature at point A is given by

$$T_A = T_1 \frac{(\gamma-1)}{(\gamma+1)^2} \frac{p_1}{\rho_1 U^2} \left\{ \frac{2\rho_1^2}{p_1^2} U^4 - \frac{\rho_1}{p_1} \frac{(\gamma^2-6\gamma+1)}{\gamma-1} U^2 - 2\gamma \right\} .$$

Pressure is determined from

$$\frac{p_A}{p_1} = \xi_A = \frac{2\rho_1}{p_1(\gamma+1)} U^2 - \frac{1}{\eta_\infty}$$

and density from

$$\frac{\rho_A}{\rho_1} = \eta_A = \frac{\eta_\infty \xi_A + 1}{\xi_A + \eta_\infty}$$

where

$$\eta_{\infty} = \frac{\gamma+1}{\gamma-1} .$$

(Derivation of these equations is indicated in Part III, section 4.)

If we knew the cross-sections for all the various atomic interactions that take place in a shock front, it should be possible to compute the rate of transfer of energy from the translational degrees of freedom to the other degrees of freedom, i.e., the rate at which true thermal equilibrium is established. For argon, the interactions involved are fairly simple and many of the cross-sections are known. In the following sections these interactions are considered in some detail and it is shown how they may be used to compute conditions in the non-equilibrium region.

If $n_e$ is the electron concentration, the rate of change of the number of electrons per $cm^3$ is

$$\frac{dn_e}{dt} = q-p.$$

q represents the rate at which electrons are produced and p the rate at which recombination takes place. (See, however, Part III, section 4.)

2. Production of Electrons in the Shock Front.

We first consider the means by which electrons are produced in the shock front and then, in section 3, consider how they recombine with the argon ions. There are numerous processes by which electrons are produced in forming a plasma. Hence the production term is written

$$q = \sum_i q_i$$

where the summing is over all possible processes. Some of the processes will be neglected because the concentrations of one or more of the interacting components is small and some will be neglected because the interaction is small. **In the final computation (cf Part III) only the processes (1) and (3) listed below are used, although one could easily include others.**

We start with a maxwellian distribution of neutral argon atoms with a sufficient number in the high-energy tail to produce ionization by the reaction

$$A + A \longrightarrow A + A^+ + e \qquad (1)$$

This produces small concentrations of electrons and argon ions, $A^+$, which then enter into the following reactions:

$$A + A^+ \longrightarrow A^+ + A^+ + e \qquad (2)$$

$$e + A \longrightarrow e + A^+ + e \qquad (3)$$

$$e + A \longrightarrow e + A^{++} + 2e \qquad (4)$$

$$e + A \longrightarrow e + A^{+++} + 3e. \qquad (5)$$

Reactions (4) and (5) offer small contributions compared to (3) but their cross-sections are known.

The reaction

$$e + A^+ \longrightarrow e + A^{++} + e \qquad (6)$$

is not included because the concentration of each of the reactants is

small. However, this reaction may be of more importance than (5) but the cross-section is not available.

The reactions

$$A^+ + A \longrightarrow A^{++} + A + e \qquad (7)$$

and

$$A^+ + A^+ \longrightarrow A^{++} + A^+ + e \qquad (8)$$

are neglected because of the higher ionization potential of A II (27.62 ev) compared to that of A I (15.76 ev) as well as the low concentration of one or both of the reactants. In addition, the cross-sections are not available.

Finally, the absorption reaction,

$$h\nu + A \longrightarrow e + A^+ \qquad (9)$$

is neglected because of the long lifetime involved (cf Part I, section 5), and because the photons escape from the system.

Finally, the argon atom may be excited by processes similar to the ones listed above. Once excited it can drop into a meta-stable state from which ionization can take place either by collisions of the second kind or by a photo-process. In both cases radiative transitions are involved and, as pointed out above, the lifetimes of radiative transitions are of such lengths as to warrant neglect of excitation. It is possible, however, that excitation processes compete with some of the one-step processes but the cross-sections are not known very well (although cf Ref 76).

If all processes are included the production term is

$$q = \sum_{i=1}^{9} q_i \qquad (10)$$

where $q_1$, $q_2$, $q_3$, etc., represent the reactions (1) to (9) respectively.

2.1. Collisions between Atoms and Ions.

Since, at the peak of the shock (point A, Fig 1), only the translational degrees of freedom are excited and there are no electrons present, we consider first the reactions between argon atoms. $q_1$ and $q_2$ and the cross-sections involved in (1) and (2) are similar so only $q_1$ need be discussed in detail.

We write

$$q_1 = \iint f(v_1) f(v_2) \sigma_i(v_r) v_r d\vec{v}_1 d\vec{v}_2 \qquad (11)$$

where $f(v_1)$, $f(v_2)$ are the maxwellian distributions for the two reactants (in this case, neutral argon atoms), $\sigma_i(v_r)$ is the ionization cross-section, $v_r$ is the relative velocity, and $d\vec{v}_1$, $d\vec{v}_2$ are the elements of volume in velocity space. The use of maxwellian distributions here is particularly good because of the high shock velocities to be considered (Ref 48) and because the masses of the reactants are equal. However, the cross-section $\sigma_i(v_r)$ is not well known and some assumptions must be made.

Very* little theoretical work has been done for the case of two heavy atoms colliding and not much more experimental work. The observed cross-sections for argon in argon are sketched in Fig. 2.

*Text which is typed in single-space may be omitted without interrupting the continuity.

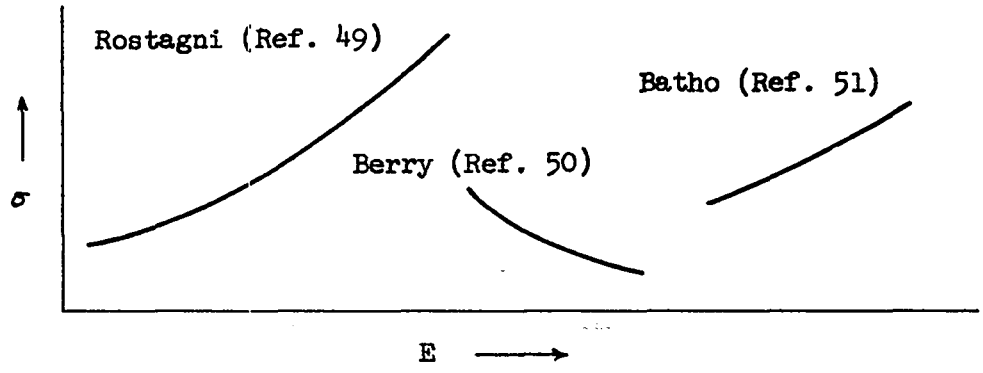


Fig. 2

Since agreement between the various observers is not good, we consider the reasons for the discrepancies.

To obtain a source of fast neutral particles, use is made of the charge transfer process which occurs without the direction of the neutralized ion being altered. A source of the appropriate ion is obtained which is then accelerated to the desired energy by an ion gun and allowed to pass through a chamber of neutral atoms. Charge exchange takes place and a beam of neutral atoms is emitted and the ions remaining in the beam are removed by an electrical field. The energy of the neutral beam is nearly the same as that of the original ion beam.

For the detection of fast neutral beams, three methods have been used. In the ionization method a neutral beam enters an ionization chamber and the relative ionization is measured. In the thermal method the neutral beam is allowed to impinge on a thermo-element and the beam intensity determined by the heating effect produced. In the secondary emission method the neutral beam strikes a metal surface and the secondary electrons produced are collected by an electrode held positive with respect to the surface. These methods of detection give relative intensities but, since only total cross-sections are required here, this is sufficient. The discrepancy between the observed cross-sections as measured by different observers is probably due to employment of different methods of measuring the neutral beam intensity.

Of the numerous methods used for measuring the cross-sections, one will be briefly described. A homogeneous beam of ions, e.g. $A^+$, is caused to enter a collision chamber which is filled with neutral atoms. If the beam energy is small, charge exchange without ionization will take place and the

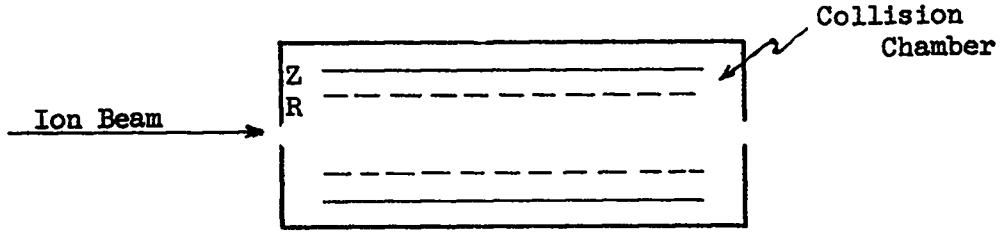


Fig. 3

flux of slow ions produced may be measured. The slow ions are attracted to the collecting cylinder Z which has in front of it a grid R. The saturation current $i_c$ represents slow

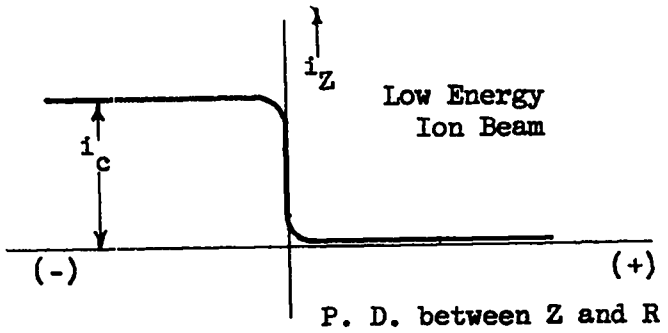


Fig. 4

ions produced by charge exchange.

If the beam energy is large, not only will charge exchange take place but there will be ionization. If Z is positive with respect to R the saturation value for the electron

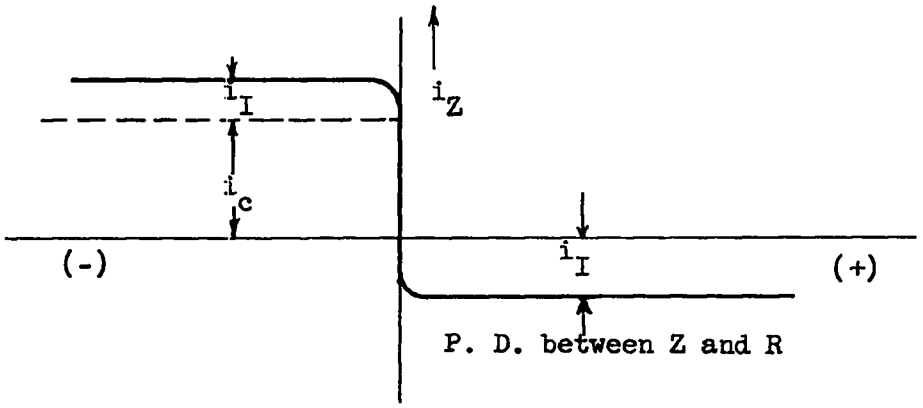


Fig. 5

current $i_I$ will be measured from which the ionization cross-section may be computed. If Z is negative with respect to R, the total current measured will be that due to charge exchange $i_c$ plus that due to ionization $i_I$. Knowing $i_I$ it is then possible to calculated $i_c$, thus both charge exchange and ionization cross-sections may be computed.

Actually, as indicated by Fig. 2, the measurement of accurate ionization cross-sections is extremely difficult for the following reasons. The ionization currents produced are small, and the electrons which have to be collected in order to measure the ionization are produced in the presence of large quantities of slow positive ions produced both in the ionization process itself, and, more often, by charge exchange. The positive ions, when collected, may give rise to considerable quantities of secondary electrons. Also, the saturation electron current must be measured at a potential below that needed to ionize the gas by electron impact. Finally, particularly in argon and other inert gas atoms and ions, metastable atoms may be present which have the property of freeing electrons from surfaces on which they are incident.

It is appropriate to mention here that the chief difficulty in measuring excitation cross-sections arises from the low intensity of the effects produced. There will, of course, be a loss in intensity due to the presence of the gas itself, but, in addition, there will be losses in intensity due to the necessity of spectral analysis of the radiation emitted. This partially explains why excitation cross-sections for very low energies have not been measured.

If v is the velocity of relative motion of the two colliding atomic systems and u the orbital velocity of the electrons concerned in the particular excitation process, then, in discussing inelastic collisions, two regions are distinguished, viz., $|v/u| >> 1$ and $|v/u| << 1$. For the high-velocity region Born's approximation may be used but since we are primarily interested in the low velocity region for which no suitable theory exists, we must, as pointed out above, use the observed cross-sections. The low velocity or near-adiabatic region is defined such that collisions occur so gradually that the chance of any ultimate transfer of energy is slight.

As indicated in Fig. 6, the cross-section in the near-adiabatic region is extremely small. The correspondence principle argument for this is the following. If the collision time $\tau$ of the atomic systems is large compared to the period T of the electron involved in the particular excitation (or ionization) collision, then the orbital electrons have time to readjust themselves to the slowly changing conditions without a transition taking place. If $\underline{a}$ is the range of interaction between the atoms and v their relative velocity, the condition for weak excitation becomes

$$\frac{a}{v} >> \frac{1}{\nu} \quad .$$

The frequency $\nu$ is given by $\Delta E/h$ where $\Delta E$ is the internal energy involved in the electronic transition. The relative velocity is given by

$$v = 2\sqrt{\frac{\mathcal{E}}{M}}$$

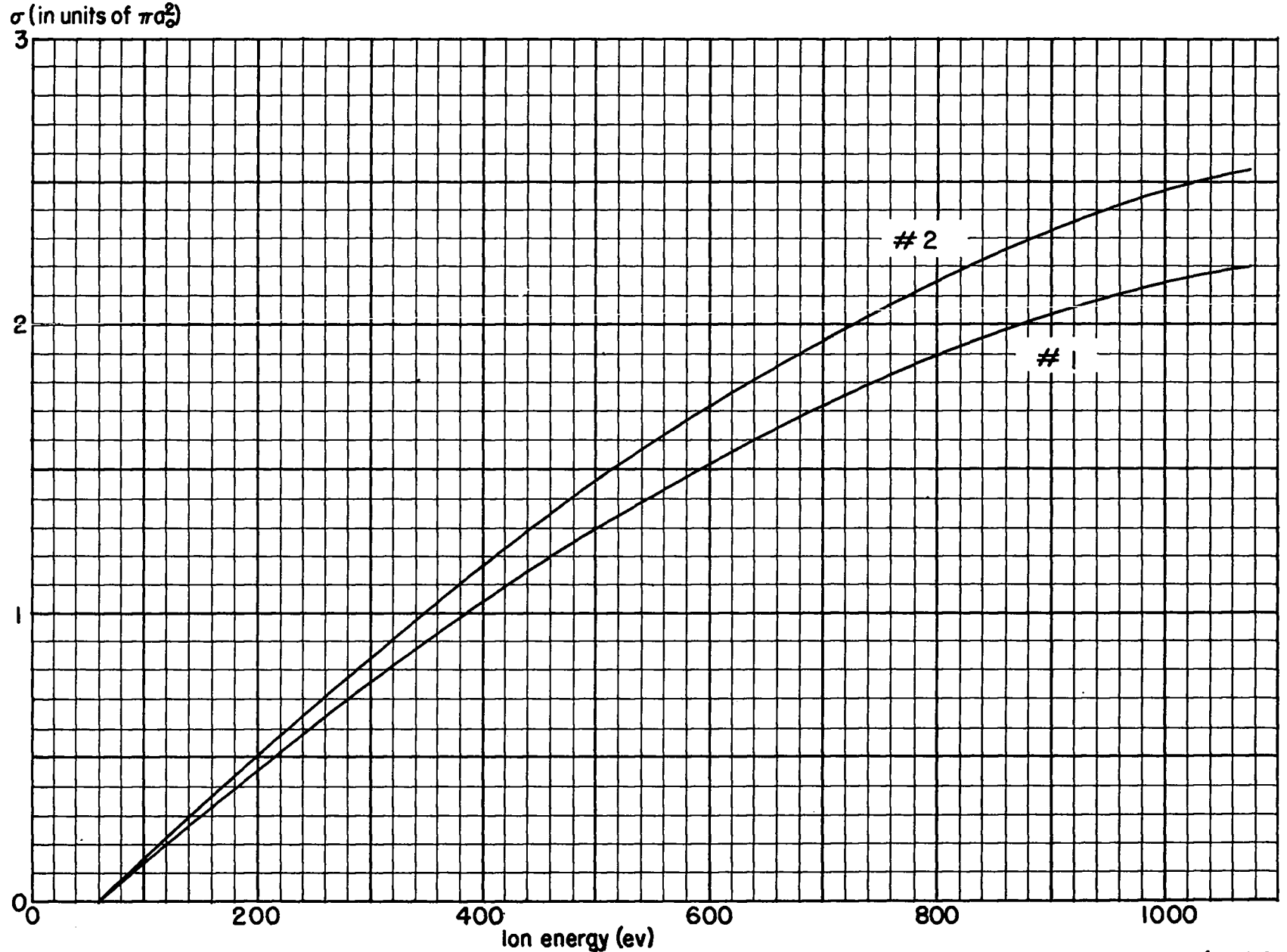


Fig. 6 Cross-sections for ionization by impact between two argon atoms or an argon atom and an argon ion. (Ref, 49)

#2: $A + A^+ \rightarrow A^+ + A^+ + e$ #1: $A + A \rightarrow A + A^+ + e$

where $\mathcal{E}$ is the relative kinetic energy and M is the mass of an argon atom.

The adiabatic condition then becomes

$$\frac{a}{2}\ \frac{\Delta E}{h}\ \sqrt{M} >> \sqrt{\mathcal{E}}$$

or, using $a = 2 \times 10^{-8}$ cm, $h = 6.62 \times 10^{-27}$ erg sec, and expressing energies in electron-volts, the conditions becomes

$$16\Delta E >> \sqrt{\mathcal{E}}$$

If $\Delta E$ is the ionization energy, then for argon $\mathcal{E} << 62$ kev. However, this is far from being a good criterion since for helium $\mathcal{E} << 15$ kev indicating the near-adiabatic region for argon should extend to about four times that of helium whereas experiment shows that it is less (cf Ref 52, p 530).

Since there is no reliable theory for the near-adiabatic region, one would be inclined to believe, on the basis of the above argument, that the ionization cross-section $\sigma_i$ should increase with $\mathcal{E}$ up to a rather flat maximum of the order of the gas-kinetic cross-section at $\mathcal{E} = 62$ kev at which energy the velocity of relative motion is comparable with the velocity of the atomic electrons concerned in the transition. It should then fall off perhaps with some v-power law. For the following reasons, however, the high-energy region need not concern us. First, the experimental values available extend only up to about 25 kev and, second, we are working with temperature distributions for which the number of particles in the high end of the maxwell tail is negligible.

In comparing the observed cross-sections as given in Fig. 2, it is evident that the results of two different observers may be off by a factor of two or more. The previously discussed experimental difficulties probably account for the discrepancies, with the error in measurement of the incoming flux being chiefly responsible. In view of the correspondence principle argument given above, the results of Berry showing a decrease in cross-section with increasing relative ion energy in the range 1 to 5 kev seem somewhat unlikely (Ref 52).

In order to obtain an integrable function approximating Rostagni's results, the curve (Fig. 6) was fitted in the following way. The zero-value was obtained by simply extrapolating the experimental values. The maximum cross-section was assumed to be at $\mathcal{E} \doteq 62$ kev at which point the slope is zero. In Table I, $\sigma_1$ and $\sigma_2$ are the cross-sections for reactions (1) and (2), $\mathcal{E}_a$ is the initial relative kinetic energy in electron volts and v is the relative velocity in cm per sec where

$$v = 3.106 \cdot 10^5 \ \mathcal{E}_a^{1/2}$$

Table I

| $\mathcal{E}_a$(ev) | $v\left(\frac{cm}{sec}\right)$ | $\sigma_1(cm^2)$ | $\sigma_2(cm^2)$ |
|---|---|---|---|
| 60 | $2.406 \cdot 10^6$ | 0 | 0 |
| 100 | $3.106 \cdot 10^6$ | $.119 \cdot 10^{-16}$ | $.129 \cdot 10^{-16}$ |
| 500 | $6.945 \cdot 10^6$ | 1.140 | 1.280 |
| 1000 | $9.822 \cdot 10^6$ | 1.891 | 2.174 |
| 62000 | $7.734 \cdot 10^7$ | | |

A cubic equation was fitted to these values where

$$\sigma_1(v) = a_1 v^3 + b_1 v^2 + c_1 v + d_1 \qquad (12)$$

$$\sigma_2(v) = a_2 v^3 + b_2 v^2 + c_2 v + d_2 \qquad (13)$$

with the constant factors being given in Table II.

Table II

| | a | b | c | d |
|---|---|---|---|---|
| $10^{16} \cdot \sigma_1$ | $-2.948 \times 10^{-23}$ | $1.897 \times 10^{-15}$ | $2.355 \times 10^{-7}$ | -.5772 |
| $10^{16} \cdot \sigma_2$ | $-5.602 \times 10^{-23}$ | $4.949 \times 10^{-15}$ | $2.397 \times 10^{-7}$ | -.6045 |

Above $\mathcal{E}_a$ = 62 kev $\sigma_i$ was assumed to drop off as 1/v which is perhaps incorrect but not important anyway, as will be shown below. In the neighborhood of $\mathcal{E}_a$ = 62 kev the cross-section should have approximately its gas-kinetic value. Equations (12) and (13) give for this energy, $\sigma_1 = 15 \times 10^{-16}$ cm$^2$ and $\sigma_2 = 21 \times 10^{-16}$ cm$^2$, values of the same order of magnitude as the gas-kinetic values.

By carrying out the integration in (11) using (12) it was found that energies above 1000 ev give no contribution. Hence we only need to use the cross-sections over their experimentally determined energy range. This is because the number of particles in the high end of the maxwell distribution is insignificant above 1000 ev for the range of temperatures involved. (Actually, 100 ev is probably high enough.)

Rostagni's results have been used for two reasons. First, his measurements on other gases are in agreement with other observers, indicating his method is good. And second, his measurements are in the lowest energy range, which is desirable for our problem.

In the very low energy range, say below 100 ev, the measurement of the cross-section is particularly difficult because the chance of energy transfer is so minute that it is not easy to reduce background effects to an unimportant magnitude. Wayland (Ref 72) found a low energy tail with a threshold value of 48 ev; however, this has not been incorporated into our computations. This should be done because of the maxwellian distributions involved. But, as yet, there is no satisfactory theoretical calculation available (Ref 75). The values we use in this range will not have much effect on the actual shock structure but are important in determining the shock width (cf Part III, section 7). As will be shown in the next section, reaction (3) offers the most important contribution to the electron production as soon as a sufficient number of free electrons are produced from reactions (1) and (2).

Inserting the expressions for the distribution functions into (11),

$$q = A \iint e^{-\frac{mv_1^2}{2kT}} \, e^{-\frac{mv_2^2}{2kT}} \, \sigma(v) v \, d\vec{v}_1 \, d\vec{v}_2 \qquad (14)$$

where A is the normalizing factor. Change to relative coordinates v,V, the relative velocity and the center of mass velocity respectively:

$$\vec{v} = \vec{v}_1 - \vec{v}_2$$

$$\vec{V} = \frac{1}{2} (\vec{v}_1 + \vec{v}_2).$$

Since the Jacobian is unity,

$$d\vec{v}_1 d\vec{v}_2 = d\vec{v}d\vec{V}.$$

We then have

$$q = A \iint e^{-\frac{m}{2kT}(2v^2 + \frac{1}{2}v^2)} \sigma(v) v d\vec{v} d\vec{V} \qquad (15)$$

or, integrating out the center of mass,

$$q = 4\pi A \left(\frac{\pi kT}{m}\right)^{3/2} \int_{v_i}^{\infty} e^{-\frac{mv^2}{4kT}} \sigma(v) v^3 dv \qquad (16)$$

The integration over v is carried from the minimum ionizing velocity to infinity although, as pointed out above, 1000 ev is sufficient for the upper limit.

The normalizing factor A is determined from

$$\mathcal{V}^2 A \iint e^{-\frac{mv_1^2}{2kT}} e^{-\frac{mv_2^2}{2kT}} d\vec{v}_1 d\vec{v}_2 = 1$$

or

$$A = \frac{1}{\mathcal{V}^2} \left(\frac{m}{2\pi kT}\right)^3 \qquad (17)$$

where $\mathcal{V}$ is the volume per particle. If n is the number density of particles at an arbitrary point in the shock front then

$$q_1 = \frac{\pi}{2} n^2 \left(\frac{m}{\pi kT}\right)^{3/2} \int_{v_i}^{\infty} e^{-\frac{mv^2}{4kT}} \sigma_1(v) v^3 dv \qquad (18)$$

where we have now written $q_1$, since this derivation holds for reaction (1).

Only a minor change is necessary in (18) to write the corresponding expression for $q_2$. For reaction (2) the normalizing factor, eq (17), becomes

$$A = \frac{1}{\mathcal{V}\mathcal{V}^+} \left(\frac{m}{2\pi kT}\right)^{3/2} \left(\frac{m^+}{2\pi kT^+}\right)^{3/2}$$

$\mathcal{V}^+$, $m^+$, $T^+$ are the volume, mass, and mean temperature of the argon ions; however, under our assumptions $T^+ = T$. Also $m^+ \doteq m$ and

$$\mathcal{V}^+ = \frac{1}{n^+} = \frac{1}{n_e}$$

where $n^+$ is the number density for the argon ions and $n_e$ that for the electrons. Hence

$$q_2 = \frac{\pi}{2} nn_e \left(\frac{m}{\pi kT}\right)^{3/2} \int_{v_1}^{\infty} e^{-\frac{mv^2}{4kT}} \sigma_2(v) v^3 dv \qquad (19)$$

In the relations for $q_1$, $q_2$, the quantities $n, n_e$, and T occur outside the integral and T also occurs inside each integral. These quantities all vary across the shock front as shown in the following table:

Table III

| Position on the Shock Front (cf Fig. 1) → / Quantity | Shock Velocity, U = $6 \times 10^5$ cm/sec | | |
|---|---|---|---|
| | 1 | A | B |
| T (degr) | 285 | 32741 | 18400 |
| $\eta = \rho/\rho_1$ | 1 | 3.9674 | 7.123 |
| $n_e(cm^{-3})$ | 0 | 0 | $.160n = 1.974 \cdot 10^{19}$ |
| $\gamma$ | 5/3 | 5/3 | 1.3216 |
| $\xi$ | 1 | 456 | 523 |

($\gamma$ is the ratio of specific heats, and $\xi$ the pressure ratio.)

## 2.2 Collisions between Electrons and Atoms.

Once electrons have been produced by the A+A reaction, then reactions between electrons and atoms take place. We consider reactions(3), (4), and (5), although, as pointed out previously, (3) is by far the most important reaction. It is sufficient to discuss $q_3$ in detail as $q_4$ and $q_5$ may be written immediately from $q_3$.

As in (11), $q_3$ may be written

$$q_3 = B \iint f(v_1) f(v_2) \sigma_3(v) v d\vec{v}_1 d\vec{v}_2 \qquad (20)$$

where B is the normalization factor, $v_1$ is the electron velocity, and $v_2$ the velocity of the neutral atoms. The relative and center-of-mass velocities are

$$\vec{v} = \vec{v}_1 - \vec{v}_2$$

and

$$\vec{V} = \frac{m_e}{M}\vec{v}_1 + \frac{m}{M}\vec{v}_2 , \qquad M = m_e + m.$$

Substituting these relations in (20) and remembering that the Jacobian for the transformation is one,

$$q_3 = B \iint e^{-\frac{1}{2kT}(MV^2+\mu v^2)} \sigma_3(v) v d\vec{v} d\vec{V}.$$

$\mu$ is the reduced mass,

$$\mu = \frac{m_e m}{M} . \tag{21}$$

Integrating over V,

$$q_3 = 16\pi^2 B \sqrt{\frac{\pi}{2}} \left(\frac{kT}{M}\right)^{3/2} \int_{v_i}^{\infty} e^{-\frac{\mu v^2}{2kT}} \sigma_3(v) v^3 dv.$$

The normalization factor is obtained as before and is

$$B = n_e n \frac{(m_e m)^{3/2}}{(2\pi kT)^3} \tag{22}$$

$v_i$ is the minimum ionizing velocity, which, in this case, corresponds to the first ionization potential. $n_e$ is the number density for electrons and n is the number density for the argon atoms. Thus we have

$$q_3 = \sqrt{\frac{2}{\pi}}\, n_e n \left(\frac{\mu}{kT}\right)^{3/2} \int_{v_i}^{\infty} e^{-\frac{\mu v^2}{2kT}} \sigma_3(v) v^3 dv \tag{23}$$

Similarly,

$$q_4 = \sqrt{\frac{2}{\pi}}\, n_e n \left(\frac{\mu}{kT}\right)^{3/2} \int_{v_i'}^{\infty} e^{-\frac{\mu v^2}{2kT}}\, \sigma_4(v) v^3 dv \qquad (24)$$

and

$$q_5 = \sqrt{\frac{2}{\pi}}\, n_e n \left(\frac{\mu}{kT}\right)^{3/2} \int_{v_i''}^{\infty} e^{-\frac{\mu v^2}{2kT}}\, \sigma_5(v) v^3 dv \qquad (25)$$

$v_i'$ corresponds to the second ionization potential, 44.0 ev, and $v_i''$ to the third ionization potential, 88 ev. The observed cross-sections, $\sigma_3$, $\sigma_4$, and $\sigma_5$ are shown in Fig. 7 (Ref 53). Because of the greater weight attached to the low energy cross-sections, values for $\sigma_3$ and $\sigma_4$ near the threshold are shown in Figs. 8A and 8B (Ref 54).

3. Recombination Processes.

After some electrons have been created by ionizing impacts between heavy particles, electron production increases with extreme rapidity due to the processes discussed in section 2.2. However, there are opposing processes, viz, recombination between electrons and ions. These are the following:

(a) Dielectronic recombination

$A^+ + e \longrightarrow A''$ (doubly excited atom, i.e., two electrons are excited)

$A'' \longrightarrow A^+ + e$

$A'' \longrightarrow A' + h\nu$ ($A'$ = singly excited atom)

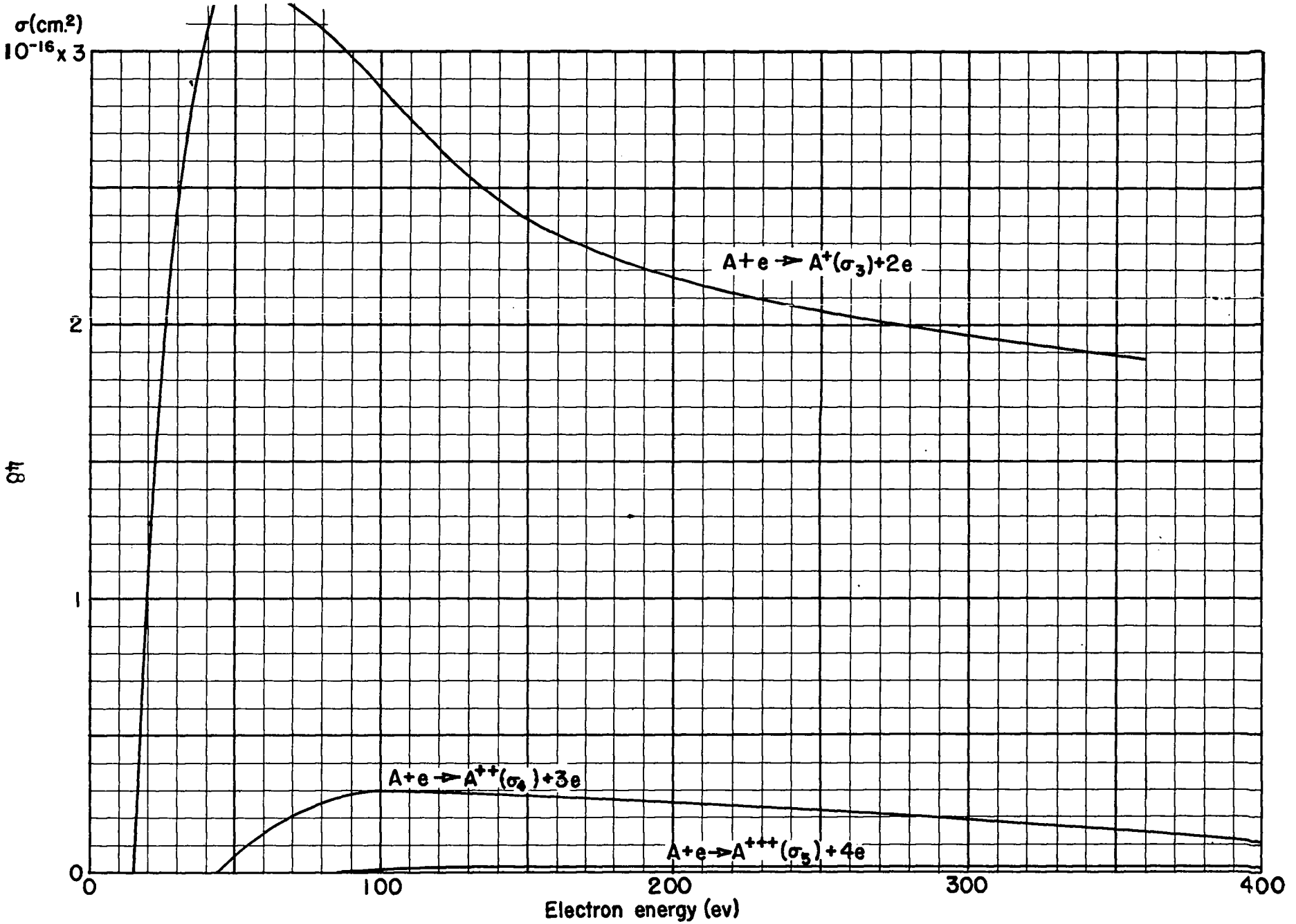


Fig. 7 Cross-sections for ionization by impact between an argon atom and an electron. (Ref. 53)

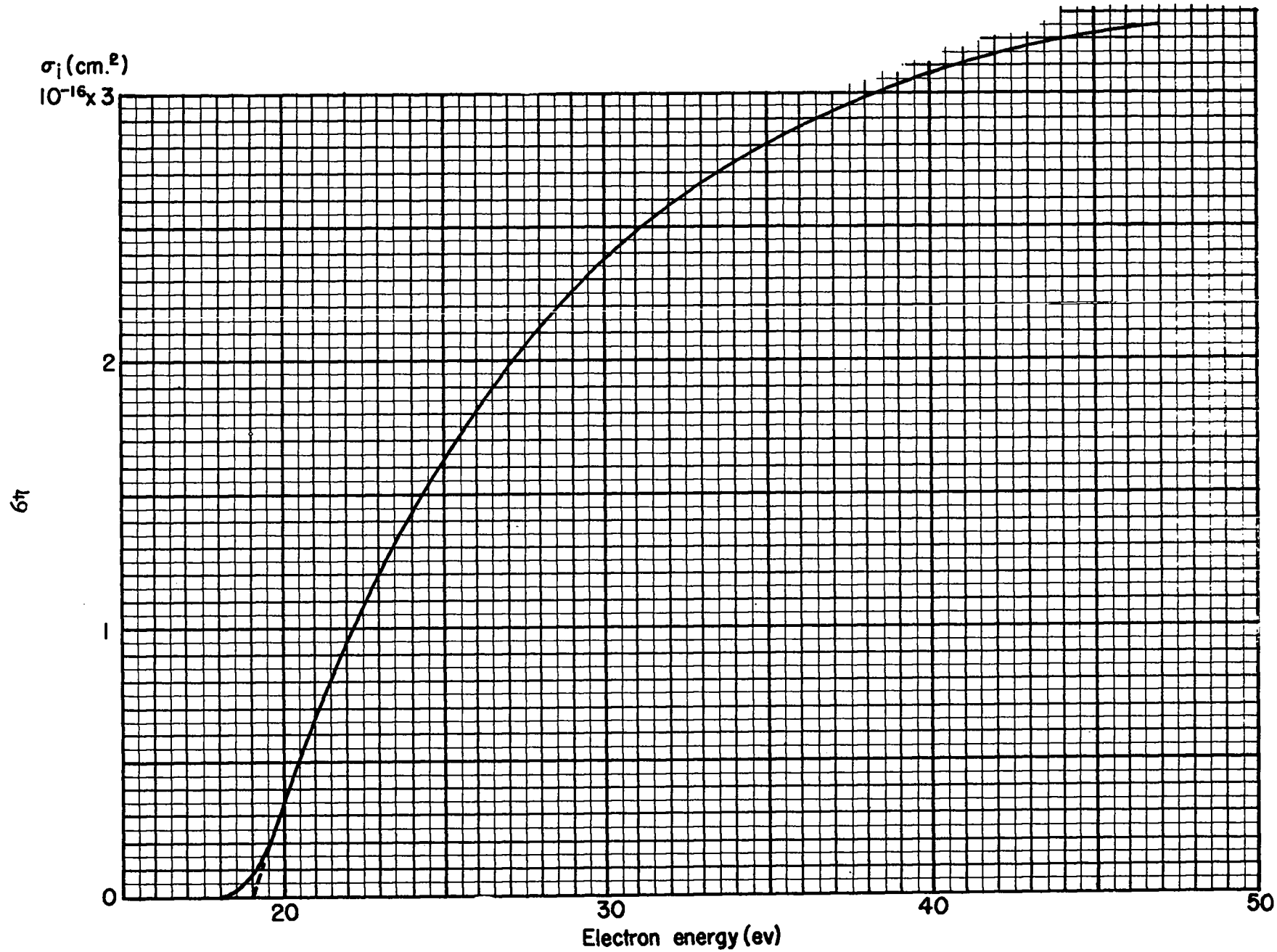


Fig. 8A Threshold cross-section for the reacton $e + A \rightarrow e + A^+ + e$ (Ref. 54)

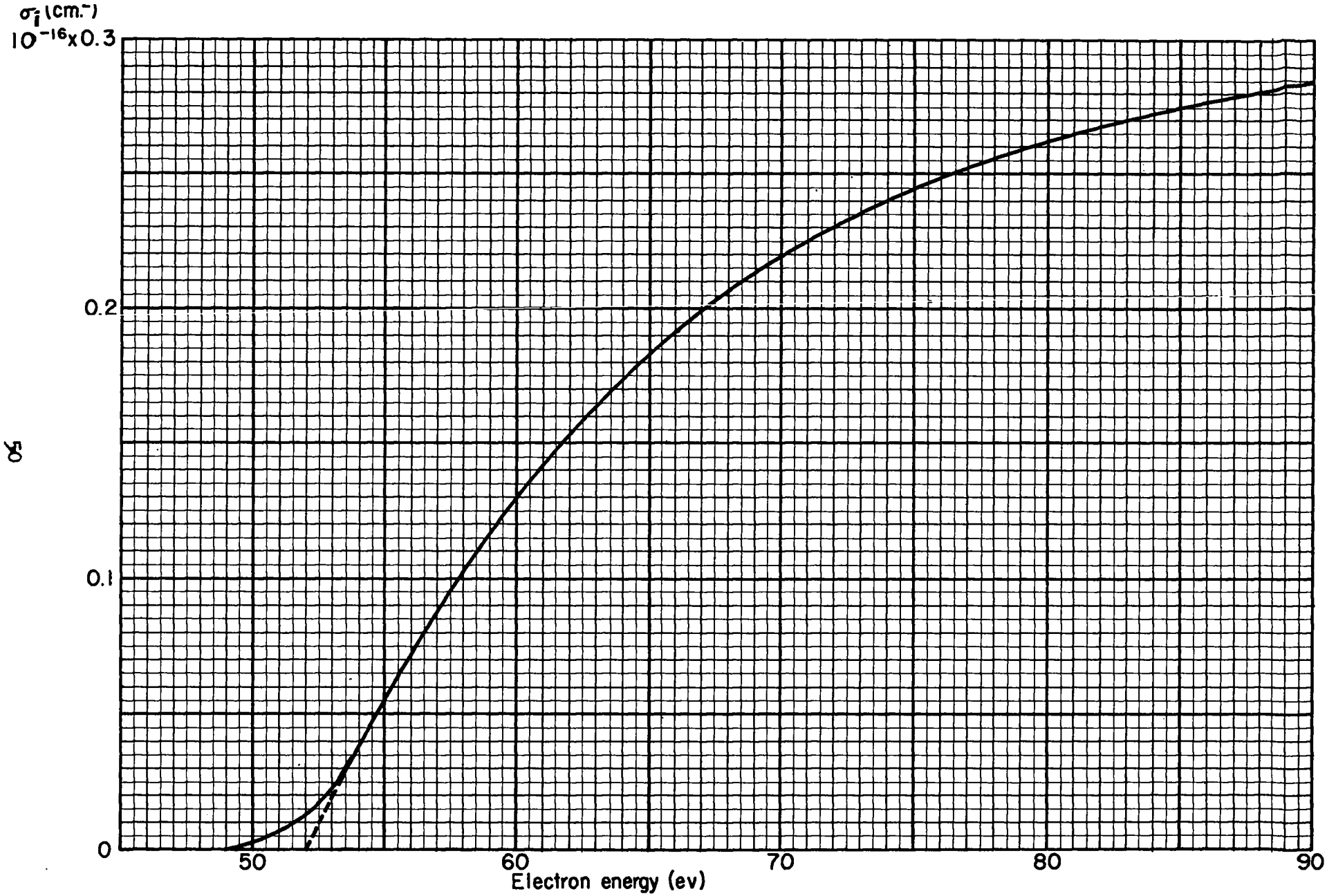


Fig. 8B Threshold cross-section for the reaction $e + A \rightarrow e + A^{++} + 2e$ (Ref. 54)

(b) Dissociative recombination

$$A_2^+ + e \longrightarrow A' + A'$$

(c) Radiative recombination

$$A^+ + e \longrightarrow A' + h\nu$$

(d) Three-body recombination

$$A^+ + e + A \longrightarrow A + A.$$

The first three processes, being two-body processes, are most important at low pressures whereas the fourth process becomes most important at higher pressures.

The recombination term p in equation (4) becomes

$$p = \sum_i p_i$$

where $p_i$ is summed over all possible processes, i.e.,

$p_1$ = dielectronic recombination

$p_2$ = dissociative recombination

$p_3$ = radiative recombination

$p_4$ = three-body recombination.

## 3.1 Dielectronic Recombination.

When an electron recombines with an ion some energy is released. If this energy is taken up by a second atomic electron, a doubly excited atom will be formed,

$$A^+ + e \longrightarrow A''.$$

Because of the length of the lifetimes involved, we will probably not be interested in how A" decays. That is, A" will either revert to its ini-

tial state, ejecting one electron and leaving the other excited electron in its initial bound state,

$$A'' \longrightarrow A^+ + e,$$

or, the doubly excited atom will undergo a radiative transition going over to a stable, singly excited state,

$$A'' \longrightarrow A' + h\nu .$$

We have then

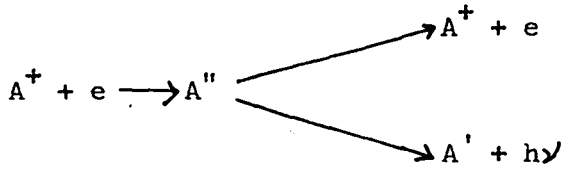


It has not been possible to obtain an accurate cross-section for this process but we can gain some information by using a computation of Massey and Bates (Ref 22). There is a chance that the lifetime of $A''$ for decay to $A^+ + e$ is much greater than the time required for a radiative transition, i.e., $10^{-8}$ sec. Assuming such a possibility, then we may compute the contribution in the following way: The Saha equation may be written

$$\frac{n''}{n_e\, n^+} = \frac{1}{K} = \left(\frac{h^2}{2\pi\mu kT}\right)^{3/2} \frac{Z_n(A'')}{Z_n(e)\, Z_n(A^+)}$$

where K is the equilibrium constant and the $Z_n$ are the partition functions described in Part I. This of course assumes the process is one of equilibrium which is not strictly true.

Each time an electron disappears a doubly excited complex appears,

hence

$$\left(\frac{dn_e}{dt}\right)'' = -\frac{dn''}{dt} = -\frac{n''}{\tau} = -p_1$$

where $\tau$ is the lifetime. In case there is more than one state for A" then

$$p_1 = \left(\frac{h^2}{2\pi\mu kT}\right)^{3/2} \frac{\sum_s \frac{w_s e^{-\frac{E_s}{kT}}}{\tau_s}}{2w^+} \cdot n_e^2 \qquad (\text{since } n_e = n^+)$$

$w_s$ is the statistical weight of the collision complex A", $w^+$ is the statistical weight of the ion, and $E_s$ is the energy excess of A" above $A^+$.

Substituting numerical values and assuming $\tau = 10^{-8}$ sec., $T = 20{,}000^\circ$, and that the statistical weights are of the order of unity then

$$p_1 \cong 10^{-14} n_e^2 \sum_s e^{-\frac{E_s}{kT}}$$

The lowest state for A" will have an energy such that $\left(\frac{E_s}{kT}\right)$ is about 5, hence

$$p_1 \cong 10^{-16} n_e^2.$$

As will be seen later, this term can be neglected compared to $p_3$ and $p_4$.

If the cross-section for this case is $\sigma_{r1}$ then, neglecting the velocity distribution,

$$p_1 = \sigma_{r1} v n_e^2$$

and, for $T = 20{,}000^\circ$,

$$\sigma_{r1} \cong 10^{-24} \text{ cm}^2.$$

On the basis of the above computation and because the concentrations of the reactants is small, this reaction will not be included in the final calculations of Part III.

3.2 Dissociative Recombination.

An argon atom and an argon ion may unite in a triple impact to form a molecular ion, $A_2^+$. Because of the short duration of the time of formation, the process

$$A_2^+ + e \longrightarrow A' + A'$$

could be of considerable importance. And, in fact, at low temperatures this is thought to be the case (Ref 30, 31, 32). However, molecular binding energies are low and since the mean temperatures we are considering are in the range from 2 to 3 electron volts, it is probably safe to assume that the concentration of $A_2^+$ is negligibly small.

3.3 Radiative Recombination.

In the previous sections two types of recombination processes have been briefly considered and it was indicated that their contribution to the total recombination process could be neglected. This will be verified by the discussion of the present and the following sections.

Radiative capture of an electron by an argon ion is a two-body process and may be represented by the reaction

$$A^+ + e \longrightarrow A' + h\nu \qquad (26)$$

where A' may be the ground state or any excited state of an argon atom. This can be regarded as a radiative transition of an electron from an unquantized (free) state to a bound state.

There is also the possibility of the attachment of an electron to an argon atom to form a negative ion. However, the cross-section for such a process is small, particularly for inert gas atoms (Ref 52), hence will be ignored.

So far observations of recombination rates have not been very successful for two reasons. First, as has been pointed out before, it is difficult to separate the various mechanisms involved. At low pressures and temperatures dissociative recombination occurs. As the temperature increases radiative recombination plays an increasingly important role and with increase in pressure, the three-body process enters.

The second difficulty lies in the order of magnitude of the effects produced. This may be indicated by the following consideration. The lifetime of an excited state of an atom is observed to be approximately $10^{-8}$ sec. This means that an electron must remain in an excited state in the neighborhood of an ion as long as $10^{-8}$ sec before there is considerable chance of its undergoing a radiative collision. Then if $\tau$ sec is the collision time, $\tau/10^{-8}$ is the chance of emission of radiation during an encounter. Collision times are of the order of a/v where a is the range of interaction and v is the relative velocity of the incoming electron. Taking $a = 10^{-8}$ cm and $v = 10^{8}$ cm/sec gives $\tau = 10^{-16}$ sec, hence the chance of capture to a particular quantum state is $10^{-8}$, i.e., $10^{8}$ encounters are required before an electron is captured.

In the first experiments in which recombination was studied (Ref 35, 55) a discharge tube was employed. After short-circuiting the discharge the decay of electron density in the afterglow was investigated by visual intensity, by spectrophotometric measurements, and by probe measurements. Recently, a microwave technique has been employed (Ref 24, 26, 30, 32). The gas in a microwave cavity is ionized by the microwaves and the decay time for the electrons measured by observing the change in the resonant wave-length of the cavity. However, the recombination coefficients as measured by the microwave method are 10 to 100 times greater than those measured by the probe technique. This is probably due to dissociative recombination, as the experiments were done at relatively low temperatures.

Since experimental cross-sections are not available, it is necessary to develop a theoretical expression for the radiative reaction (26). What is needed is a relation for $\alpha$ as a function of temperature for the range $T \leq 3$ ev where

$$\left(\frac{dn_e}{dt}\right)_{\text{radiative}} = -\alpha_3(T) n_e^2$$

and $\alpha_3(T) = \sigma_r v$; or, if maxwell distributions are used, $\alpha_3(T) = \overline{\sigma_r v}$. v is the relative velocity of the incoming electron and $\sigma_r$ is the cross-section for radiative capture.

It would be possible to use the inverse process, viz, photo-ionization,

$$h\nu + A \longrightarrow A^+ + e \qquad (27)$$

by applying the theory of detailed balancing. But this reaction has neither been computed or measured (see, however, Part III, section 6).

An accurate theoretical derivation has been made only for hydrogen (Ref 36, 42). An approximate (classical) theory has been given by Kramers (Ref 41) and applied by Eddington (Ref 27) and Biondi (Ref 24). Biondi found that Kramers' theory gave a result for argon that was higher than

the experimental value by a factor of ten; however, it has been pointed out that the measured recombination coefficients may include several processes whose contribution is unknown. Hence the theory could well be in error by several orders of magnitude.

To restate the problem, we have a plasma consisting of free electrons and neutral and singly-ionized argon atoms in various states of excitation with respective concentrations $n_e$, n and $n^+$ where $n^+ = n_e$ and the velocity distributions are maxwellian. The radiative capture cross-section for an electron by an argon ion, reaction (26), is to be estimated.

Classical Theory. When an electron passes through an electric field in which the charge distribution is uniform, it loses energy at a rate dependent upon the square of the acceleration. If the accelerating force is exerted by a positive charge, the path of the electron will be hyperbolic and such that the greatest acceleration, and consequently the greatest energy loss, will be at the point of closest approach to the positive charge. Kramers used this classical picture to develop the following theory for radiative recombination. Let us assume a uniform charge distribution to surround each argon nucleus. This charge distribution may be obtained by taking the self-consistent field calculations of Hartree (Ref.43) for a neutral argon atom and reducing the outer orbital charge by unity with appropriate adjustment of the radius and charge density. The result is shown in Figs. 9, 10, 11. When the electron penetrates this charge distribution, it radiates energy at a

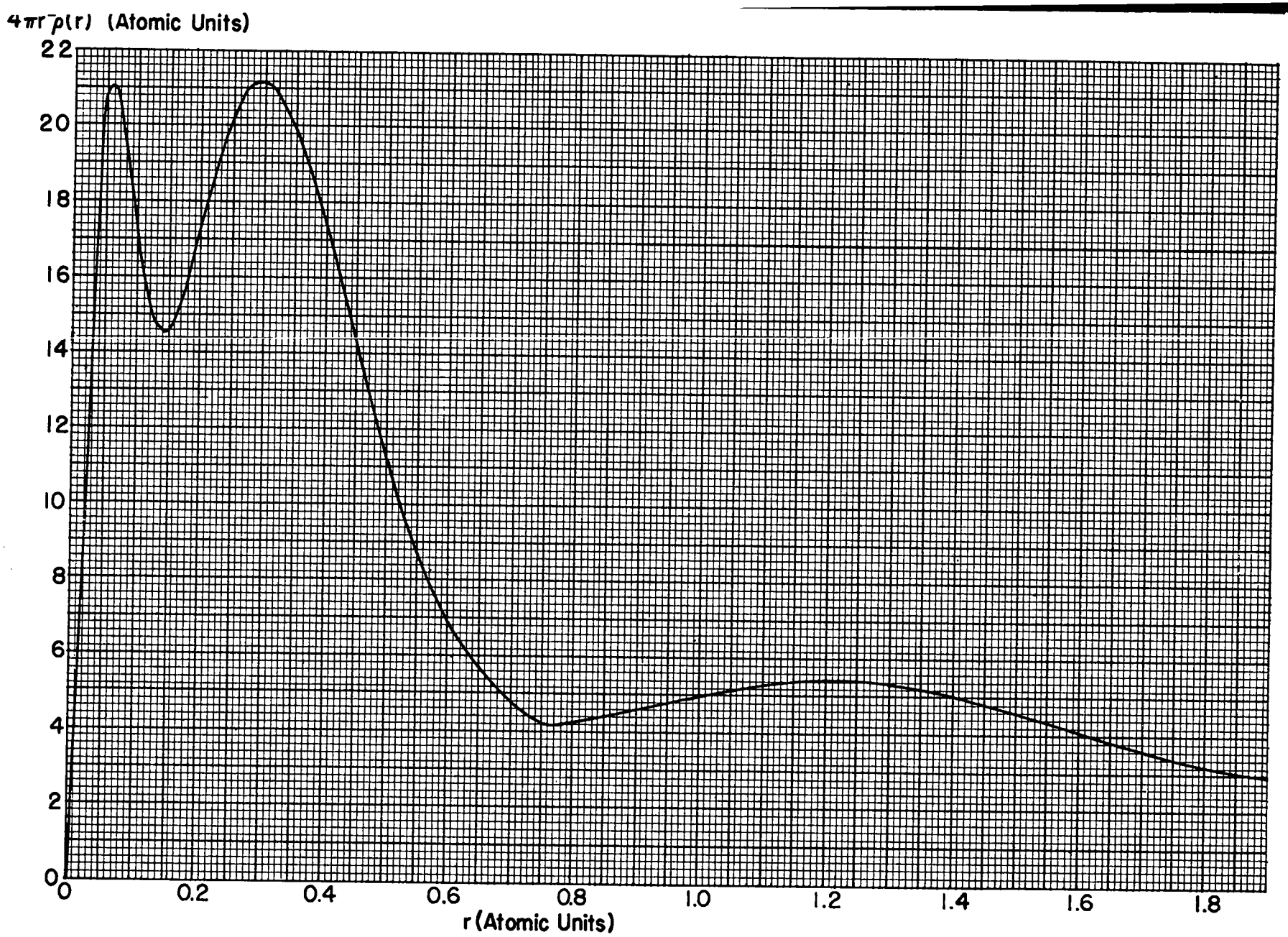


Fig. 9 Charge distribution for a singly-ionized argon atom.

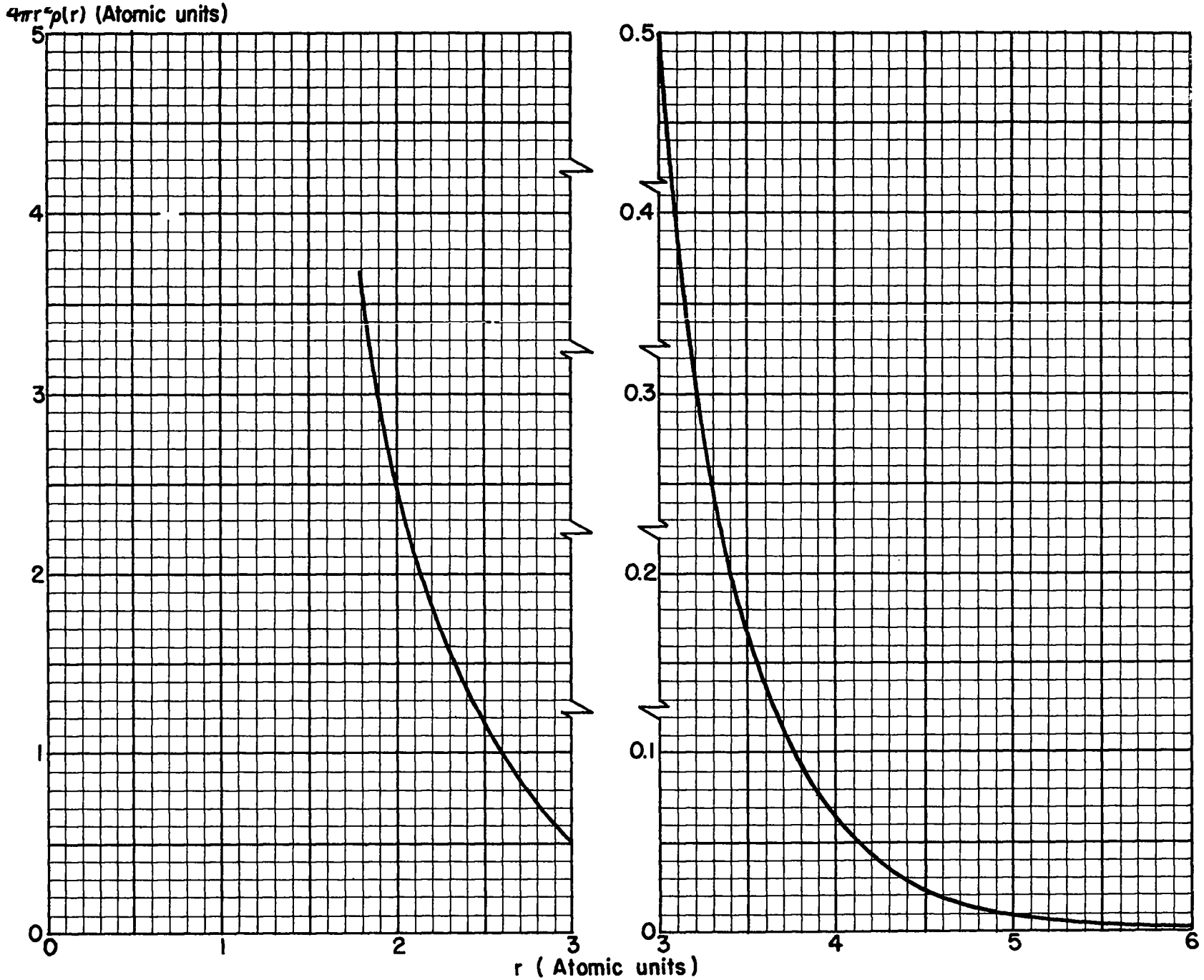


Fig. 10 Charge distribution for a singly-ionized argon atom.

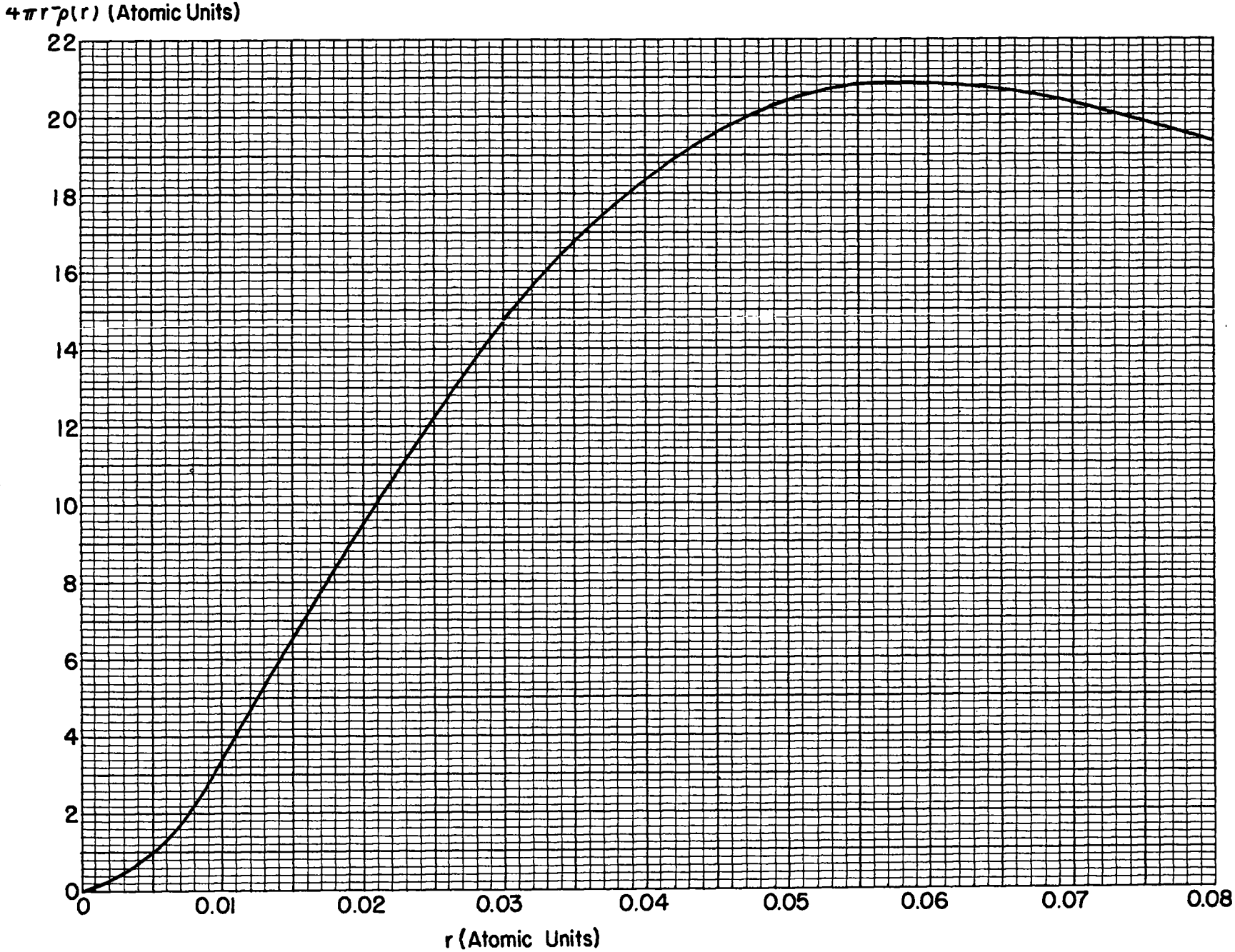


Fig. 11 Charge distribution for a singly-ionized argon atom.

rate given by

$$R = \frac{2}{3c^3} |\ddot{\vec{D}}|^2 \quad \left( = \frac{2e^2 \dot{v}^2}{3c^3} \right) \tag{28}$$

where $\vec{D}$ is the dipole moment. For a spherical charge distribution the dipole moment is zero, hence the only contribution to $\vec{D}$ is from the incoming electron, i.e.

$$\vec{D} = e\vec{r} \tag{29}$$

where $\vec{r}$ is the distance between the center of the atom and the impinging electron.

The equation of motion is

$$\mu \ddot{\vec{r}} = - e^2 Z_e \frac{\vec{r}}{r^3} \quad . \tag{30}$$

$Z_e$ is the effective charge as seen by the electron as it passes through the charge cloud. This has been estimated on the basis of the Thomas-Fermi model to be between 11e and 13e (Ref 24). The self-consistent-field gives the distribution shown in Fig. 12.

From (28) - (30),

$$R = \frac{2}{3c^3} \frac{e^6 Z_e^2}{\mu^2 r^4} \quad . \tag{31}$$

Since the incoming electron and the atomic ion are oppositely charged, the path of the electron through the charge cloud will be an hyperbola, the equation of which is

$$r = \frac{A}{1 - \epsilon \cos \varphi} \tag{32}$$

where A and $\epsilon$ are constants, $\epsilon$ being the eccentricity.

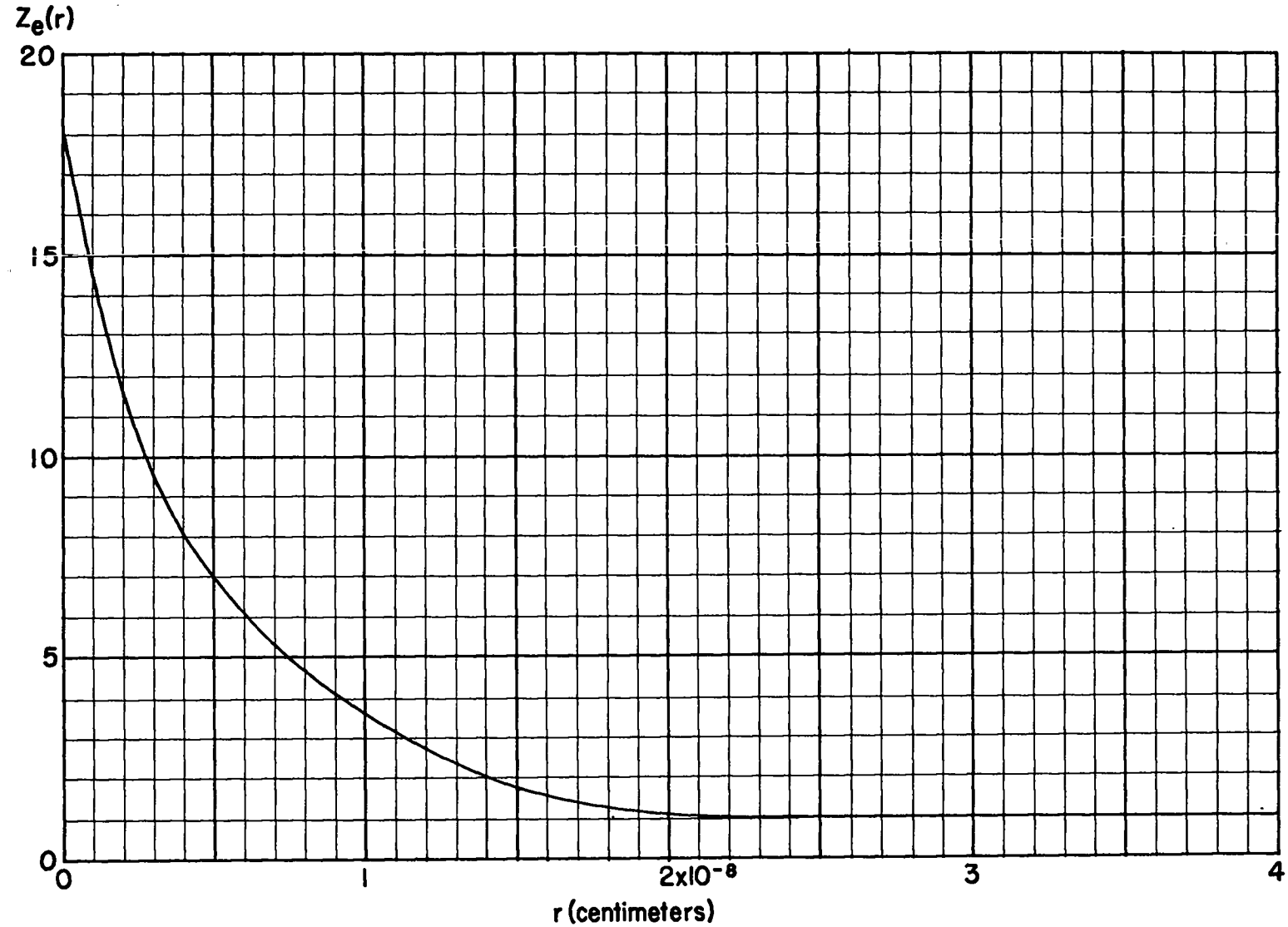


Fig. 12 Effective charge as a function of radius for singly-ionized argon.

If $\vec{n}_r$ and $\vec{n}_\varphi$ are unit vectors in the direction of increasing r and $\varphi$, then

$$\vec{r} = r\vec{n}_r$$

$$\dot{\vec{r}} = \dot{r}\vec{n}_r + r\dot{\varphi}\vec{n}_\varphi \tag{33}$$

$$\ddot{\vec{r}} = \ddot{r}\vec{n}_r + 2\dot{r}\dot{\varphi}\vec{n} + r\ddot{\varphi}\vec{n}_\varphi - r\dot{\varphi}^2\vec{n}_r \ .$$

Substituting in (30) the radial equation of motion is

$$\mu(\ddot{r}-r\dot{\varphi}^2) = -\frac{e^2Z_e}{r^2} \ . \tag{34}$$

For the angular momentum

$$L = \mu r^2\dot{\varphi} = \text{constant}. \tag{35}$$

Let

$$r = \frac{1}{u} \ , \quad \dot{r} = -\frac{1}{u^2}\frac{du}{dt} \ , \tag{36}$$

then, from (35),

$$\mu\dot{\varphi} = Lu^2, \quad \dot{r} = -\frac{L}{\mu}\frac{du}{d\varphi} \ , \quad \ddot{r} = -\left(\frac{L}{\mu}\right)^2 u^2\frac{d^2u}{d\varphi^2} \ . \tag{37}$$

Substitute in (34) obtaining,

$$\frac{d^2u}{d\varphi^2} + u = e^2Z_e\frac{\mu}{L^2} \ . \tag{38}$$

From (32),

$$u = \frac{1-\epsilon\cos\varphi}{A} \ , \quad \frac{d^2u}{d\varphi^2} = \frac{\epsilon}{A}\cos\varphi \ . \tag{39}$$

Hence, from (38) and (39),

$$A = \frac{L^2}{e^2Z_e\mu} \ , \tag{40}$$

and, for the equation of path,

$$u = \frac{e^2 Z_e \mu}{L^2} (1 - \epsilon \cos \varphi) . \qquad (41)$$

We now assume the total radiative energy loss to be given by

$$W = \int_{+\varphi_o}^{2\pi - \varphi_o} R dt$$

where $2\varphi_o$ is the angle between the asymptotes. Actually, if the electron loses energy, the incoming angle must differ from the outgoing angle; however, the assumption of equality is approximately justified classically as will be seen below. And, quantum mechanically, the assumption is even better. Substituting (31), (37), and (41) in W,

$$W = \frac{4}{3c^3} \frac{e^{10} Z_e^4 \mu}{L^5} \left[ \left( 1 + \frac{\epsilon^2}{2} \right) (\pi - \varphi_o) + 2\epsilon \sin \varphi_o - \frac{\epsilon^2}{4} \sin 2\varphi_o \right] . \qquad (42)$$

If v is the initial velocity and b the impact parameter, the angular momentum is

$$L = b\mu v .$$

The total energy of the system is

$$E = \frac{\mu}{2} (\dot{r}^2 + r^2 \dot{\varphi}^2) - \frac{e^2 Z_e}{r} .$$

From (41),

$$\frac{du}{d\varphi} = + \frac{\epsilon e^2 Z_e \mu}{L^2} \sin \varphi ,$$

and, using (37),

$$\dot{r} = -\frac{\epsilon e^2 Z_e \sin\varphi}{L}, \quad r\dot{\varphi} = \frac{e^2 Z_e}{L}(1-\epsilon\cos\varphi).$$

Substituting in E,

$$E = \frac{e^4 Z_e^2}{\mu b^2 v^2}\left(\frac{\epsilon^2-1}{2}\right).$$

Since

$$E = \frac{1}{2}\mu v^2,$$

and, from (32),

$$\epsilon = \frac{1}{\cos\varphi_o},$$

$$b = \frac{e^2 Z_e}{\mu v^2}\tan\varphi_o. \tag{43}$$

Eliminating $\epsilon$ and L in (42),

$$W = \frac{2}{3c^3}\frac{e^{10} Z_e^4}{\mu^4 b^5 v^5}\left[(\sec^2\varphi_o+2)(\pi-\varphi_o) + 3\tan\varphi_o\right]. \tag{44}$$

Substitution of (43) into (44) shows that for our range of temperatures ($T \lesssim 3$ ev) $\varphi_o$ is close to zero, hence, to this approximation,

$$W = \frac{2\pi e^{10} Z_e^4}{c^3 \mu^4 b^5 v^5}. \tag{45}$$

The assumption is now made that if the energy lost by radiation W is greater than the initial kinetic energy of the electron, then capture takes place. Quantum mechanically this means that if the incoming angle differs from the outgoing angle, the electron falls into some quantum

state $n, \ell$.

Let $W = \frac{1}{2}\mu v^2$ and solve for b:

$$b = \frac{(4\pi)^{1/5} Z_e^{4/5}}{\beta^{7/5}} r_o = \frac{217.68 Z_e^{4/5}}{v^{7/5}} \tag{46}$$

where

$$r_o = \frac{e^2}{mc^2}, \qquad \beta = \frac{v}{c}.$$

The cross-section is

$$\sigma(v) = \pi b^2 = \frac{1.4885 \cdot 10^5 Z_e^{8/5}}{v^{14/5}} \tag{47}$$

in agreement with Ref 24.

Up to now the variation of $Z_e$ has not been taken into account. Combining equation (46) and Fig. 12, $Z_e$ may be obtained as a function of v. This is plotted in Fig. 13. Similarly $\sigma(v)$ is shown in Fig. 14.

The recombination term $p_3$ is

$$p_3 = \iint f(v_1) f(v_2) \sigma(v) v d\vec{v}_1 d\vec{v}_2$$

where the notation is the same as in section 2.2. Changing to relative coordinates, from equation (23)

$$p_3 = \sqrt{\frac{2}{\pi}} \left(\frac{\mu}{kT}\right)^{3/2} n_e^2 \int_0^\infty e^{-\frac{\mu v^2}{2kT}} \sigma(v) v^3 dv. \tag{48}$$

It will be shown in Part III that the above result is incorrect;

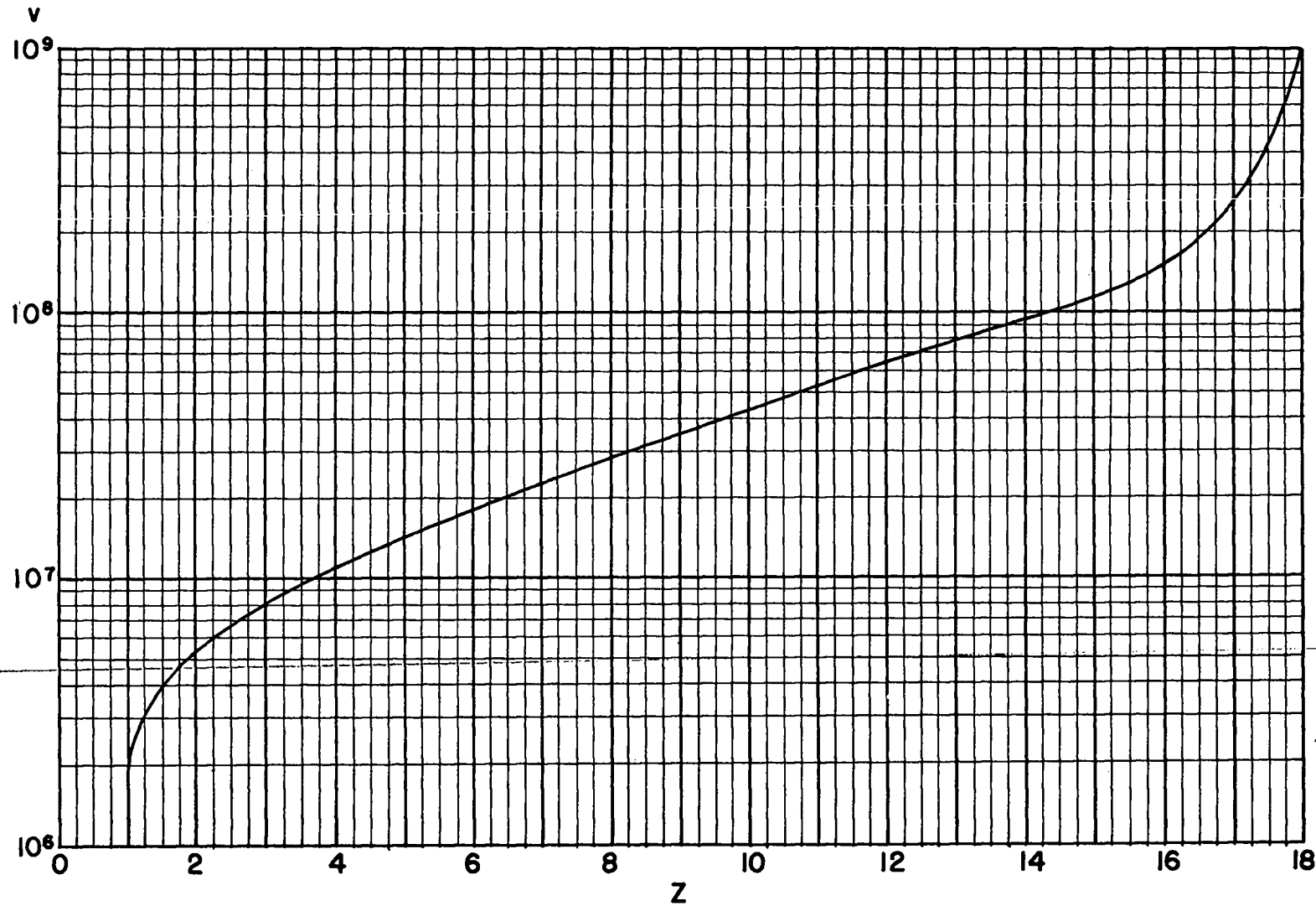


Fig. 13 Effective charge as a function of relative velocity for radiative capture of an electron by a singly charged argon ion.

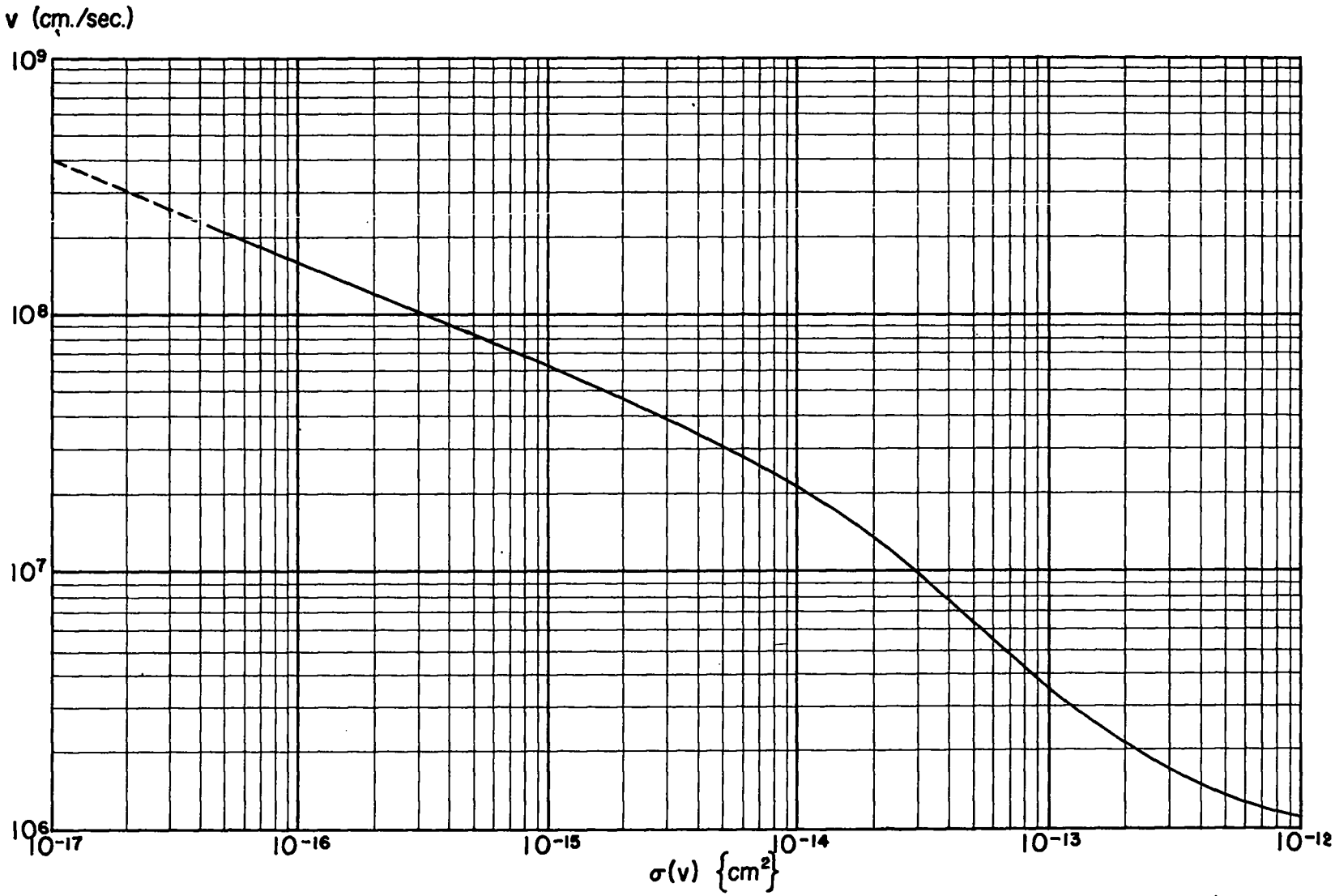


Fig. 14 Cross-section for radiative capture of an electron by a singly charged argon ion. *(Classical theory)*

hence, we present below the quantum theory which should give the correct answer but for which accurate computations have not been made.

Quantum Theory. Following the radiative capture of an electron by an argon ion, as indicated by (26), the resulting argon atom may be in its ground state which is a $3p^6$ level with an occupation number 1/Z(A) (cf Table IV, Part III), or in any one of its discrete excited states. The reaction is a transition of a free electron of energy $1/2\mu v^2$ to a bound state for which quantal theory gives an effective cross-section of

$$\sigma_e(n,\ell) = \frac{64\pi^4 e^2 \nu^3}{3hvc^3} \left|\vec{M}\right|^2.$$

The bound state is specified by the quantum numbers $n,\ell$, and v is the initial relative velocity, $\nu$ the frequency of the emitted radiation and $e\vec{M}$ the dipole moment where

$$\vec{D} = e\vec{M} = \int \psi_f e\vec{r}\, \psi_i^* d\tau.$$

The distance between the incoming electron and the center of the atom is $\vec{r}$, $\psi_f$ is the normalized wave function for the bound state, and $\psi_i$ is the wave function for the initial free state which is normalized to have the asymptotic form of a modified plane wave and the corresponding scattered wave. The amplitude of the plane wave is normalized for a flux of one electron/$cm^2$/sec in the direction of the wave so that

$$\psi_i = \frac{N}{v^{1/2}} \cdot \left[ e^{ikz} + \frac{e^{ikr}}{r} f(\theta) \right]$$

where $N/v^{1/2}$ is the normalization factor, $k = mv/\hbar$, $e^{ikz}$ is the plane wave travelling in the z-direction, $\frac{e^{ikr}}{r} f(\theta)$ represents the scattered

wave and $f(\theta)$ gives the angular dependence of the scattered wave. The total radiative capture cross-section will then be

$$\sigma_r = \sum_{n,\ell} \sigma_e(n,\ell)$$

where the summation is over all possible bound states of the argon atom. In Part I we saw that the number of bound states is limited by pressure ionization such that, for our range of temperature and pressure, there is no state for which $n \geq 8$.

We now assume (Bates et al, Ref 78) that for all excited states the wave functions $\psi_f$ may be taken as those of the hydrogen atom since, for the excited states, the effective core charge is about one. However, the ground state wave function and the initial wave function must be evaluated numerically. The wave function for the ground state of the argon atom has been computed by Hartree using the method of self-consistent fields and is tabulated in Ref 8.

The initial wave function may be represented by

$$\psi_i = \sum_{\ell} (2\ell+1)\, \psi_i^{\ell}(r) P_{\ell}(\cos\theta).$$

$P_{\ell}(\cos\theta)$ is the $\ell$th Legendre coefficient with $\ell$ the orbital quantum number. The ground state of argon, being a 3p level, can combine only with an s or a d state, hence only $\psi_i^{\,0}$ and $\psi_i^{\,2}$ need be determined. The wave functions $\psi_i^{\ell}$ may be found by solving the Schrödinger equation

$$\frac{d^2}{dr^2}(r\psi_i^{\ell}) + \frac{2\mu}{\hbar^2}\left[(E-V) - \frac{\hbar^2\ell(\ell+1)}{2\mu r^2}\right](r\psi_i^{\ell}) = 0$$

where E is the kinetic energy of the incident electron and V the potential energy of interaction between an electron and an argon atom. In Ref 78 computations were made for hydrogen and oxygen, and for the latter the unmodified potential energy of the ionic field as given by Hartree was used. However, for argon, as well as other inert gas atoms, polarization effects are important (compare the discussion of the diffusion cross-section in section 3.4), hence the Hartree field should be correspondingly modified. Using such a modified V the above equations could be integrated numerically.

Normalization of the argon wave functions has not been considered; however, this is discussed for oxygen in the above reference. Once the normalized wave functions $\psi_i$ and $\psi_f$, have been obtained the cross-section for capture into the ground state, $\sigma_e(3p)$, may be computed by performing another numerical integration.

In the self-consistent field approximation used by Hartree the complete wave function is the product of wave functions for each separate electron. In evaluating $\vec{M}$ the integral is over the coordinates of the incoming electron and this is independent of the other electronic coordinates. In obtaining $\sigma_e(3p)$ above the effect of the other electrons was omitted. Bates has shown that this omission may be approximately corrected for by multiplying by a numerical factor which for oxygen is .93.

The ground state cross-section for both hydrogen and oxygen amounts to about one-fourth of the total cross-section. The two cross-sections are not far different, that for oxygen being slightly smaller than that

for hydrogen. We will use these facts in estimating the total cross-section for argon.

In evaluating the cross-sections for capture into excited states the assumption is made that the wave functions are hydrogen-like. If the energy E of the incoming electron is small, then this assumption is good. This is because, for small E, the phase shift produced by the inner field of the ion is also small. Hence if $\psi_f$ for an excited state is large, then $\psi_i$ will not differ much from the corresponding function for atomic hydrogen. This point was considered in Part I.

The computations made by Bates were for energies of less than .28 ev. His results are plotted in Fig. 18 of Part III where it is seen, that for this energy range, $\sigma$ decreases with energy. This is to be expected because the wave-length of the incoming electron is large compared to the dimensions of the atomic system upon which it impinges. However, for our energy range, i.e., one to three electron volts, the electron wave-length becomes comparable to the size of the atomic system. In such a case one or more complete wave-lengths of zero angular momentum may be obtained within the range of the potential well without affecting waves of higher angular momentum. This means that at an energy of approximately one electron volt, the capture cross-section should show a sharp increase (Ref 79). In Part III, section 6, a method of detailed balancing is used to compute the capture cross-section for energies between .1 and 3.0 electron volts. The results are plotted along with those of Bates, where it may be seen that the

predicted increase of cross-section with energy is not obtained.

Unfortunately, experimental values are unavailable for either oxygen or argon. Also, computations have not been made for energies greater than .28 ev for oxygen and none for argon. However, the method of detailed balancing used to obtain the argon cross-sections has received a fair amount of verification in its application to the shock front. This will be discussed in greater detail in Part III.

It has been suggested by Morse and Stueckelberg (Ref 28) that the cross-section $\sigma_r(Z,n,\ell,v)$ for capture of electrons of velocity v by a heavy ion of charge Ze into a state of quantum numbers $n,\ell$ is related to that $\sigma_r(1,n,\ell,v)$ for capture into the corresponding state for a hydrogen atom by (see also Ref 52)

$$\sigma_r(Z,n,\ell,v) = Z^2 \sigma_r(1,n,\ell,v).$$

This formula does not apply to the ground state for which separate computations must be made as explained previously. In order to apply this formula to our case the computations for hydrogen need to be extended to higher energies. In addition, as will be pointed out in Part III, the argon calculations for the equilibrium region need to be extended; however, this is at present limited by the equation of state used here.

## 3.4 Three-body Recombination.

There are two ways in which electrons can be lost from the plasma:

(1) by the electron being captured in a two-body collision, the excess energy being removed by photons, or by excita-

tion of the atom, and

(2) by the electron being captured in a three-body collision, the excess energy being given to the third particle.

The first of these has been discussed in the previous sections and the cross-sections given. The second will be considered in the present section.

Theory of J. J. Thomson. We consider first the theory developed by Thomson for a plasma of oppositely charged ions A and B and neutral atoms C, and later modify the theory to apply to our plasma of ions, electrons, and atoms. We wish to find the condition that an ion B should, after making a collision with a neutral atom, proceed to describe a closed orbit around A. Assume that just after the collision the kinetic energy of the B ion is equal to the mean kinetic energy of an atom at the temperature of the gas. If $m_1$, $m_2$ are the masses of the A and B ions, then if B makes a collision at a distance r from A, the ions will describe closed orbits around each other if r is less than $r_o$ where $r_o$ is prescribed by

$$\frac{1}{2}\,\frac{m_1 m_2}{m_1+m_2}\,v^2 = \frac{e^2}{r_o} \tag{49}$$

and v is the relative velocity of the ions at a separation $r_o$. This follows since a bound orbit is one for which the total energy, E = T+V, is negative.

The inherent assumption here that the attractive energy $e^2/r$ for $r > r_o$ is lost upon collision with a neutral atom seems rather drastic;

however, in support of this is the moderate agreement between theory and experiment under conditions for which the theory seems valid. In addition, we have previously adopted the concept of a local temperature, hence

$$r_o = \frac{2e^2}{3kT} \quad . \tag{50}$$

Draw a sphere of radius $r_o$ about ion A (cf Fig. 16). Then the number of times per second that ion B comes within a distance $r_o$ of an A ion is $\pi r_o^2 v n_A$ where $n_A$, $n_B$ are the number of A,B ions per $cm^3$. Ion B will have acquired an additional amount of kinetic energy equal to $e^2/r_o$ by the time it approaches ion A within a distance $r_o$, i.e., if $\mathcal{E}_\infty$ represents the kinetic energy of B at a distance $r = \infty$ from A and $\mathcal{E}_o$ is the kinetic energy of B at $r = r_o$, then

$$\mathcal{E}_\infty = \mathcal{E}_o - \frac{e^2}{r_o} \quad .$$

But $\mathcal{E}_\infty = \frac{3}{2}$ kT and from(50), $e^2/r_o = 3/2$ kT, hence $\mathcal{E}_o = 2\left(\frac{3}{2}\text{ kT}\right)$.

Thus, for recombination to take place, we require that B lose an amount of energy of order kT when within a distance $r_o$ of A. We have assumed that this amount of energy is lost upon collision with a neutral atom. If B and C have equal masses, then, on the average, this assumption is exactly obeyed, which can be shown as follows: Let $m_1$, $m_2$ be two particles where, initially, $m_2$ is at rest and $m_1$ has velocity $v_1$. After the particles collide, $m_1$ has velocity $v_1'$ and is moving at an angle $\theta$ with its original direction. $m_2$ has final velocity $v_2'$ and

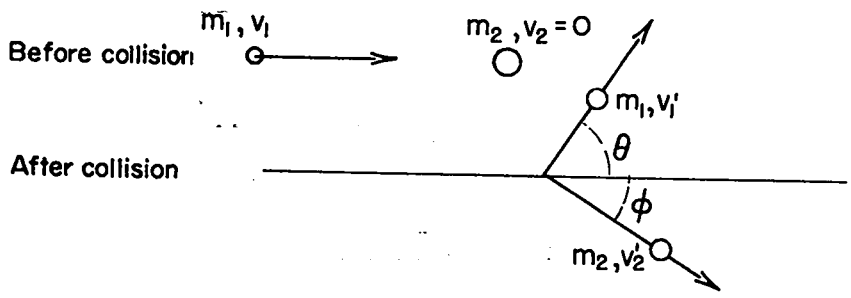


Fig. 15

angle $\varphi$. Then, from conservation of energy,

$$\frac{1}{2} m_1 v_1^2 = \frac{1}{2} m_1 v_1'^2 + \frac{1}{2} m_2 v_2'^2, \tag{51}$$

and, from conservation of momentum,

$$m_1 v_1' \sin\theta = m_2 v_2' \sin\varphi,$$

$$m_1 v_1 = m_1 v_1' \cos\theta + m_2 v_2' \cos\varphi.$$

Eliminating $\varphi$,

$$m_1^2 \left[ v_1'^2 \sin^2\theta + v_1^2 + v_1'^2 \cos^2\theta - 2 v_1 v_1' \cos\theta \right] = m_2^2 v_2'^2.$$

Combine this with (51) obtaining

$$m_1 (v_1^2 + v_1'^2 - 2 v_1 v_1' \cos\theta) - m_2 (v_1^2 - v_1'^2) = 0, \tag{52}$$

from which,

$$\frac{v_1'}{v_1} = \frac{m_1}{m_1+m_2} \cos\theta + \frac{m_2}{m_1+m_2} \left[ 1 - \frac{m_1^2}{m_2^2} (1-\cos^2\theta) \right]^{1/2}.$$

If $m_1 << m_2$, then, to the order of terms in $(m_1/m_2)^2$,

$$\frac{v_1'}{v_1} = \frac{m_1 \cos\theta + m_2}{m_1 + m_2} . \tag{53}$$

Since

$$\frac{\Delta E}{E} = \frac{2\Delta v}{v} ,$$

$$\frac{\Delta E}{E} = \frac{2(v_1 - v_1')}{v_1} = 2\left(1 - \frac{v_1'}{v_1}\right) = \frac{2m_1}{m_1+m_2}(1-\cos\theta), \quad (m_1 << m_2). \tag{54}$$

The average energy loss is, since $\overline{\cos\theta} = 0$,

$$\overline{\frac{\Delta E}{E}} = \frac{2m_1}{m_1+m_2} . \tag{55}$$

This follows also from (52), i.e.,

$$\overline{\frac{\Delta E}{E}} = \frac{\frac{1}{2} m_1 v_1^2 - \frac{1}{2} m_1 v_1'^2}{\frac{1}{2} m_1 v_1^2} = 1 - \left(\frac{v_1'}{v_1}\right)^2 = \frac{2m_1}{m_1+m_2} .$$

Hence we need to calculate the chance that ion B suffers an elastic collision with a neutral atom C within a distance $r_o$ of A and such that B loses an appreciable amount of energy and recombines in a closed orbit with A. Let this chance be $s_B$ and let $s_A$ be the chance for A colliding with C and recombining with B. Th chance that ion B should be at a distance between $\rho$ and $\rho + d\rho$ from a line drawn through A parallel

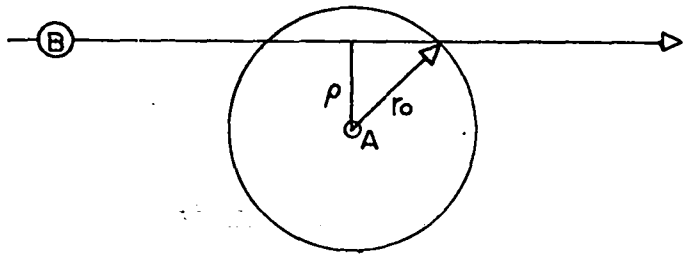


Fig. 16

to the relative velocity of the two ions is $2\rho d\rho/r_o^2$ and the chance that B will go through the sphere of radius $r_o$ drawn about A at this distance without a collision is

$$e^{-\frac{2\sqrt{r_o^2-\rho^2}}{\ell_B}}$$

where $\ell_B$ is the mean free path for ions B in a collection of atoms C. If B and C are of approximately equal masses equation (55) and the preceding argument show that, since, on the average, the energy lost in a collision is about kT, the energy-loss mean free path $\ell_B$ is, to a sufficient degree of approximation, equal to the geometric mean free path. Thus the chance that ion B should pass without making a collision is

$$Q = \int_o^{r_o} e^{-\frac{2\sqrt{r_o^2-\rho^2}}{\ell_B}} \cdot \frac{2\rho d\rho}{r_o^2} = \int_o^1 e^{-\frac{2r_o}{\ell_B}(1-z^2)^{1/2}} \cdot 2zdz$$

where $z = \rho/r_o$. Let $y = \frac{2r_o}{\ell_B}(1-z^2)^{1/2}$, $2zdz = -\frac{\ell_B^2 ydy}{2r_o^2}$, then

$$Q = -\frac{\ell_B^2}{2r_o^2}\int_{g_B}^{o} e^{-y} y dy.$$

Let

$$J = \int_o^y e^{-ay} dy = \frac{1}{a}(1-e^{-ay}),$$

$$\frac{\partial J}{\partial a} = -\int_o^y e^{-ay} y dy = -\frac{1}{a^2}(1-e^{-ay}) + \frac{y}{a} e^{-ay};$$

hence

$$Q = -\frac{2}{g_B^2}\left[g_B e^{-g_B} + e^{-g_B} - 1\right].$$

Thus the chance that ion B will make a collision is

$$s_B = 1 + 2\left(\frac{e^{-g_B}}{g_B^2} + \frac{e^{-g_B}}{g_B} - \frac{1}{g_B^2}\right) \tag{56}$$

with a similar expression for $s_A$ and where

$$g_B = \frac{2r_o}{\ell_B}, \quad g_A = \frac{2r_o}{\ell_A}. \tag{57}$$

It should be kept in mind that $\ell_A$, $\ell_B$ are really the energy mean free paths and not the geometric mean free paths. The relation between the two is, from (55),

$$\ell_{energy} = \frac{(m_1+m_2)}{2m_1} \ell_{geom.} \tag{58}$$

This is because $1\Big/\frac{\overline{\Delta E}}{E}$ collisions are required for the particle $m_1$ to lose an amount of energy about equal to E.

If A,B are of approximately equal masses then, as they approach each other they each acquire additional kinetic energy due to their attraction which is then lost upon collision. Hence the chance that when the two ions come within a distance $r_o$ one or the other of them should make a collision within this distance is

$$s_A + s_B - s_A\, s_B$$

where $s_A\, s_B$ is the chance that they both make collisions within this distance, and this has been included in both $s_A$ and $s_B$. In case the mass of the incoming ion B is much greater than the mass of A most of the attractive energy will go into increasing the kinetic energy of A and the velocity of B will remain about the same; hence, upon collision only A will lose energy. Therefore, in this case, the chance of making a recombining collision is simply $s_A$ or s where

$$s = 1+2\left(\frac{e^{-g}}{g^2} + \frac{e^{-g}}{g} - \frac{1}{g^2}\right) \tag{59}$$

and, from (57), (58),

$$g = \frac{2r_o}{\ell_{geom}} \cdot \frac{2m_e}{M} = \frac{4r_o m_e n \sigma_d}{M} \tag{60}$$

where

$m_e$ = mass of electron,

$M = m + m_e$,

$m$ = mass of argon atom,

$\sigma_d$ = diffusion cross-section (see below),

$n$ = number of gas atoms,

and, the geometric mean free path is

$$\ell_{geom.} = \frac{1}{n\sigma_d} \quad . \tag{61}$$

Finally, then, the rate at which electrons recombine with argon ions by three-body collisions is given by the number of times per second an electron comes within a distance $r_o$ of an argon ion, $\pi r_o^2 v n^+$, times the chance of making a recombining collision, s, times the number of electrons, $n_e$, or

$$p_4 = \pi r_o^2 s v n_e n^+ = \pi r_o^2 s v n_e^2 \tag{62}$$

where

$n^+$ = number of argon ions per $cm^3$,

$n_e$ = number of electrons per $cm^3$;

and

$$n_e = n^+.$$

In case $g << 1$,

$$s = \frac{2g}{3} = \frac{8}{3} \frac{r_o m_e n \sigma_d}{M}$$

and

$$p_4 = \frac{8\pi}{3} r_o^3 \frac{m_e n \sigma_d}{M} v n_e^2 , \tag{63}$$

from which

$$\sigma_4 = \frac{8\pi}{3} r_o^3 \frac{m_e n \sigma_d}{M} \quad , \qquad (g \ll 1). \tag{64}$$

At a temperature of 30,000° and a compression ratio of 5, $\sigma_4 = 10^{-22}$ cm$^2$ which is much less than the classical cross-section for radiative capture (see, however, Part III, section 6).

To complete the discussion of the Thomson theory its limitations should be considered and, in addition, use of the diffusion cross-section, $\sigma_d$, should be justified.

No allowance has been made for the possibility of more than one collision while the electron is still within a distance $r_o$ of the ion and before it has recombined. If such a collision could restore the original hyperbolic motion and if the chance of such an occurrence were high, then the above theory would not give the correct result. This is born out experimentally since theory and experiment agree at low pressures where $\sigma_4$ shows an increase with pressure. However, at high pressures the theory breaks down and since pressures are high in a shock front (in our case between 100 and 1000 atmospheres), it is necessary to obtain a pressure limit for the theory. This is done by defining a saturation condition such that $r_o = \ell$. The corresponding saturation pressure then lies at the upper limit of the conditions considered in this report.

Langevin's Theory. Thomson's theory verifies the increase of the three-body recombination coefficient $\alpha_4$ with pressure in the low-

pressure region; however, at high pressures $\alpha_4$ drops off with pressure. Hence we consider a theory due to Langevin (Ref 52, 58) which predicts $\alpha_4$ nicely in this region. In this theory the electrons are attracted toward the ions by the respective coulomb fields. They attain a relative drift velocity which is inhibited by collisions with neutral gas atoms. If $k_A$ and $k_B$ are the respective mobilities of ions and electrons, then the relative drift velocity at a distance r will be

$$\left(k_A + k_B\right) \frac{e}{r^2} .$$

The number of electrons drifting radially inwards across a spherical surface of radius r about an ion is then

$$4\pi n_B e(k_A+k_B) .$$

The electrons will drift up to and neutralize the ions unless deflected by collisions with other charged particles. Assuming small ion density and isotropic distribution, this possibility can be neglected, hence the rate of recombination is given by

$$4\pi e(k_A+k_B)n_A n_B$$

and

$$\alpha_4 = 4\pi e(k_A+k_B).$$

Evaluation of the mobilities for the plasma state behind the shock front has not been made, however, for normal conditions it is found that k drops off with pressure, verifying the decrease of $\alpha$ with pressure (at high pressures).

The Diffusion Cross-Section. As indicated above, we wish to justify use of the diffusion cross-section in the Thomson theory. If velocity distributions are used, the recombination rate would be expressed as

$$p_4 = \iint \sigma_4(v) f_e(\vec{v}_1) f^+(\vec{v}_2) d\vec{v}_1 d\vec{v}_2$$

where $f_e(\vec{v}_1)$ is the maxwellian velocity distribution for electrons and $f^+(\vec{v}_2)$ that for the argon ions. $\sigma_4$ is given by (64) and contains the diffusion cross-section $\sigma_d(v)$. It would be convenient if an analytic expression for $\sigma_d(v)$ were available, hence we examine this possibility.

The elastic scattering cross-section may be written as

$$\sigma = \frac{4\pi}{k^2} \sum_{\ell} (2\ell+1) \sin^2 \eta_\ell$$

where

$$k = \frac{\sqrt{2m_e E}}{\hbar}$$

and $\eta_\ell$ is the phase shift produced in the de Broglie waves of angular momentum $\left[\ell(\ell+1)\right]^{1/2}\hbar$. We wish an analytic expression for $\sigma$ which is explicit in v. However, $\eta_\ell$ will depend on the scattering potential V(r) which, for argon, is quite complicated. This was discussed in section 3.3. Holtsmark (Ref 16), using the Hartree field modified by a polarization effect, was able to obtain a theoretical value for $\sigma$ which agreed well with the observed $\sigma$ in the low energy range, i.e., his results led to the Ramsauer-Townsend effect. He was able to show that

$$\sigma_{expt} \doteq \sigma_{theor} = \sum_{\ell=0}^{\ell=2} (2\ell+1) \sin^2 \eta_\ell \quad \text{(for .3 ev} \lesssim \mathcal{E} \lesssim \text{13 ev)};$$

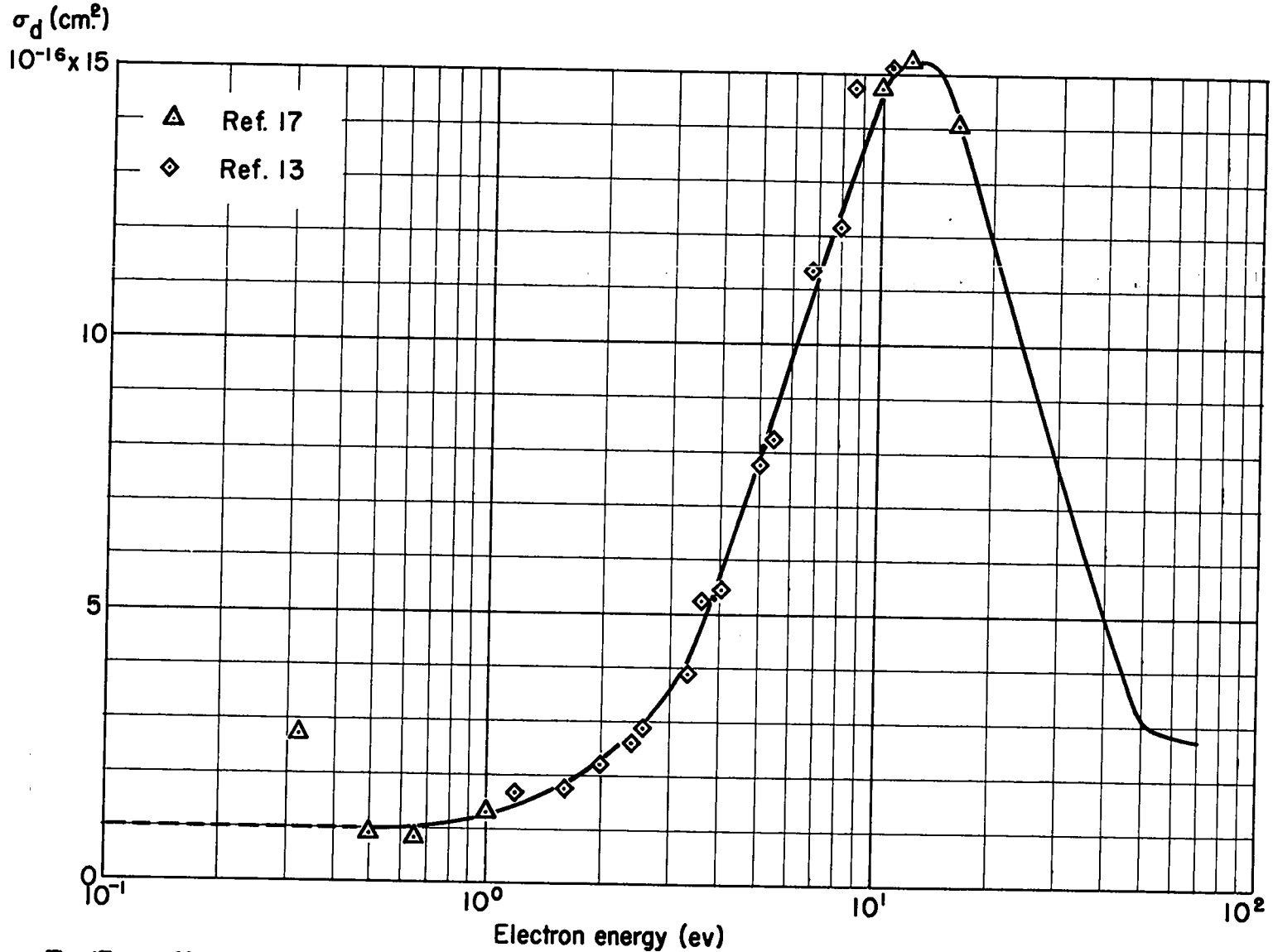


Fig. 17 Diffusion cross-section for electrons in argon.

but in order to obtain values for $\eta_\ell$ ($\ell = 0,1,2,\cdots$) a numerical integration was necessary.

Thus it is possible to obtain an empirical relation for $\eta_\ell(v)$ but not an analytic expression. Hence we may fit an empirical curve directly to the observed values for $\sigma_d$ (cf Fig. 17). There is some disagreement between observers, particularly in the region below 1 ev, so an approximate curve is used.

The value for the cross-section at zero energy is given as about $7 \times 10^{-16}$ cm$^2$ (Ref 18, 19) while Wahlin (Ref 20) measured $\sigma_d = .73 \times 10^{-16}$ cm$^2$ at $\mathcal{E} = .03$ ev. Again because of the nature of the maxwell distribution, it is somewhat immaterial what $\sigma_d(0)$ is; so we use $\sigma_d(0) = 1 \times 10^{-16}$ cm$^2$.

The interest here is only in low-energy cross-sections hence we do not need to discuss inelastic, superelastic, or radiative cross-sections, i.e. only elastic collisions are to be considered. A superelastic collision occurs between an electron and an excited atom where the electron gains energy from the internal motion of the atom. Collisions involving radiation are rare compared with other types of collisions and have been previously considered.

If $\sigma_o$ is the total elastic cross-section and $I_o(\theta)$ the differential cross-section for elastic scattering then

$$\sigma_o = \int_o^{\pi} \int_o^{2\pi} I_o(\theta) \sin\theta \, d\theta \, d\varphi.$$

If $\sigma$ is the total collision cross-section where

$$\sigma = \sum_{n=0}^{n} \sigma_n$$

is summed over all types of collision, then in the energy range of interest $\sigma_o = \sigma$.

The total collision cross-section may be measured by the following method (cf Fig. 18). Electrons are ejected photoelectrically from a source F into a circular collimating channel with a magnetic field directed perpendicular to the paper. Electrons which suffer no collision enter a collector at C, while those which are scattered fail to pass through the slits and those which collide inelastically move in new circular paths of smaller radii.

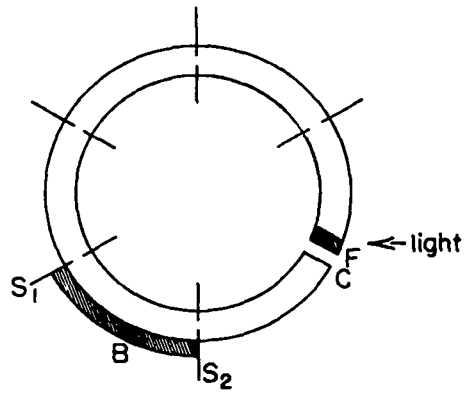


Fig. 18

If $i_C$ is the current to C alone and $i_B$ the current to B alone then $i_{C1} = i_{BC1} e^{-\alpha p_1 x}$ where $i_{BC1} = i_{B1} + i_{C1}$, $\alpha$ is the absorption coefficient, and $p_1$ is the pressure. Similarly at a pressure $p_2$,

$$i_{C2} = i_{BC2}\, e^{-\alpha p_2 x}$$

and

$$\alpha(p_1 - p_2)x = \ell n \frac{i_{C2}}{i_{BC2}} \frac{i_{BC1}}{i_{C1}} .$$

Hence $\alpha$ may be determined and consequently $\sigma$.

In case the electrons are very slow (say ~1 ev) it is possible to use the Townsend method (Ref 21) (cf Fig. 19) in which a swarm of electrons is introduced into a diffusion chamber through a slit A across which an electric field F is directed as shown. The current may then be measured at $C_1$, B, and $C_2$. Guard rings 2, 3, 4 may be added to insure uniformity of the field.

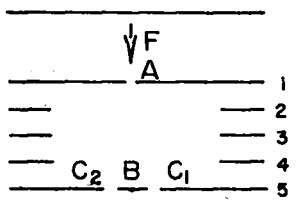


Fig. 19

Now, as the electrons diffuse through the chamber they gain energy from the field but, in the steady state, this gain in energy is equal to the loss in energy by collision with the gas atoms. (We are assuming the electron energy so low that only elastic collision with gas atoms need be considered). Let the drift velocity be u in the direction x of the field and assume a definite mean energy $\epsilon$ for the electrons.

Let the mean free path $\ell$ and the fractional energy loss $\lambda$ be constant. Then, if c is the mean velocity of the random motion of the electron, the actual path length is cx/u and the number of collisions made in travelling a distance x is $cx/u\ell$. Then, from conservation of energy,

$$\lambda\epsilon \frac{cx}{u\ell} = Fex,$$

or, if $\epsilon = 1/2\ m_e c^2$,

$$\frac{\lambda c^3}{u} = 2\frac{Fe\ell}{m_e}.$$

If $\delta t$ is the time between collisions then $u\delta t$ is the mean distance travelled in the direction of the field in this time. Assuming isotropic scattering then

$$u\delta t = \frac{1}{2}\frac{Fe}{m}(\delta t)^2,$$

or, if $\delta t = \ell/c$,

$$2uc = Fe\ell/m.$$

Now $\ell \sim 1/p$ where p is the pressure, hence u should be a linear function of $\frac{F}{p}$.

u may be determined by directing a magnetic field H perpendicular to the electric field F. Then the stream of electrons will be deviated through an angle $\theta$ such that

$$\tan \theta \sim \frac{Hu}{F}.$$

If u is plotted against F/p, the mean free path $\ell$ may be computed from the slope of the curve.

In this discussion the effect of diffusion is neglected; however, the method is discussed in more detail in Ref 52, Chapter I.

If we assume that in the electron swarm the mean energy is so small that inelastic collisions with gas atoms do not occur, then the only energy loss will occur in elastic collisions and will be due to the finite ratio of the masses, $m_e/M$. Also, we assume the electron concentration in the stream to be so small that interaction between electrons can be ignored.

Considering only elastic impacts between electrons and atoms, then since $m_e << m$, the fractional energy loss per impact by an electron is (cf eq (54))

$$2(1-\cos \theta) \frac{m_e}{m}$$

where terms of order $(m_e/m)^2$ have been dropped.

If $p(\theta)d\Omega$ is the probability that the electron will be scattered into a solid angle $d\Omega$ then the mean fractional energy loss per impact will be

$$2 \frac{m_e}{m} \int (1-\cos \theta)p(\theta)d\Omega.$$

But the differential cross-section for elastic scattering into the solid angle $d\Omega$ is given by

$$I_o(\theta)d\Omega = \sigma_o p(\theta)d\Omega$$

where $\sigma_o$ is the total cross-section for elastic scattering. The mean fractional energy loss per impact then becomes

$$2\frac{m_e}{m}\frac{\sigma_d}{\sigma_o}$$

where

$$\sigma_d = \int_o^{\pi}\int_o^{2\pi} I_o(\theta)(1-\cos\theta)\sin\theta d\theta d\varphi .$$

$\sigma_d$ is the diffusion or momentum transfer cross-section.

The fractional amount of energy lost by an electron in moving a distance x is then

$$2\frac{m_e}{m}\frac{\sigma_d}{\sigma_o}\cdot nx\sigma_o = 2\frac{m_e}{m}\cdot n\sigma_d\cdot x.$$

Hence for elastic collisions the mean free path should be $\ell = 1/n\sigma_d$ and the mean fractional energy loss $\lambda = 2m_e/m$.

4. Summary.

In the above sections the individual atomic interactions that take place in an argon shock front have been detailed. It has been indicated that the production of electrons is a two-stage process. First, starting from a state of translational equilibrium where only argon atoms exist, electrons are produced by ionizing collisions between the argon atoms. Once a sufficient number of electrons have been produced, then ionizing collisions between argon atoms and electrons predominate. If maxwell distributions are replaced by averages, then the two production

coefficients for the above reactions may be written as $\overline{\beta_1} = \overline{\sigma_1 v}$ and $\overline{\beta_3} = \overline{\sigma_3 v}$ where $\beta_1$ and $\beta_3$ are functions of temperature only. Theoretical values for these cross-sections have not been derived, hence we have used the experiment cross-sections. Other production reactions have been considered and assumed to be unimportant.

As soon as electrons have been produced in quantity, recombination processes must be considered. It was shown that, for the pressure and temperature conditions existing in a shock front, only two recombination processes are of importance. The first is radiative recombination which depends on temperature only, and the second is three-body recombination which depends on temperature and pressure.

Experimental values for the cross-sections corresponding to the two recombination reactions are unavailable, hence theoretical derivations have been made. Radiative capture of electrons by argon ions has been considered both classically and quantum mechanically. It is indicated that the classical theory gives too large an answer by several orders of magnitude. Thomson's theory for the three-body process has been presented and its limitations discussed.

If we combine the above processes the source term which expresses the rate of production of electrons may be written as

$$S = \frac{dn_e}{dt} = \beta_1 n^2 + \beta_3 n n_e - \alpha n_e^2.$$

Quantitative evaluation of $\beta_1(T)$, $\beta_3(T)$ and $\alpha(n,T)$ is made in Part III.

## PART III: COMPUTATIONS AND RESULTS

### 1. Introduction.

In Parts I and II the theoretical basis for the computations involved has been presented in some detail. In Part III the theory will be applied to a few special cases. It should be remembered that the theory is somewhat limited, viz, there is an upper limit to the temperature because doubly ionized argon has been ignored and there is a lower limit to the pressure and temperature due to effects discussed in the sections on recombination. Also, as pointed out in Part I, if the degree of ionization is too high, the method used to calculate the partition functions breaks down. The theory as presented is probably good for shock velocities in argon between 3 and 9 times $10^5$ cm per sec.

If higher shock velocities are of interest then doubly ionized argon must not be neglected which means a different equation of state than the one used here (cf Ref 69). However, one would still be limited because there is not sufficient cross-section data available for reactions involving multiple-ionized atoms.

The extension to lower shock velocities is not difficult for argon because, below about $3.10^5$ cm per sec the ionization is negligible, i.e., only translational degrees of freedom are important. This case has been thoroughly treated as we have previously indicated.

### 2. Equation of State of Argon.

Using the method of Part I, sections 2-4, we write down the complete equation of state for argon for a rather wide range of density

and temperature. The partition functions are given by eqs I: (22) to I: (24). The energy levels and multiplicites for the low states of the neutral argon atom A and the argon ion $A^+$ are listed in Table II. This table enables us to calculate $Z_{low}(T)$ and $Z_{ion}(T)$. There are a number of higher levels for the argon ion which are not listed in the Table. These levels are fairly closely spaced with an average number of levels per degree, $\bar{n}$, and an average multiplicity $\bar{g}$. Then, for $Z_{ion}$,

$$Z_{ion} = \sum_{n(E_1)}^{n(E_2)} g_n e^{-E_n/T} + \int_{E_2}^{E_3} \bar{n}\bar{g} e^{-E/T}\, dE$$

where the energies are expressed in degrees. For argon we have used $E_1 = 0$, $E_2 = 268920$, $E_3 = 320800$ and $\bar{n}\bar{g} = 4.05 \cdot 10^{-3}$. The integral on the right represents a correction to the higher states which is small but is easy to make. Because the ion is more tightly bound than the atom, pressure ionization will not be important and no correction has been made for this.

$Z_{high}$, eq I: (24), is not only a function of temperature but is also a function of density. Values of the energy $E_{n\ell}$ and the effective multiplicity are listed in Table III.

Using Tables II and III the partition functions for the atoms and ions have been calculated and are listed in Table IV as functions of the temperature and density ratio. The equilibrium constant K, eq I: (17), is given in Table IV* for the initial condition of 59.38 cm Hg,

*Actually, K divided by the partition function for electrons is listed, or, for our case, K/2.

which is local atmospheric pressure at Los Alamos, (see Table I).

From equations (16) and (17) in Part I it is clear that the equilibrium constant for an initial pressure of h cm Hg can be obtained from the value of K in Table IV by multiplying by 59.38/h. (Although, the internal partition functions may change slightly due to the cut-off criterion.) The concentrations, $[A]$ and $[A^+]$, of course depend upon the initial conditions through the equilibrium constant.

The energy content of the neutral argon atoms is given by

$$\beta(A) = 2.5 + \frac{W}{Z}$$

and that for the argon ions by

$$\beta(A^+) = 2.5 + \frac{W_{ion}}{Z_{ion}} \quad .$$

3. Shock Conditions in the Equilibrium Region.

It has been shown in Part I, section 6, that heat conduction and viscosity do not enter into the shock conditions in the equilibrium region. It has already been indicated that the equations to be used are those of Part I, section 5, and specifically, equations (42) and (43) of that paragraph. These two equations are solved simultaneously for $\eta$ and T with the shock velocity U as a parameter. The quantities g and $\beta$ occur in these equations and are rather complicated functions of $\eta$ and T. They are obtained from the equation of state as explained in Part I.

It is possible to simplify the computation of $\beta$ considerably by the

following approximation. The ionization ratio x is given by

$$x = \frac{n_e}{n+n_e} = \frac{n_e/n}{1+n_e/n} \tag{1}$$

and the average number of particles per original atom by

$$g = 1+x. \tag{2}$$

x may be computed directly from the equilibrium constant (listed in Table IV) by the relation

$$K = \frac{x^2}{1-x} .$$

Since the temperatures we are considering are low enough so that the number of singly ionized argon atoms in higher excited states is small, it is a good assumption that

$$\beta(A^+) = 2.5.$$

Then, from eq I: (10),

$$\epsilon = \beta(A)(1-x) + \beta(A^+)x + \beta(\mathcal{E}\ell) \cdot x + \frac{I}{kT} \cdot x$$

or

$$\epsilon = \beta(A)(1-x) + 5.0x + \frac{183000}{T} \cdot x \tag{3}$$

where $\beta(\mathcal{E}\ell) = 2.5$ and the first ionization potential for argon is I = 183,000 degrees. If we knew $\beta(A)$, we could obtain $\epsilon$ and hence $\beta$ from

$$\beta = \frac{\epsilon}{g} .$$

$\beta(A)$ has been calculated and a good fit is

$$\beta(A) = \frac{1}{2}\left(\frac{5+x}{1-x}\right). \tag{4}$$

If (4) is substituted in (3),

$$\epsilon = 2.5+5.5x + \frac{183000}{T} x,$$

or

$$\beta = \frac{2.5+5.5x + \frac{183000}{T} x}{1+x} . \qquad (5)$$

If we substitute the relations for $\beta(A)$ and $\beta(A^+)$ given in section 2 into $\epsilon$,

$$\epsilon = \left(2.5 + \frac{W}{Z}\right) (1-x) + \left(2.5 + \frac{W_{ion}}{Z_{ion}}\right) x + 2.5x + \frac{I}{kT} x,$$

or

$$\epsilon = 2.5+2.5x + \frac{I}{kT} x + \frac{W}{Z} - x\left(\frac{W}{Z} - \frac{W_{ion}}{Z_{ion}}\right).$$

Thus we see that our approximation is that

$$3x = \frac{W}{Z} + x\left(\frac{W_{ion}}{Z_{ion}} - \frac{W}{Z}\right)$$

or

$$x = \frac{W/Z}{3 + \frac{W}{Z} - \frac{W_{ion}}{Z_{ion}}} .$$

If

$$\epsilon' = 2.5+2.5x + \frac{I}{kT} x$$

then

$$\epsilon = \epsilon' + 3x.$$

The term $3x$ is less than 10% of $\epsilon'$ in even the most extreme case. Hence, as shown in the following table, the maximum error made in com-

puting $\epsilon$ by this method is not more than .5% and will, in most cases, be far less.

| T | $\frac{W}{Z}$ | $\frac{W_{ion}}{Z_{ion}}$ | x (correct) | x (approximate) |
|---|---|---|---|---|
| 16000 | .12 | .04 | .05 | .04 |
| 19000 | .45 | .04 | .12 | .13 |
| 22000 | .97 | .05 | .22 | .24 |
| 24000 | 1.46 | .08 | .28 | .33 |

Results of the computations for the two initial conditions, $p_1$ = 59.38 cm Hg and $p_1$ = 1 cm Hg are plotted in Figs. 1 to 6 and listed in Table V.

Some measurements have been made on strong shocks in argon at Los Alamos (Ref 74). The shocks were produced by high explosives for which the detonation velocities are known and the material velocity u behind the shock front was measured. The results are plotted along with the theoretical curve in Fig. 1.

4. Electron Balance in the Shock Front.

The equation for the rate of electron production, i.e., the source term, is given in Part II, section 1. In order to apply this equation to the non-equilibrium part of the shock front, we need to incorporate a term that expresses the change in macroscopic density. This comes about as follows: Let S represent the source term, i.e.,

$$S = q - p,$$

or,

$$S = \beta_1(T)n^2 + \beta_3(T)nn_e - \alpha(T)n_e^2. \qquad (6)$$

(Note that $\alpha$ has been written as a function of temperature only. This is not quite correct but is discussed further in section 6.)

S is the number of electrons produced per $cm^3$ per sec by interatomic collision processes. If $\Delta X$ is the Eulerian element of displacement perpendicular to the shock front, then the number of electrons in the volume element $\Delta X \Delta A$ is

$$N_e = n_e \cdot \Delta X \Delta A$$

and the number of argon atoms is

$$N = n \cdot \Delta X \Delta A.$$

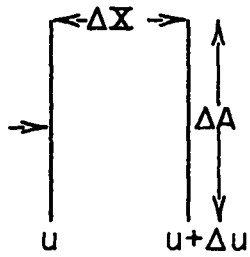


Hence the electron flux through $\Delta A$ is

$$\frac{\Delta\left(N_e/\Delta A\right)}{\Delta t} = S\Delta X - \Delta(un_e).$$

Dividing through by $\Delta X$ and taking limits, we obtain the ordinary continuity equation expressed in terms of electron density

$$\frac{\partial n_e}{\partial t} + \frac{\partial(un_e)}{\partial X} = S,$$

or,

$$\frac{\partial n_e}{\partial t} + u \frac{\partial n_e}{\partial X} = S - n_e \frac{\partial u}{\partial X} .$$

If x is the Lagrange coordinate, then

$$\frac{\rho_1}{\rho} = \frac{\partial X}{\partial x}$$

and

$$\left.\frac{\partial n_e}{\partial t}\right)_x = S - n_e \frac{\rho}{\rho_1} \frac{\partial u}{\partial x} .$$

To an observer on the shock front the shock wave appears stationary, hence we may make the similarity transformation,

$$f(t) \longrightarrow f(\tau) = f(t - \frac{x}{U}) \qquad (7)$$

and obtain

$$\frac{dn_e}{d\tau} = S + \frac{n_e \rho}{U \rho_1} \frac{du}{d\tau} = S + \frac{n_e \rho}{M} \frac{du}{d\tau} \qquad (8)$$

where

$$M = \rho_1 U.$$

The Rankine-Hugoniot equations may also be transformed as follows:

$$\rho_1 \frac{\partial u}{\partial t} = - \frac{\partial p}{\partial x} \text{ becomes } M \frac{du}{d\tau} = \frac{dp}{d\tau} ,$$

$$\rho_1 \frac{\partial v}{\partial t} = \frac{\partial u}{\partial x} \text{ becomes } M \frac{dv}{d\tau} = - \frac{du}{d\tau} ,$$

and

$$\rho_1 \frac{\partial}{\partial t} \left(E + \frac{u^2}{2}\right) = - \frac{\partial}{\partial x} (pu) \text{ becomes } M \frac{d}{d\tau} \left(E + \frac{u^2}{2}\right) = \frac{d(pu)}{d\tau}$$

where v is the specific volume. These last three equations lead to the

ordinary shock conditions discussed previously, viz,

$$Mu = p-p_1,$$

$$M(v-v_1) = - u,$$

and

$$M(E-E_o + \frac{u^2}{2}) = pu.$$

From the $\gamma$-law equation for the energy,

$$E = \frac{p/\rho}{\gamma-1} ,$$

and the three shock equations we obtain the following relations given in Part II, section 1:

$$\xi = \frac{2\rho_1 u^2}{p_1(\gamma+1)} - \frac{1}{\eta_\infty} \tag{9}$$

and

$$\eta = \frac{\eta_\infty \xi + 1}{\xi + \eta_\infty} \tag{10}$$

where

$$\eta_\infty = \frac{\gamma+1}{\gamma-1} .$$

From the equation of state

$$p = gR^*\rho T$$

we have that

$$T = \frac{\eta_A T_A}{\xi_A} \cdot \frac{\xi}{\eta g} . \tag{11}$$

These relations enable us to calculate $p,\rho,T$ as well as other quantities at any point in the shock front provided $\gamma$ is known (assuming the shock velocity U and the initial conditions in front of the shock to be given). To calculate $\gamma$ we return to the equation for the electron balance (8) into which we first substitute

$$\frac{1}{M}\frac{du}{dt} = -\frac{dv}{dt} \quad .$$

This gives

$$\frac{1}{n_e}\frac{dn_e}{dt} + \frac{1}{v}\frac{dv}{dt} = \frac{S}{n_e} \quad .$$

Using (6) we obtain

$$\frac{d\ln(n_e v)}{dt} = \beta_1(T)\frac{n^2}{n_e} + \beta_3(T)n - \alpha(T)n_e. \tag{12}$$

n is the number density of argon atoms at temperature T and $n_1$ is the corresponding value at $T_1$. Also, $n_e$ is the number density of electrons, which, of course, is equal to the ion density. Conservation of mass may be written

$$(n+n_e)V = n_1V_1 = k. \tag{13}$$

From (1) and (13)

$$n_eV = kx, \quad n = \frac{k(1-x)}{V} \quad . \tag{14}$$

Substituting in (12),

$$\frac{dx}{dt} = \frac{\beta_1 k}{V} + x\left(\frac{\beta_3 k - 2\beta_1 k}{V}\right) + x^2\left(\frac{\beta_1 k - \beta_3 k - \alpha k}{V}\right). \tag{15}$$

This equation can be integrated by completing the square. Let

$$a' = \frac{(\beta_1 - \beta_3 - \alpha)k}{V} \quad , \qquad b' = \frac{(\beta_3 - 2\beta_1)k}{V} \quad , \qquad c' = \frac{\beta_1 k}{V} \quad .$$

Then

$$\Delta t = \int_{x_1}^{x_2} \frac{dx}{a'x^2 + b'x + c'} = \frac{1}{a'} \int_{x_1}^{x_2} \frac{dx}{\left(x + \frac{b'}{2a'}\right)^2 - \left[\left(\frac{b'}{2a'}\right)^2 - \frac{c'}{a'}\right]} \quad .$$

Let

$$a = \left[\left(\frac{b'}{2a'}\right)^2 - \frac{c'}{a'}\right]^{1/2} = \left[b^2 - \frac{c'}{a'}\right]^{1/2}$$

and

$$b = \frac{b'}{2a'} \quad .$$

The integral then becomes

$$aa' \Delta t = \tanh^{-1}\left(\frac{x_1 + b}{a}\right) - \tanh^{-1}\left(\frac{x_2 + b}{a}\right)$$

or

$$x_2 = -b + a \tanh\left[\tanh^{-1}\left(\frac{x_1 + b}{a}\right) - aa' \Delta t\right] . \qquad (16)$$

This equation enables us to compute the degree of ionization $x_2$ at a point specified by an interval $\Delta t$ seconds behind a point at which the degree of ionization $x_1$ is known. In this time interval $\beta_1$, $\beta_3$, and $\alpha$ are assumed to be constant. In the integration one iteration was used.

5. Production of Electrons in the Shock Front.

We have previously discussed how electrons are produced (Part II, section 2). It remains here only to evaluate the electron production coefficients, $\beta_1$ and $\beta_3$.

Initially there are no electrons, hence the only means by which electrons are produced is by ionizing collisions between argon atoms. The cross-section for this reaction has a relatively high threshold value, hence the coefficient $\beta_1$ is quite small for the temperatures we are considering. This means that $\gamma$ remains essentially constant until a sufficient number of electrons are present for the ionizing collisions between electrons and atoms to predominate. This point is called the onset of ionization.

From eq (18), Part II, $\beta_1$ is given as

$$\beta_1 = \frac{\pi}{2}\left(\frac{m}{\pi kT}\right)^{3/2}\int_{v_i}^{\infty} e^{-\frac{mv^2}{4kT}}\,\sigma_1(v)v^3dv \qquad (17)$$

and is plotted in Fig. 7. As will be shown in section 7 $\beta_1$ is the most important quantity in determining the actual width of the shock front.

Once the onset of ionization has been reached reactions between electrons and atoms take over and $\beta_3$ becomes the important production coefficient. $\beta_3$ is defined from eq (23), Part II, to be

$$\beta_3 = \sqrt{\frac{2}{\pi}}\left(\frac{\mu}{kT}\right)^{3/2}\int_{v_i}^{\infty} e^{-\frac{\mu v^2}{2kT}}\,\sigma_3(v)v^3dv. \qquad (18)$$

A graph of $\beta_3(T)$ is shown in Fig. 8.

In the computations to follow only the two reactions discussed above have been considered. In a more refined analysis some of the other reactions listed in Part II might be included; however, because of the approximate nature of some of the quantities involved and because their contribution is small, this was not done.

6. The Recombination Coefficient.

There appear to be no experimental measurements of the recombination coefficient in the temperature and density regions of importance in the shocks we are considering. We therefore consider the theoretical formulae for radiative recombination derived by Kramers, and for three-body recombination as given by the Thomson theory. These formulae were discussed in sections (3.3) and (3.4) of Part II. We shall see later in this section, however, that the region of validity of the Thomson theory does not include the conditions of interest, hence its use would be suspect. Moreover, we will also show that the Kramers' theory gives values for the radiative recombination coefficient which are much too large to permit the equilibrium degree of ionization behind the shock. We must therefore proceed in a different manner to obtain the recombination coefficients. Our method will be to use recombination coefficients determined by detailed balancing from the inverse reactions.

We can readily see that Kramers' formula for the radiative recombination coefficient gives values which are too large. His values, which we denote by $\alpha_3(cl)$, as discussed in Part II, are considerably

larger than the corresponding values obtained from the theoretical three-body recombination coefficient $\alpha_4$(theor). If Kramers' formula were correct, we could neglect $\alpha_4$ and simply replace $\alpha$ by $\alpha_3$ where

$$\alpha_3 = \sqrt{\frac{2}{\pi}} \left(\frac{\mu}{kT}\right)^{3/2} \int_0^\infty e^{-\frac{\mu v^2}{kT}} \sigma_r(v) v^3 dv, \qquad (19)$$

$\sigma_r(v)$ being the cross-section for radiative capture of electrons by argon ions given by Kramers' classical relation (eq II: (47) or Fig. II: 13). A plot of $\alpha_3$(cl) is shown in Fig. 9. With our assumption that $\alpha$ may be replaced by $\alpha_3$(cl) in eq (15), the production and recombination coefficients, $\beta_1$, $\beta_3$ and $\alpha$ are all known as functions of temperature and the equation could be numerically integrated across the shock front. If this is done, we obtain a degree of ionization in the steady state region behind the shock (region 4 of Fig. II; (1)) which is smaller than that computed in section 3 by a factor of about $10^4$.

In view of the failure of Kramers' classical theory for the radiative recombination coefficient, we turn to the quantum theory for this process. Usually the cross-section $\sigma_{ph}$ for the inverse process; that is, photoelectric absorption, is what is calculated. This causes but little difficulty, for the radiative capture cross-section $\sigma_r$ can be obtained from it by detailed balancing. In fact (Ref 82)

$$\frac{\sigma_r}{\sigma_{ph}} = \frac{p_{ph}^2}{p_{el}^2} = \frac{(h\nu)^2}{2mc^2 E} \quad , \qquad (20)$$

where $P_{ph} = h\nu/c$ is the photon momentum and $P_{el} = \sqrt{2mE}$ is the electron momentum, E being the electron kinetic energy.

It is possible to use a rather simple approximation for the photoelectric cross-section, for we are interested in processes where the kinetic energy of the electron in the ionized state is small compared to the ionization energy. For this case it is valid to expand the continuum wave function occurring in the matrix elements of the transition probability about the function for zero energy. If a similar expansion (which is a priori much less justified, but which nevertheless gives good numerical results) is used for the bound state functions, and the resulting cross-section averaged over all values of the orbital angular momentum of the bound state, we obtain the cross-section derived by Menzel and Pekeris (Ref 80) and discussed by Mayer (Ref 81, p 12),

$$\sigma_{ph}(n \longrightarrow f) = \frac{2^5\pi}{3\sqrt{3}} \alpha^3 a_o^2 \frac{mc^2(Rhc)^2}{(h\nu)^3} \frac{Z_n^{*4}}{n^5} .$$

Here $\alpha = e^2/\hbar c \sim 1/137$ is the fine structure constant,

$a_o$ is the first Bohr radius,

Rhc is the Rydberg energy (13.61 ev),

n is the principle quantum number of the photoelectron in its bound state, and

$Z_n^*$ is the effective nuclear charge which the photoelectron feels. This formula is derived using the approximation to hydrogenic wave functions, and the only adjustment possible to take into account the actual form of the wave functions is $Z_n^*$.

Using (20) the radiative capture cross-section for an electron of kinetic energy E in its initial state making a transition to a bound state of principle quantum number n is

$$\sigma_r(f \longrightarrow n) = \frac{2^4\pi}{3\sqrt{3}} \alpha^3 a_o^2 \frac{(Rhc)^2}{E(I_n+E)} \frac{Z_n^{*4}}{n^5}, \qquad (21)$$

where we have substituted $h\nu = I_n+E$, $I_n$ being the ionization potential of the electron in its bound state. We are interested in capture from states near the ionization limit, and hence we can neglect E compared to $I_n$. Further, putting

$$I_n = \frac{Z_n^{*2}}{n^2} Rhc,$$

(21) becomes

$$\sigma_r(f \longrightarrow n) = \frac{2^4\pi}{3\sqrt{3}} \alpha^3 a_o^2 \frac{Rhc}{E} \frac{Z_n^{*2}}{n^3} . \qquad (22)$$

To get the total radiative capture cross-section, we must sum (22) over all available bound states. For the argon ion it is possible to capture an electron into one 3p orbital, or into $2n^2$ orbitals of n greater than 3. For the latter orbitals we use an effective nuclear charge $Z_n^* = 1$. For the 3p orbital, the device of the effective nuclear charge is only approximate, since the orbital is far from hydrogenic. However, we will not be making order of magnitude errors if we choose $Z_{3p}^* = 5$, a value gotten by using the screening constants in Mayer's paper.

Finally, we apply the quantum cut-off, equation (19) of Part I, in summing (22). For our range of shock strengths and for a fore-pressure $p_1 \sim 60$ cm Hg we can, to a good approximation, assume that states for which $n \geq 7$ are non-existent. This cuts the series off so that it is finite and thus convergent. However, convergence of the sum is only an apparent difficulty of our formula (22). For higher values of n the approximation that $h\nu \doteq I_n$ is no longer valid, and we must keep the kinetic energy term, as included in (21). In this case the sum over n even if it were infinite clearly converges.

Making the above substitutions in (33) we obtain for the total capture cross-section

$$\sigma_r = \frac{3.018 \times 10^{-21}}{E} \quad cm^2 \qquad (23)$$

with E in electron volts. Values for $\sigma_r$ are plotted in Fig. 18 where it is seen that they are in good agreement with values for argon obtained by adjusting Bates' results on hydrogen and oxygen as discussed in Part II, section 3.3.

If we substitute (23) into (19) we obtain the coefficient for radiative recombination $\alpha_3$ where

$$\alpha_3 = \frac{2.174 \times 10^{-11}}{T^{1/2}} \quad , \qquad (24)$$

with T in degrees absolute. This relation is plotted in Fig. 19. Comparison with $\alpha_3(cl)$ of Fig. 9, shows our new result to be smaller by a factor of about $10^5$. This invalidates our previous integration of

the ionization density through the shock front in which $\alpha_3(c1)$ was used.

With this new value of the radiative recombination coefficient, we can no longer neglect the three-body recombination process. We therefore consider the range of applicability of Thomson's theory of three-body recombination. On the low pressure side the pressure must be sufficiently high so that the chance for the neutral atom involved in the collision to be in the neighborhood of the interacting ion and electron is large enough. This means that the distance between an ion and a neutral atom must be less than $r_o = 2e^2/3kT$; e.g., at $T = 12000^o$ and $p_1 = 59.3$ cm Hg the compression $\eta^*$ must be greater than about 60 ($\eta^*$ of course increases as $T^3$). In terms of the atom density n this says that, for our range of temperatures and pressures, n must be greater than about $10^{22}$ atoms per $cm^3$. On the high pressure side we have already indicated that Thomson's theory breaks down for atom densities greater than $n \sim 10^{24}$ in the temperature range of 1 to 3 ev. Whereas the Thomson theory is applicable for atom densities per $cm^3$ $10^{22} \lesssim n \lesssim 10^{24}$, the atom densities achieved in the shocks we are treating lie in the range $10^{18}$ to $10^{20}$ per $cm^3$.

In view of the inapplicability of the Thomson theory, we turn to another method aimed at finding the recombination coefficient $\alpha$. To do this let us reconsider the derivation of the source term, equation (6). We assume the only important reactions occurring in our plasma, which consists of argon atoms A, argon ions $A^+$, and electrons e, are

the following:

$$A+A \underset{\alpha_4}{\overset{\beta_1}{\rightleftharpoons}} A+A^+ +e, \tag{25}$$

$$A+e \underset{\alpha_5}{\overset{\beta_3}{\rightleftharpoons}} A^+ +2e, \tag{26}$$

$$A+h\nu \underset{\alpha_3}{\overset{\beta_9}{\rightleftharpoons}} A^+ +e. \tag{27}$$

The electron production rates are given by the $\beta$'s and the recombination rates by the $\alpha$'s. From these reactions we write the source term as

$$\frac{dn_e}{dt} = \beta_1 n^2 + \beta_3 n n_e + \beta_9 n n_\nu - \alpha_4' n n_e^2 - \alpha_5' n_e^3 - \alpha_3 n_e^2 \tag{28}$$

where all the coefficients are functions of temperature only and where $\alpha_4' = \alpha_4/n$ and $\alpha_5' = \alpha_5/n$. The atom density is n, electron density $n_e$, photon density $n_\nu$, and electron and ion densities are equal. If we compare eq (24) with eq (6) we see that

$$\alpha = \alpha_4' n + \alpha_5' n_e + \alpha_3. \tag{29}$$

In the equilibrium state $dn_e/dt = 0$ or, from (28), using the asterisk to denote equilibrium values,

$$\alpha^* = \alpha_4' n^* + \alpha_5' n_e^* + \alpha_3 = \frac{n^{*2}}{n_e^{*2}} \left( \beta_1 + \beta_3 \frac{n_e^*}{n^*} + \beta_9 \frac{n_\nu^*}{n^*} \right).$$

From eq (1)

$$\frac{n^*}{n_e^*} = \frac{1-x}{x} ,$$

hence

$$\alpha^* = \alpha_4' n^* + \alpha_5' n_e^* + \alpha_3 = \beta_1 \left(\frac{1-x}{x}\right)^2 + \beta_3 \left(\frac{1-x}{x}\right) + \beta_9 \frac{n_\nu^*}{n^*} \left(\frac{1-x}{x}\right)^2 . \quad (30)$$

By the principle of microscopic reversibility, not only must the overall production of electrons be zero in the equilibrium state, but each individual reaction (25) to (27) must be balanced. Hence we have

$$\alpha_4' = \frac{1}{n^*} \beta_1 \left(\frac{1-x}{x}\right)^2 ,$$

$$\alpha_5' = \frac{1}{n_e^*} \beta_3 \left(\frac{1-x}{x}\right) ,$$

$$\alpha_3 = \frac{n_\nu^*}{n^*} \beta_9 \left(\frac{1-x}{x}\right)^2 .$$

We can therefore obtain the non-equilibrium recombination rate $\alpha$ of (29) from knowledge of the equilibrium concentrations, and $\beta_1$ and $\beta_3$ (giving $\alpha_4'$ and $\alpha_5'$) and from the quantum formula for radiative recombination (giving $\alpha_3$), i.e.,

$$\alpha = \frac{n}{n^*} \beta_1 \left(\frac{1-x}{x}\right)^2 + \frac{n_e}{n_e^*} \beta_3 \left(\frac{1-x}{x}\right) + \alpha_3 . \quad (31)$$

Actually it is unnecessary to use this general formula for many of the conditions with which we are dealing. The main point here is

that in the region in which the ionization is relatively low the recombination rate $\alpha n_e^2$ is negligible, hence the value of $\alpha$ is unimportant. The recombination rate does become important after considerable ionization has taken place. Then, however, the coefficients of the terms $\beta_1$ and $\beta_3$ in (31) become comparable at least to within several orders of magnitude and since $\beta_3$ is between $10^{11}$ to $10^{14}$ times $\beta_1$ (see Figs. 7 and 8), we may neglect the term in $\beta_1$. Moreover, as can be seen from Figs. 11, b and c, for temperatures of 15,000° and 18,000° the radiative recombination term $\alpha_3$ is small compared to $\beta_3\left(\frac{1-x}{x}\right)$ for a considerable range of densities. Hence in (31) we can neglect $\alpha_3$ for values of $n_e$ in the neighborhood of $n_e^*$. (For the 12000° case, Fig. 11a, the radiative recombination term is dominant and the approximation we make here does not apply.) Hence over a considerable range of densities and temperatures ($n \gtrsim 5\cdot 10^{19}$ and $T \gtrsim 16000°$) we can approximate $\alpha$ by

$$\alpha \sim \frac{n_e}{n_e^*}\,\beta_3\left(\frac{1-x}{x}\right). \tag{32}$$

Actually in the integrations following the degree of ionization through the shock front the value $\alpha = \beta_3\left(\frac{1-x}{x}\right)$ was used (cf section 7). This is satisfactory in the most important region near equilibrium where $n_e/n_e^*$ is close to unity, and makes some allowance for the other terms in (31) for regions far from equilibrium.

## 7. Structure of the Shock Front.

The main purpose of this report is to describe quantitatively the structure of a shock front in argon when the shock strength is high enough so that ionization takes place. The previous sections have prepared us for such a computation and in this section we present the results.

All conditions at the peak of the shock (point A, Fig. 1 of Part II) may be obtained from the ordinary shock equations with $\gamma = 5/3$, provided we know the shock velocity U and the conditions in front of the shock. The conditions thus obtained will be expressed in terms of compression $\eta$, shock strength $\xi$ and temperature ratio $T/T_1$. Thus, knowing the conditions at point A and in front of the shock and numerical relations for $\beta_1$, $\beta_3$ and $\alpha$ we may integrate equation (15) across the shock front. The method of integration is outlined in section 4 with the relations for $\beta_1$, $\beta_3$ and $\alpha$ being given in sections 5 and 6. Since specific volume V and temperature T which occur in equation (15) are slowly varying functions of time, they were replaced by an average constant value across the small interval of integration $\Delta t = t_2 - t_1$. The average was determined by an iteration procedure and one iteration was sufficient. The criterion used in determining the interval $\Delta t$ was that the corresponding temperature change $\Delta T$ must be less than $100^{\circ}$. This integration carried out in equation (16) gives a value for the degree of ionization x at $t_2$ knowing conditions at $t_1$. From x at $t_2$ we computed $\beta$, equation (5), and hence $\gamma$. The shock equations

(9), (10) and equation (11) then give $\xi$, $\eta$ and T respectively at the time $t_2$, and the Eulerian increment of distance in this time interval is given by $\Delta X = U\Delta t/\eta$. Starting at the head of the shock (point A) we thus proceed by successive small steps $\Delta t$ until we arrive at what is sensibly the equilibrium condition B (Fig. 1 Part II).

The electron production coefficients $\beta_1$ and $\beta_3$ are given as functions of temperature in Figs. 7 and 8 but, for purposes of calculation, exponential type empirical formulas were fitted to these curves. The recombination coefficient $\alpha$, equation (31) depends on the atom and electron densities n and $n_e$, as well as on the temperature. This could be incorporated into the integration where, to even a better approximation than for V used above, n could be considered as constant across the integration interval $\Delta t$. Actually equation (31) was not used, but instead the quantity $\beta_3\left(\frac{1-x}{x}\right)$ plotted in Fig. 10 was used for the recombination coefficient $\alpha$. This gives substantially the correct value for $\alpha$ in the region near the equilibrium position B where recombination has the greatest effect on the shock structure. In the less important regions away from the equilibrium position $\alpha$ is incorrectly represented by $\beta_3\left(\frac{1-x}{x}\right)$ both because of the neglect of radiative and other recombination processes, and because the density dependence of this function is incorrect.

The numerical work of this integration (as well as all other computations in this paper) was done on the IBM card programmed electronic computer (CPC) through the courtesy of Los Alamos Group T-1. A typical

integration through the shock front may take from 2 to 3 hours.

The structure of the shock obtained from this integration is given in Table VI and is plotted in Figs. 12 to 17.

We have previously described the sort of behavior to be expected in a shock front and now, on the basis of the above computations, we review this description. First let us recall that our calculations apply to a monatomic gas, viz, argon, where the initial pressure is 59.38 cm Hg and for which the shock velocity is high enough so that some ionization takes place but low enough so that the number of doubly ionized atoms may be ignored.

When such a shock wave passes a point X the translational degrees of freedom of the gas are first excited and translational equilibrium is achieved within about two collisions. This point is referred to here as the peak of the shock. The time required for translational equilibration is small compared to that for the remaining processes involved in the shock front, hence is not included in our computations. The local temperature at the peak of the shock is high enough so that a significant amount of energy may be transferred from the translational degrees of freedom to those of electronic excitation and ionization. This is clearly indicated in Fig. 12 where it is seen that the equilibrium temperature $T^*$ is considerably lower than that at the peak of the shock $T_A$. This is particularly true for increasing shock velocity as shown in the following table:

| U(cm per sec) | $T_A/T^*$ |
|---|---|
| $5.0 \cdot 10^5$ | 1.46 |
| $5.5 \cdot 10^5$ | 1.60 |
| $6.0 \cdot 10^5$ | 1.78 |

The only reactions available at first are collisions between argon atoms for which the corresponding ionization cross-section is quite small. This means that the transfer of energy takes place rather slowly until the point we have called the onset of ionization is reached. Thus the values at the peak of the shock remain approximately unchanged for some distance, resulting in a rather flat region in the shock front. This is true for all the shock parameters as Figs. 12 to 17 show (cf the table below). We refer to this distance as the onset width. If we call the relaxation point that point at which 63% of the equilibrium ionization is achieved, it may be seen that the onset width offers the most important contribution to the total relaxation width.

In determining the onset width $\beta_1$ is the most significant quantity because the degree of ionization x is small in this region. Hence, by considering the leading term in eq (15), we see that the onset width scales inversely with initial density $\rho_1$ (or pressure $p_1$) at constant initial temperature $T_1$.

Once the onset of ionization is reached transfer of energy from translational degrees of freedom to electronic excitation and ionization proceeds quite rapidly. This results in a sudden change in the

shock parameters, especially the temperature (Fig. 12) and the degree of ionization (Fig. 16). Again we see that the effect is more violent for higher shock velocities, e.g, if the distance in which this sudden change takes place is $\Delta X$, then for $U = 6 \cdot 10^5$ cm per sec, $\Delta X \doteq .001$ cm, while for $U = 5 \cdot 10^5$ cm per sec, $\Delta X \doteq .007$ cm. At first the electron production term involving $\beta_3$ is most important but soon the recombination term takes over and equilibrium is quickly achieved. The shape (or profile) of this region is rather sensitive to the value of $\alpha$ but because the region is relatively narrow $\alpha$ does not have much effect on determining the total relaxation width of the shock front.

If $\lambda_x$ is the relaxation width for the shock front, $\lambda_t$ the relaxation time, and $x_r$ the corresponding degree of ionization, we find the following approximate values for the case $p_1 = 59.38$ cm Hg:

| $U\left(\frac{cm}{sec}\right)$ | Onset width (cm) | $\lambda_x$(cm) | $\lambda_t$(sec) | $x_r$ |
|---|---|---|---|---|
| $5.0 \cdot 10^5$ | $10.5 \cdot 10^{-3}$ | $13.7 \cdot 10^{-3}$ | $1.15 \cdot 10^{-7}$ | .045 |
| $5.5 \cdot 10^5$ | $1.6 \cdot 10^{-3}$ | $2.45 \cdot 10^{-3}$ | $2.0 \cdot 10^{-8}$ | .065 |
| $6.0 \cdot 10^5$ | $.4 \cdot 10^{-3}$ | $.58 \cdot 10^{-3}$ | $3.8 \cdot 10^{-9}$ | .088 |

It is seen that the onset width is about 70% of the relaxation width. We also see that in these shocks we could assume that processes involving radiative transitions can be ignored in determining the width of the shock front since such times are of the order of $10^{-8}$ sec whereas once a significant amount of ionization is reached so that radiative

transitions could take place, the main part of the shock front has passed. For lower shock velocities, however, the relaxation widths will be considerably larger, and radiative processes assume importance. (As we have previously stated, they may also be important for lower densities.)

It is interesting to note that there is a range of shock velocities in which the width of the shock front may be significant, i.e., in which the conditions in the shock front are considerably different from the equilibrium conditions behind the shock front. At low shock velocities, i.e., for our case below about $3 \cdot 10^5$ cm per sec, there is no ionization behind the shock front, hence $\gamma$ remains constant and the conditions at the peak of the shock remain unchanged. As the shock velocity U increases above $3 \cdot 10^5$ cm per sec, $\gamma$ decreases and a long and relatively low temperature bump appears behind the head of the shock. (This is an indentation in terms of pressure and density.) As U becomes greater the bump becomes progressively higher but shorter until at $10^6$ cm per sec it is approximately $10^{-6}$ cm thick but has a peak temperature of about $90{,}000^\circ$ where the equilibrium temperature is about $26000^\circ$. However, for U $\sim 10^6$ cm per sec we can no longer ignore the number of doubly ionized atoms. This picture of the shock front is qualitatively the same if the fore-pressure is 1.0 cm Hg.

8. Effect of Impurities.

Impurities such as oxygen or other molecules in the argon would have a strong influence on two parts of our computation. In the case

of the equilibrium calculation the additional degrees of freedom, i.e., rotation, vibration, dissociation, and molecular excitation, due to their lower energy levels, will soak up a considerable amount of energy which is then not available for exciting (or ionizing) the argon atom. Calculations show that a small percentage (between about 1 to 10%) of oxygen in the argon will keep the argon from ionizing.

The second place in which impurities play an important part is in determining the onset of ionization. If the ionization cross-section between argon and $O_2$ or O is large then, even though the amount of oxygen is small, enough electrons may be furnished for the A+e reaction to take over, resulting in an effective decrease in the onset width.

9. Comparison with Experiment.

In previous sections we have referred to some of the experimental measurements made on shock fronts for the energy range considered in this report. In this section we review these measurements as well as others. In general, the experimental work is quite meager although this field is now being explored, particularly by Kantrowitz and Lin at Cornell University, by Laporte at the University of Michigan and by various workers at Los Alamos. As mentioned previously, the shock velocity is the one well-determined quantity for a shock wave; and, of course, it may be assumed that the conditions in front of the shock are known.

Material Velocity. Shreffler, Christian, and others have measured the material velocity in a shock wave immediately behind the shock

front (Ref 74). Their measurements correspond to the velocity in the equilibrium region and are plotted in Fig. 1. It is seen that experiment and theory are in good agreement in this region.

Electric Effects. Unpublished measurements at Los Alamos have shown that a strong (positive) potential rises behind the shock front. And for a given shock velocity the potential is much smaller if the gas is diatomic. This latter effect, as explained in section 8, is due to the presence of the additional degrees of freedom in the diatomic gas which absorb energy that otherwise would have gone into exciting or ionizing the atom.

Cowling (Ref 77) has shown that diffusion can be more important than viscosity or thermal conductivity in its effect on shock propagation, particularly if the gas is composed of two constituents having a large mass difference and if the pressure gradient is large, the direction being such that the heavier particles tend to move toward the regions of greater pressure. In our case such a situation exists immediately in front of the equilibrium region (cf Figs. 14 and 16), hence, a separation of ions and electrons should take place which could possibly account for the measured potential gradient in the shock front.

Shock Width. Measurements on the structure of the shock front in argon have been made at Cornell. The point at which the onset of ionization occurs is determined by a conductivity measurement and the equilibrium region is specified by the luminosity. The Cornell measurements are in fair agreement with our computations, although it is likely

that impurities affect their measurements such that their shock width is slightly less than ours*.

Spectral Distribution. Observations on spectra in shock waves show that at low shock velocities distinct lines exist whereas at high shock velocities a continuous spectrum is seen. This is because of the following reasons. First, at low shock velocities, transitions from the continuum to bound states do not occur because there are no free electrons, or at most, very few. There will, however, be many excited states of the atoms, thus one would expect a discrete spectrum to be observed.

For a high shock velocity and, consequently, a high degree of ionization, there are many electrons in free states. Since for the range of energies considered in this report these free states are in approximate maxwellian distributions with energies centered between one and three electron volts, one would expect the radiated energy to be continuously distributed. This is the ordinary recombination spectrum which is observed in shock fronts.

In addition to the continuous recombination spectrum in a shock front one might expect to observe a line spectra because of the presence of excited atoms. However the pressure and temperature are high enough so that Stark, collision, and Doppler broadening should be quite large and the spectral lines smeared out to such an extent that they are masked by the continuous recombination spectrum. Also, when the degree

*Private communication from S. C. Lin to R. E. Duff.

of ionization is high, the occupation number for a particular excited state is quite low and hence the line it emits is weak and more easily merges with the continuous background. For example, at $\eta = 7$ and $T = 20{,}000^{\circ}$ the occupation number for the excited state $3p^5(^2P^{\circ}_{1/2})4s$, which emits the persistent argon line, $\lambda = 1048\ A^{\circ}$, is only .003. That is, out of 1000 plasma particles at these conditions, 140 will be electrons, 140 will be argon ions, 666 argon atoms in the ground state, only 2 atoms in the above excited state, and the remaining 52 particles in various other excited states. Finally, there are many closely spaced lines in the argon spectrum and because of the broadening of the lines they may be expected to overlap. As the initial pressure is lowered, however, the spectral lines do begin to stand out against the continuous background. This is because, for a given shock velocity, the temperature and pressure behind a shock front decrease with decrease of initial pressure. And the lower the temperature and pressure, the sharper and more pronounced the spectral lines will be. Also, the recombination coefficient decreases with decreasing temperature and pressure, resulting in a weaker recombination spectrum, although this effect may be balanced by the increase in ionization which occurs for smaller fore-pressures.

Luminosity. As discussed previously, because of the small number of degrees of freedom available in a monatomic gas compared to a diatomic gas, much of the energy can go directly into ionization. Thus one obtains a high degree of ionization behind a shock front in an inert

gas. Consequently, an argon shock of sufficient strength will emit a brilliant flash and, because of the continuous distribution of energy in the spectrum, may be used in certain physical applications where such an energy distribution is desirable, e.g., in flash photography (Ref 84).

## 10. Summary and Critique.

A convenient method for determining the equilibrium conditions behind a shock front in argon has been presented. However, two factors limit its applicability. First, since double ionization has been neglected, there is an upper limit to the temperature. And, second, there is an upper limit to the degree of ionization due to the approximations involved in computing the partition functions. Neither of these limits has received a quantitative treatment. Numerical calculations of the equilibrium conditions have been made for shock velocities from 3 to $9 \times 10^5$ cm/sec at fore-pressures of 59.38 and 1.0 cm Hg.

The shape of the non-equilibrium part of the shock front has also been calculated. It was shown that the region between the front of the shock and the onset of ionization largely determines the shock width. In this zone the ionizing A+A reaction plays the dominant role. Hence, more accurate values for the A+A cross-section, particularly in the neighborhood of the threshold, should be obtained. Also, the effect of excitation reactions should be re-examined. Our reasons for neglecting these have been discussed qualitatively but a quantitative analysis is desirable.

Finally, a recombination coefficient $\alpha$ was derived from a method depending on the balance of the production and recombination of electrons in the equilibrium region behind the shock front. It was shown that $\alpha$ depends on temperature as well as on the atom density n and that Kramers' theory for radiative recombination, which was based on classical assumptions, is incorrect.

The two fore-pressures we have used in our calculations correspond to those used in experimental work at Cornell by Kantrowitz and his co-workers, and at Los Alamos. As pointed out previously, impurities exist in argon which have an important effect on both the equilibrium conditions and on the onset of ionization. In order to compare the above theory with the experimental results, the impurities should be included in the computations.

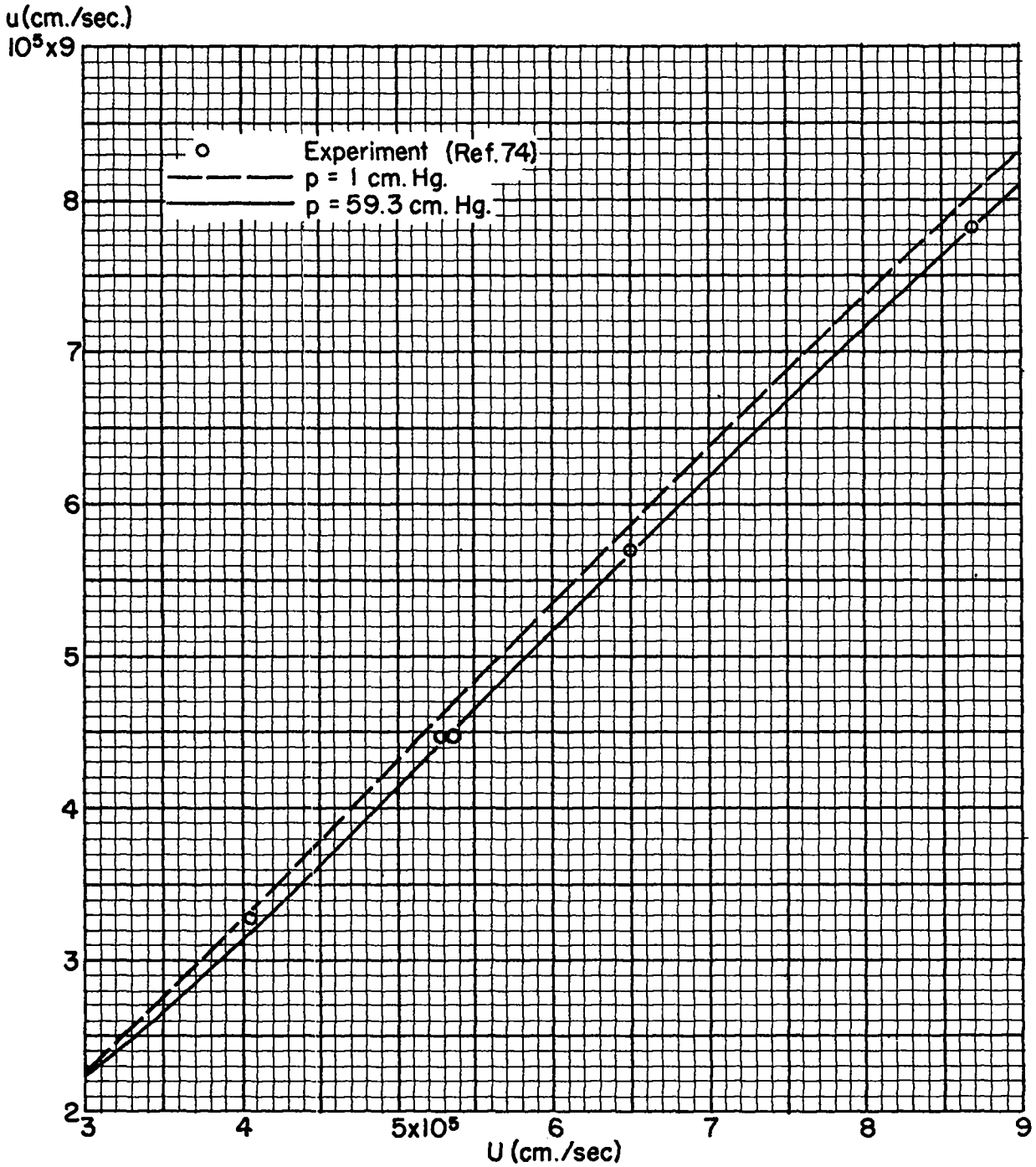


Fig. 1 Material velocity vs. shock velocity.

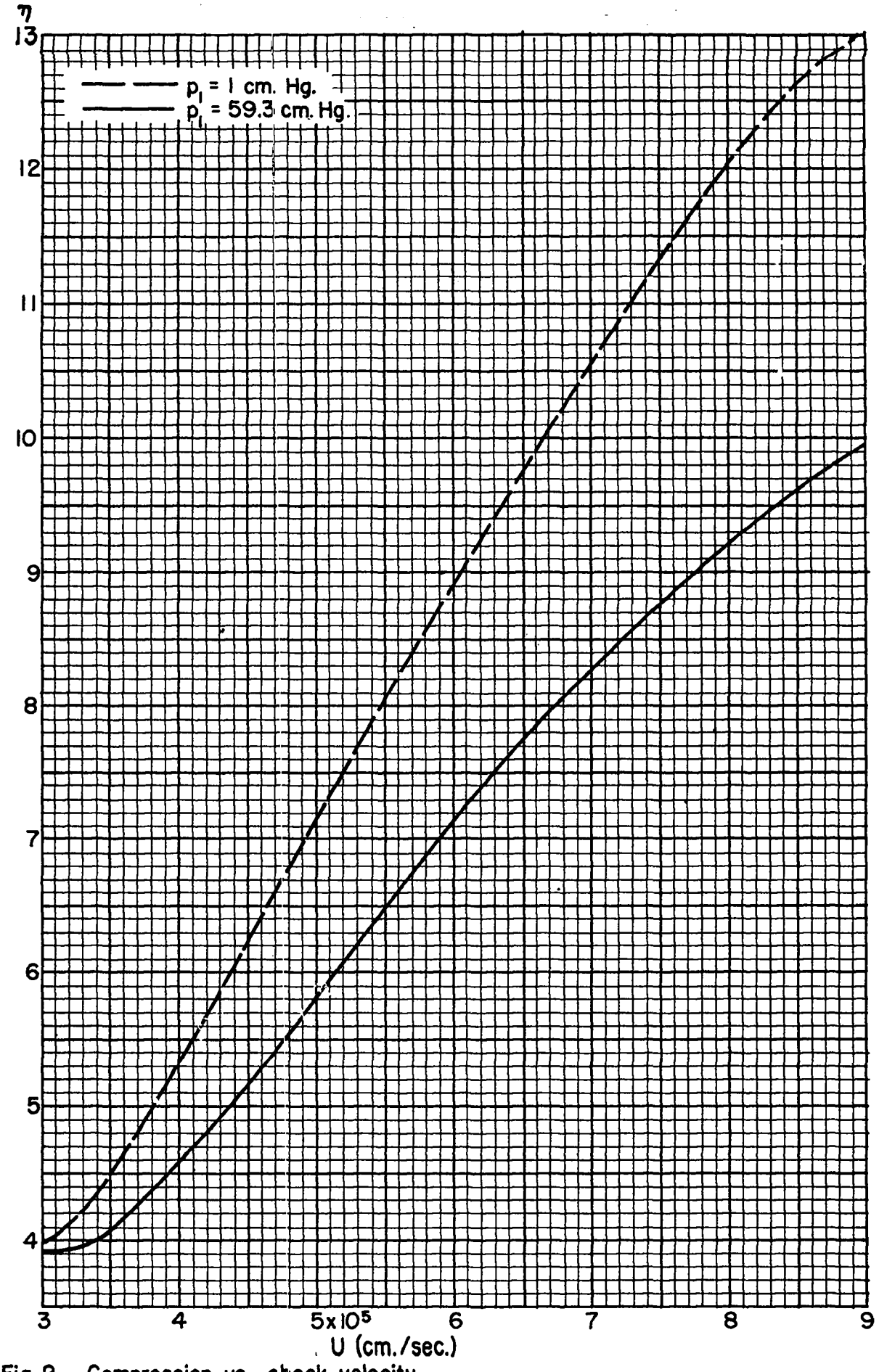


Fig. 2 Compression vs. shock velocity.

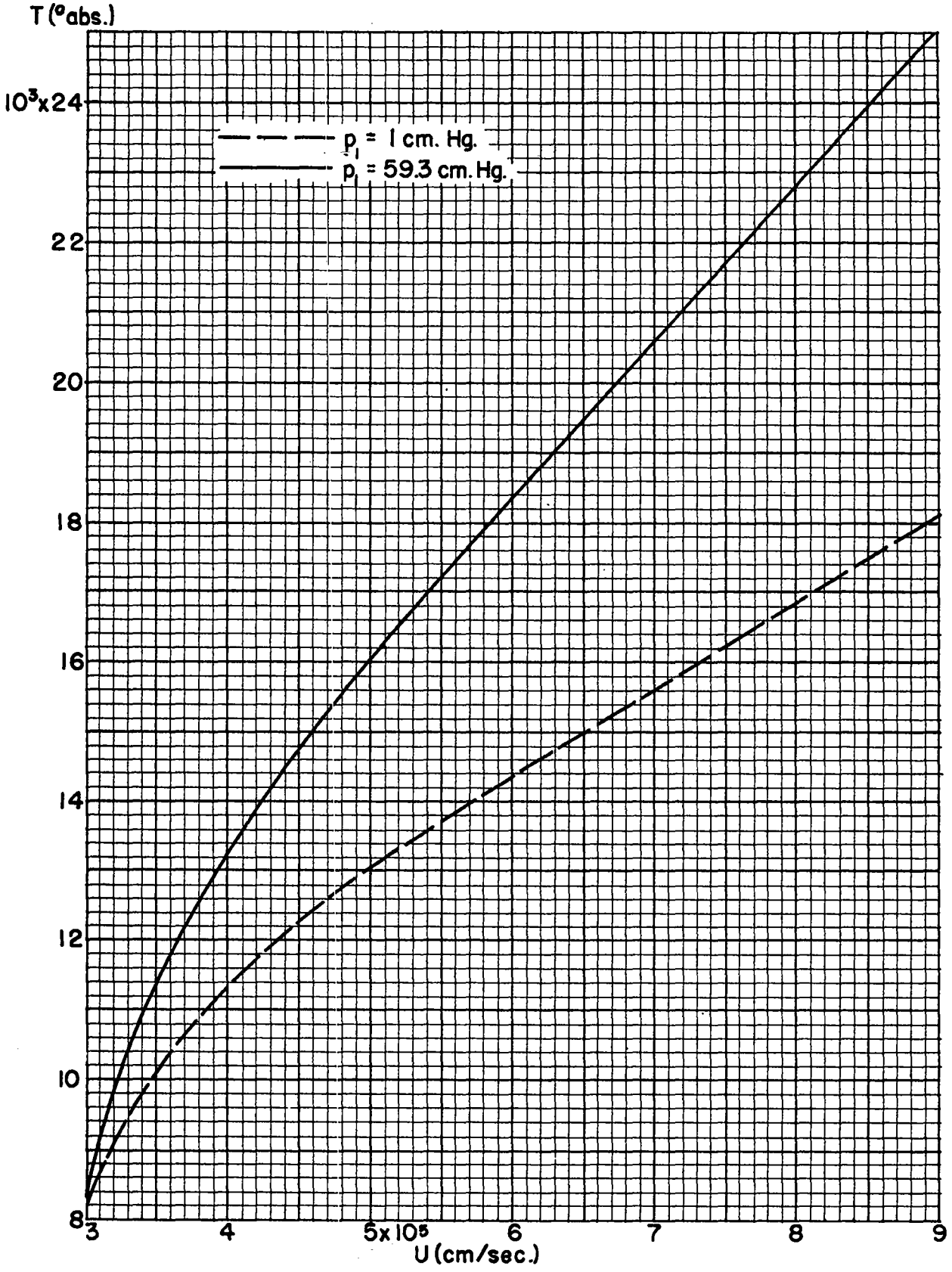


Fig. 3 Temperature vs. shock velocity.

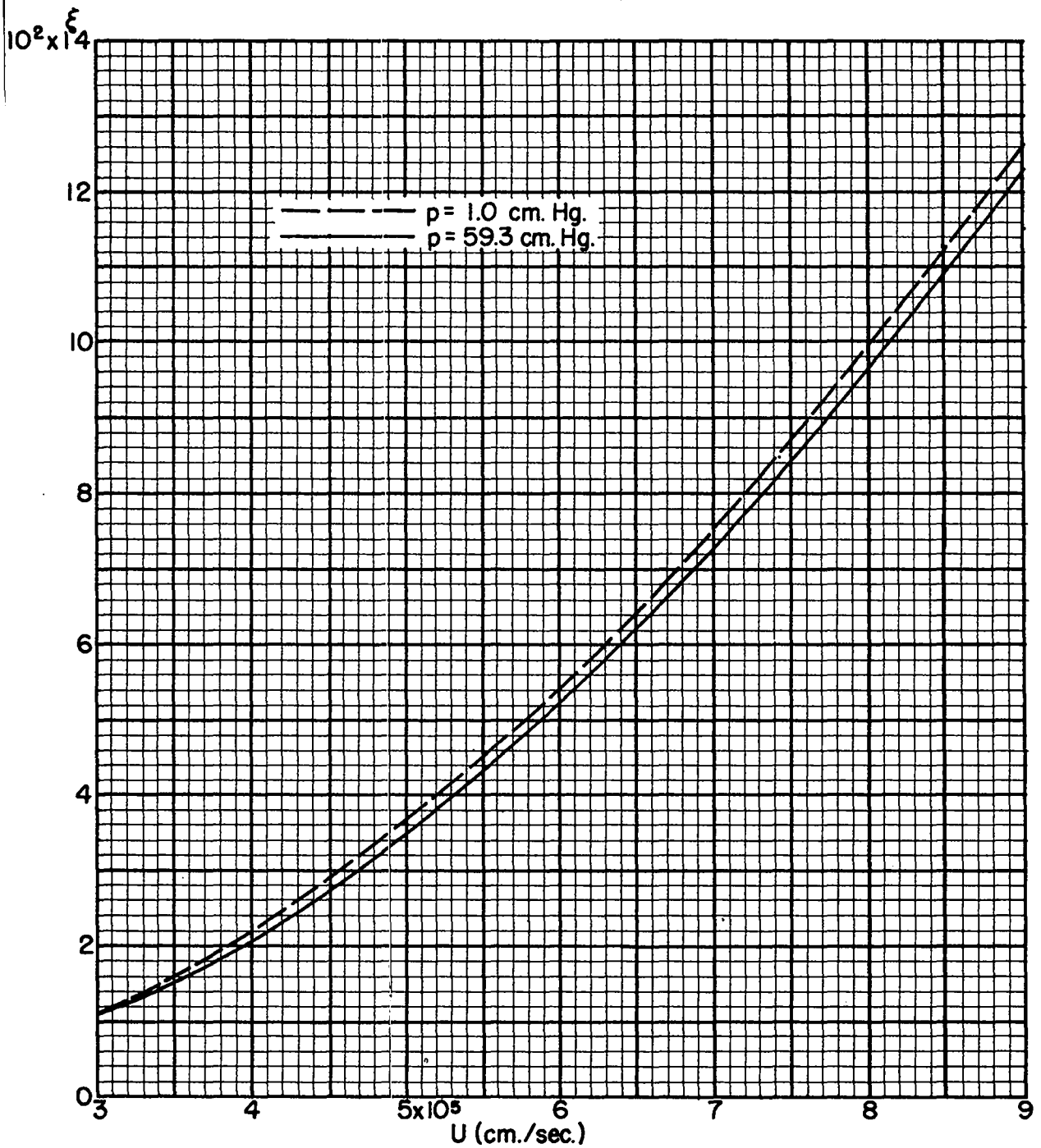


Fig. 4 Pressure ratio vs. shock velocity.

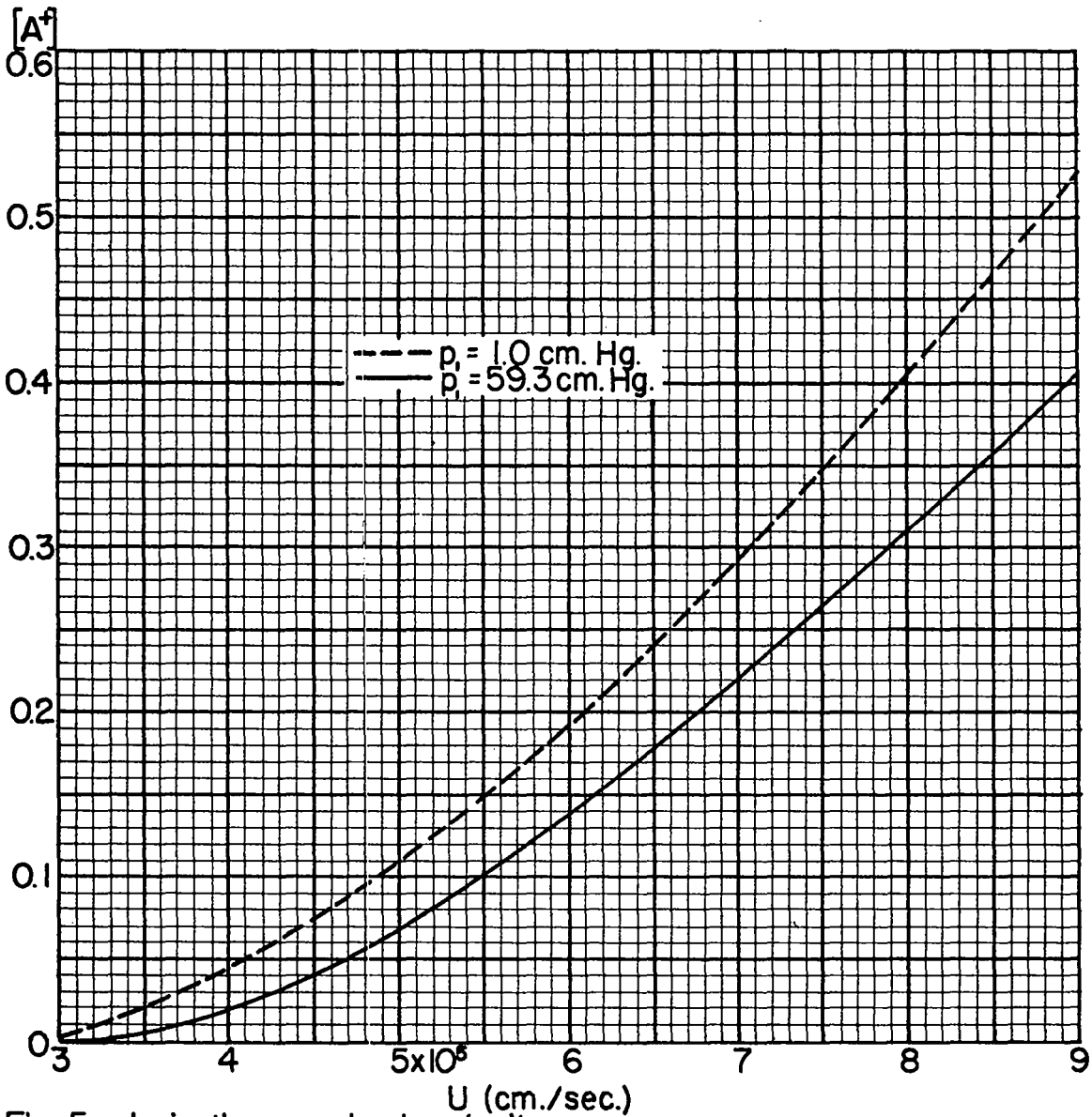


Fig. 5 Ionization vs. shock velocity

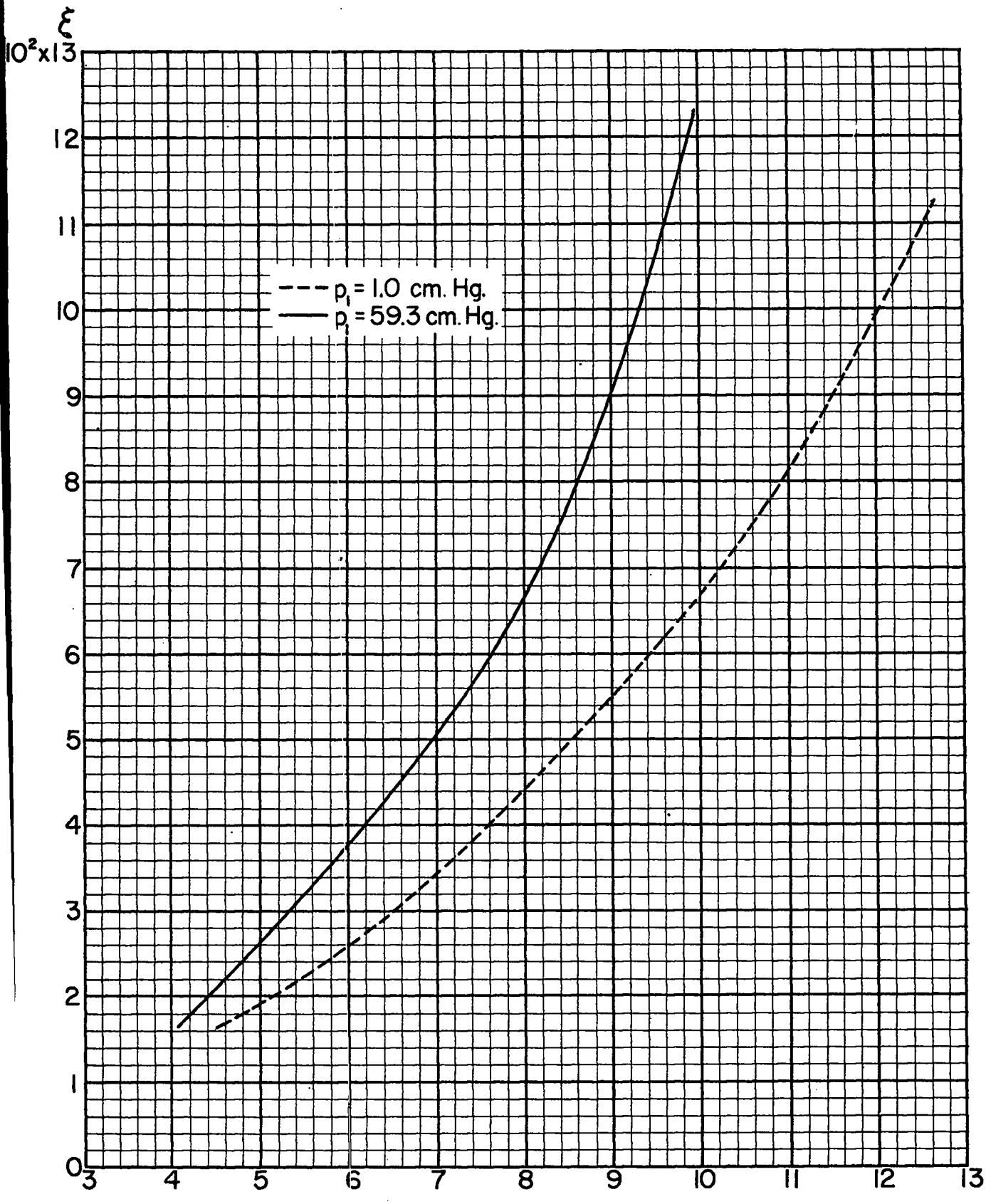


Fig. 6 Hugoniot

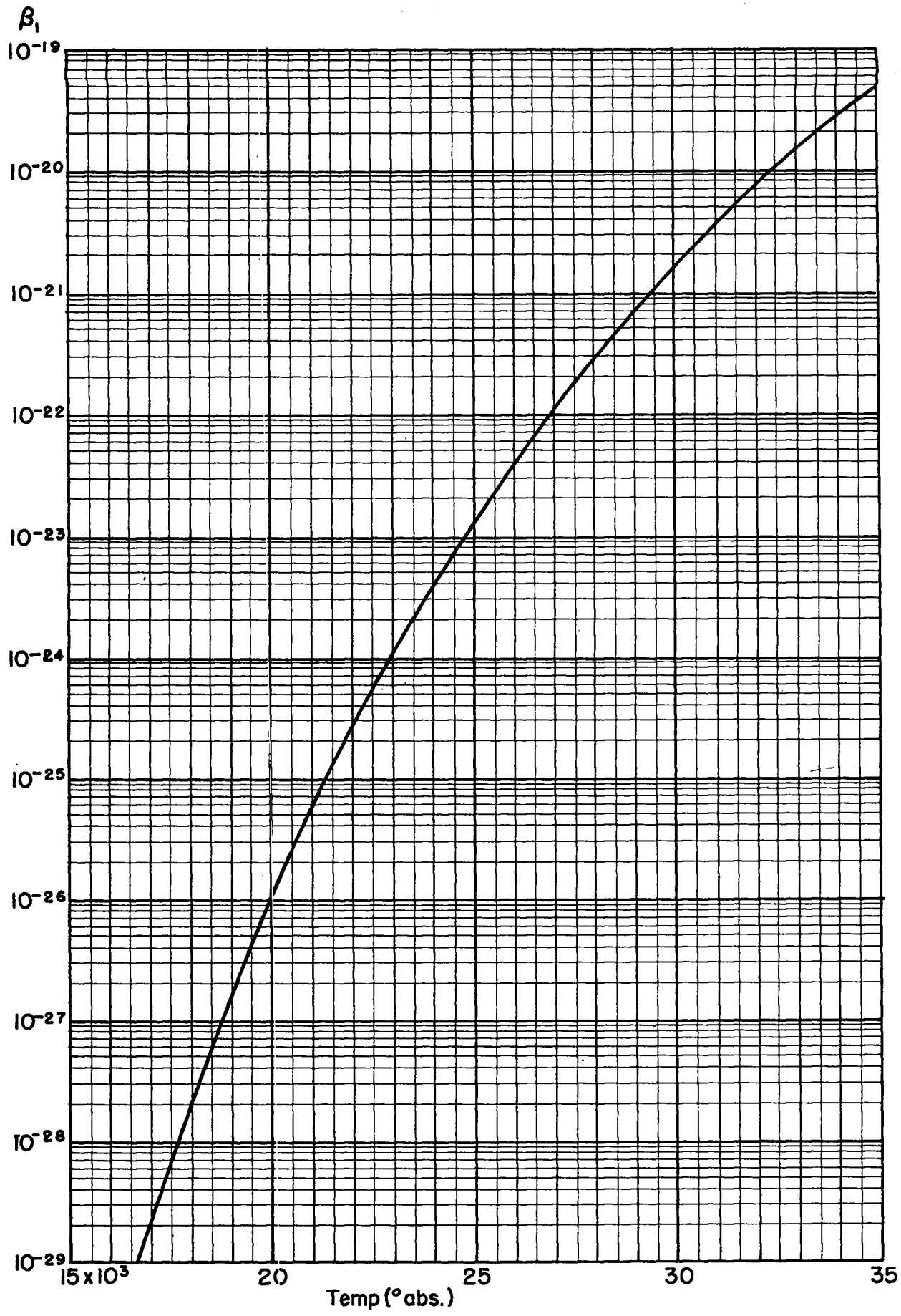


Fig. 7 Electron production coefficient for the reaction $A + A \rightarrow A + A^+ + e$

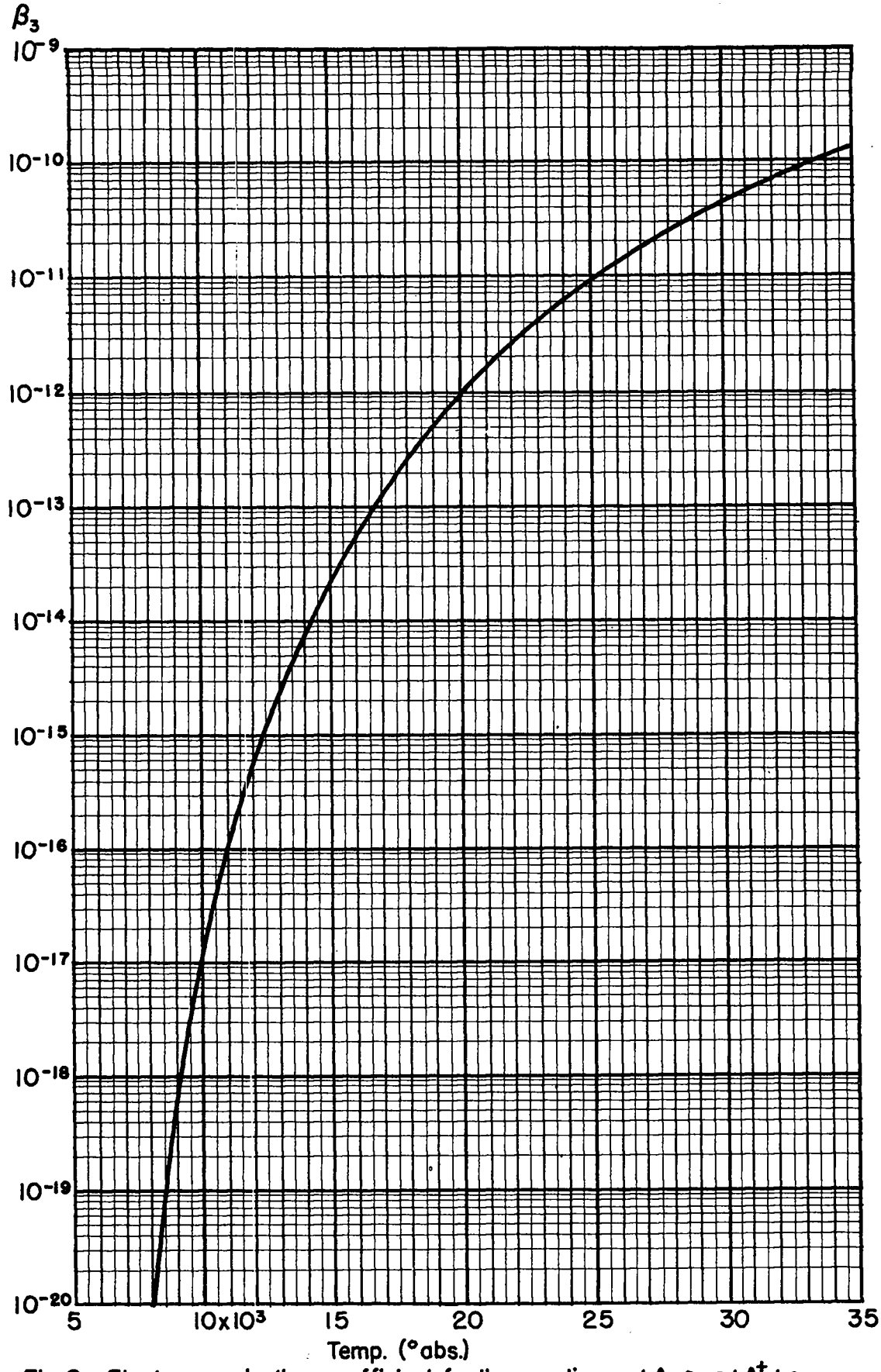


Fig. 8 Electron production coefficient for the reaction $e+A \rightarrow e+A^{+}+e$

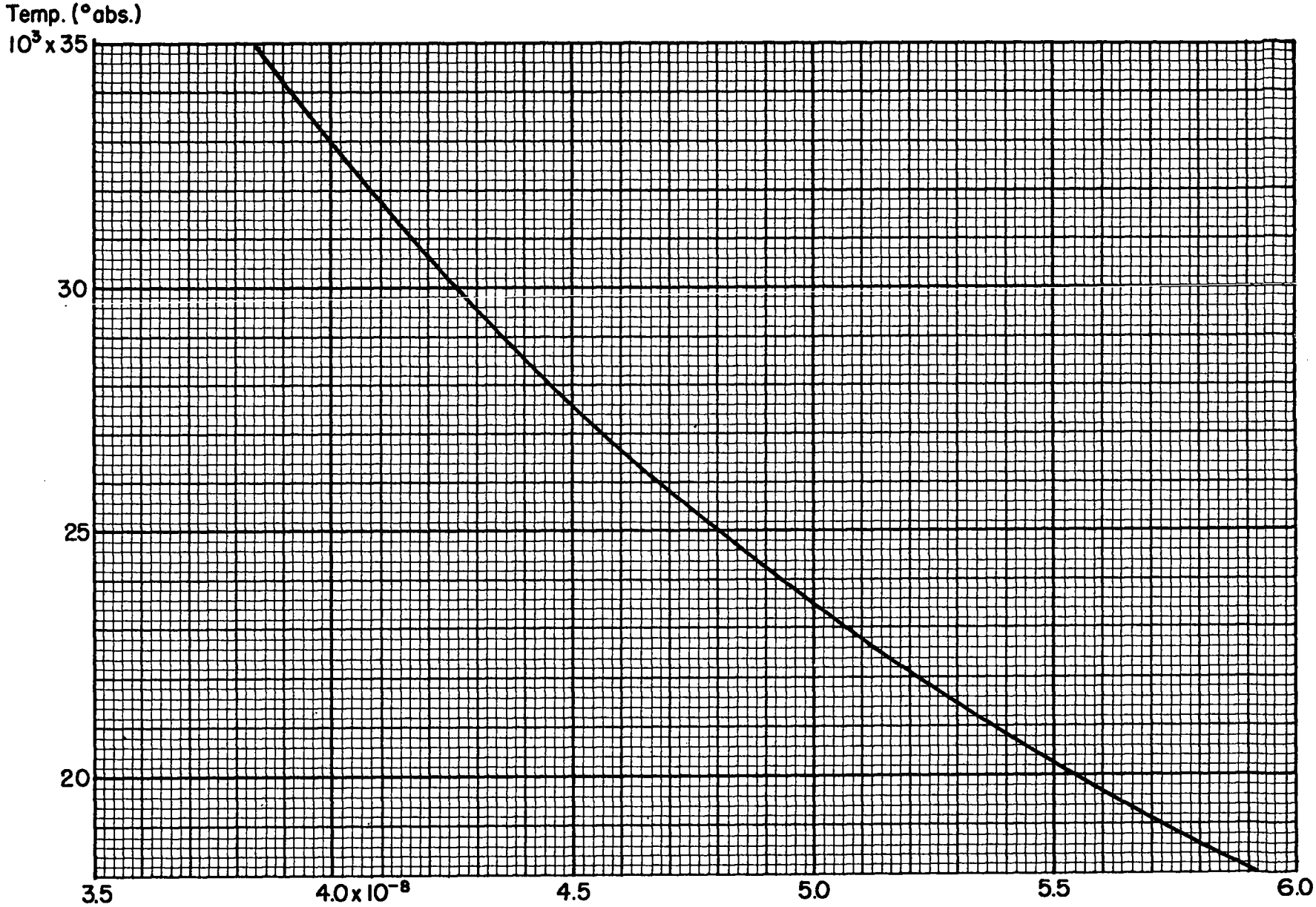


Fig. 9 Radiative recombination coefficient *(classical)* $\alpha_3$

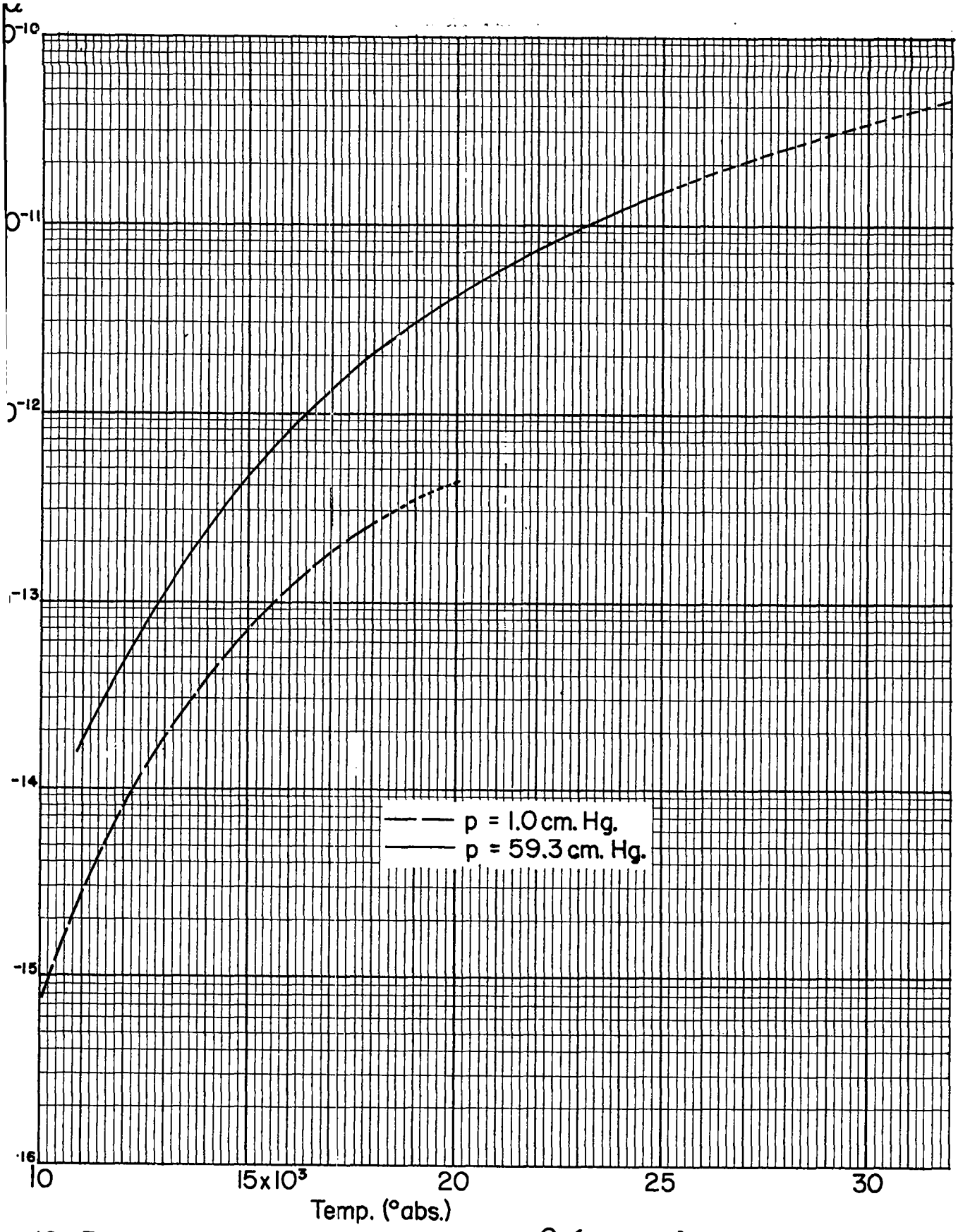


. 10 Recombination coefficient $\alpha^* = \beta \{(1-x^*)/x^*\}$

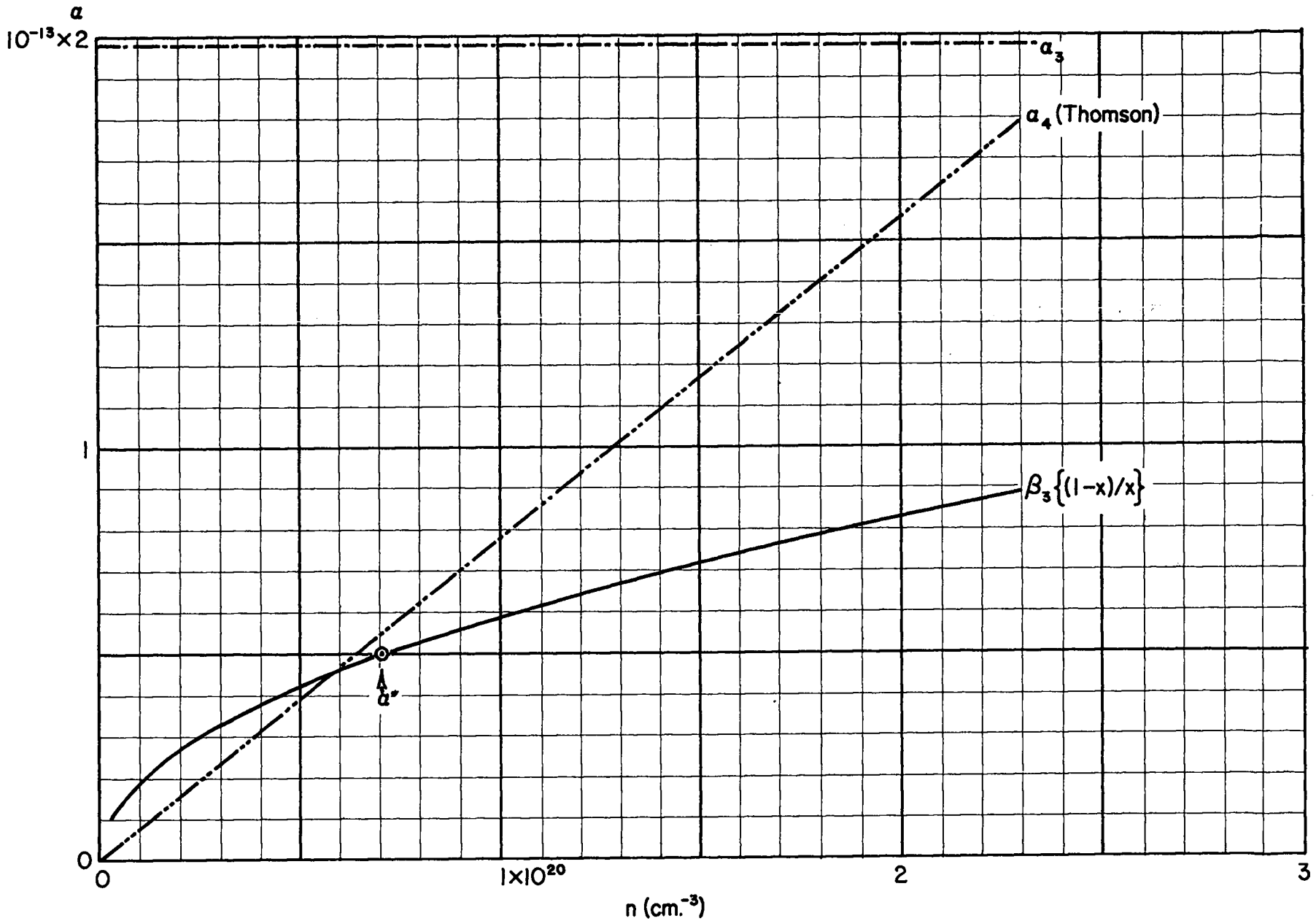


Fig. IIa Recombination coefficients for T = 12,000° abs.

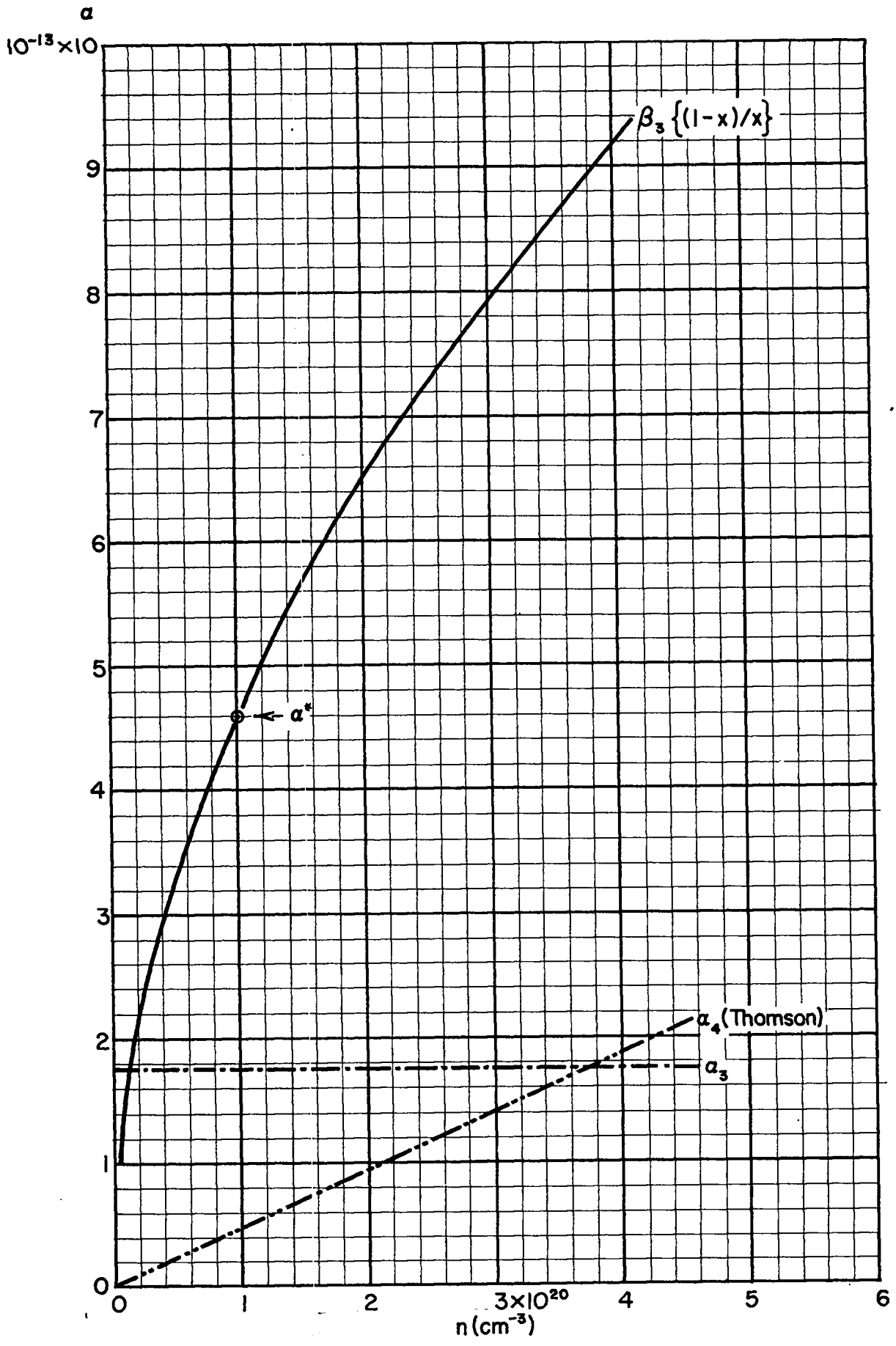


Fig. 11 b Recombination coefficients for T = 15,000° abs.

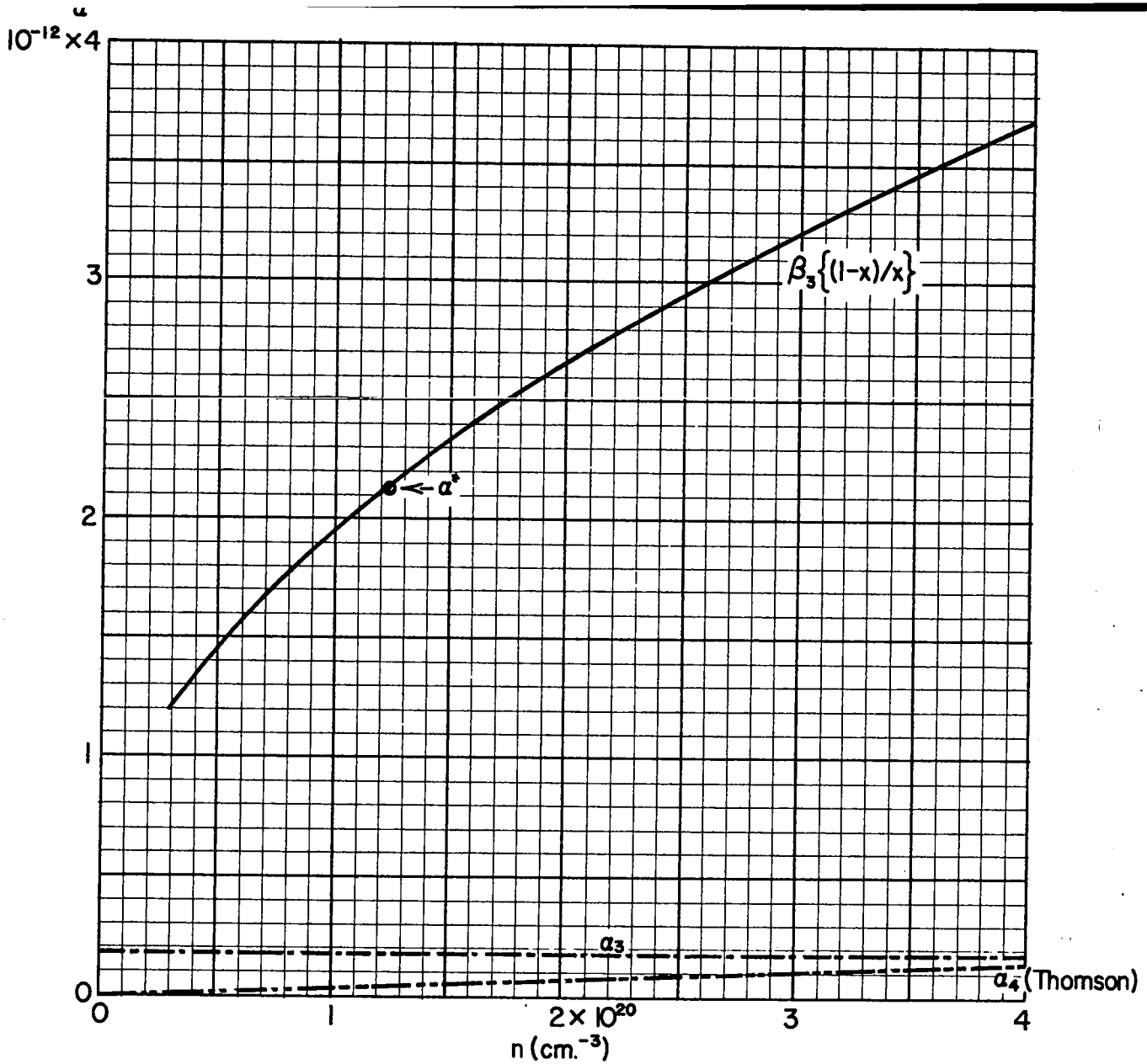


Fig. 11 c Recombination coefficients for T= 18,000° abs.

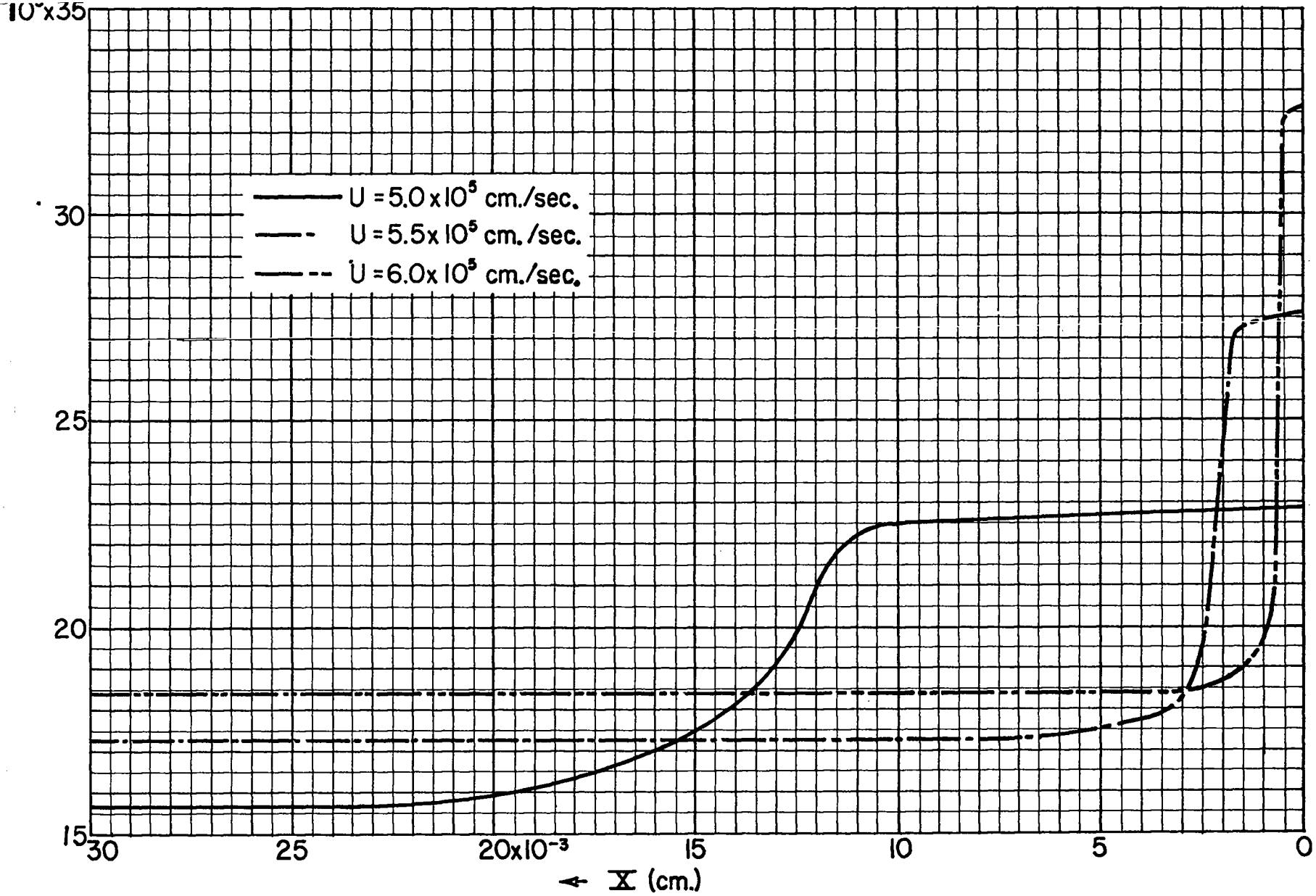


Fig. 12 Temperature vs. (Eulerian) distance behind the shock front for various shock velocities. ($p_1$ = 59.3 cm. Hg.)

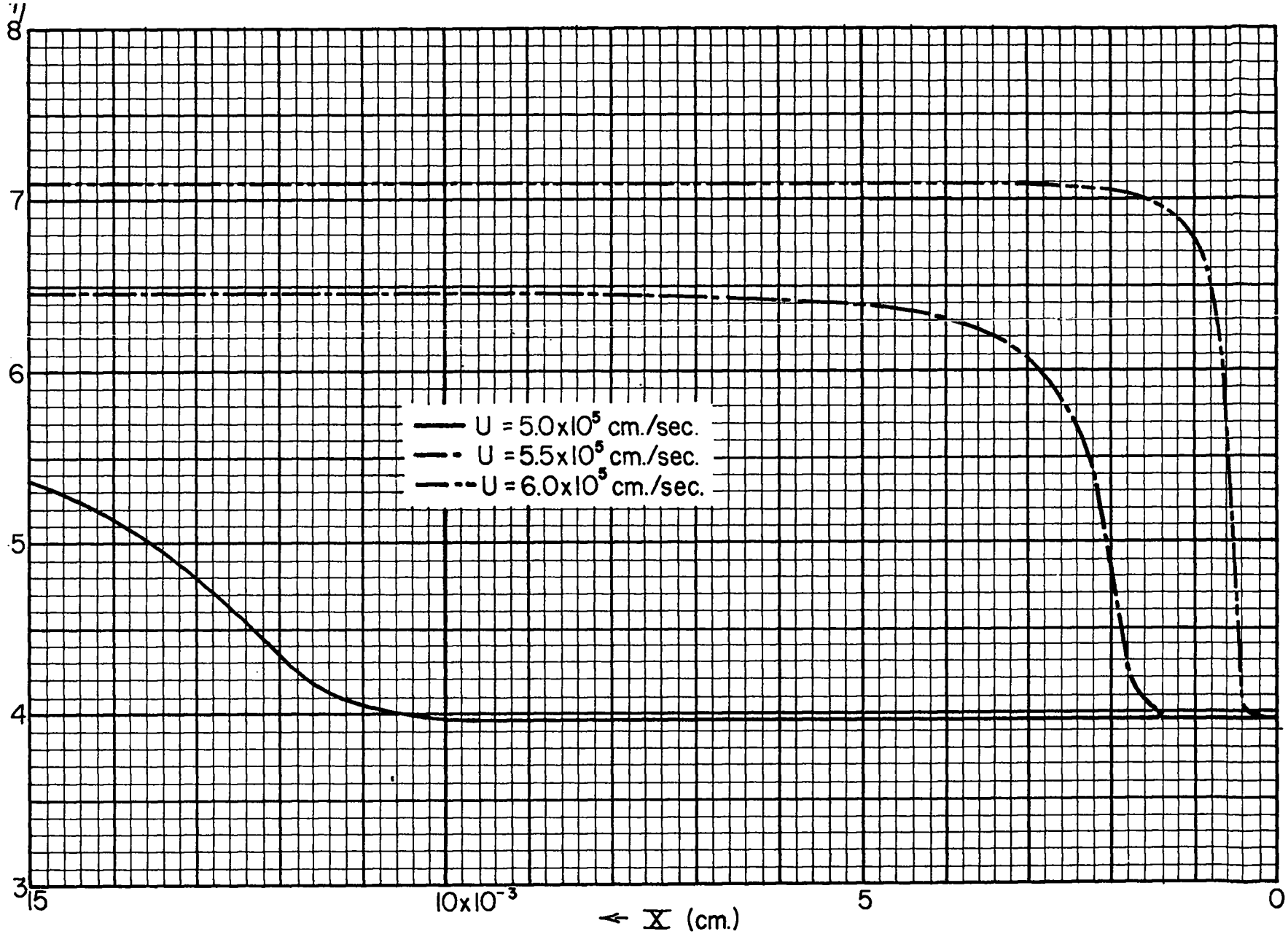


Fig. 13 Compression vs. (Eulerian) distance behind the shock front for various shock velocities. ($p_i$=59.3 cm. Hg.)

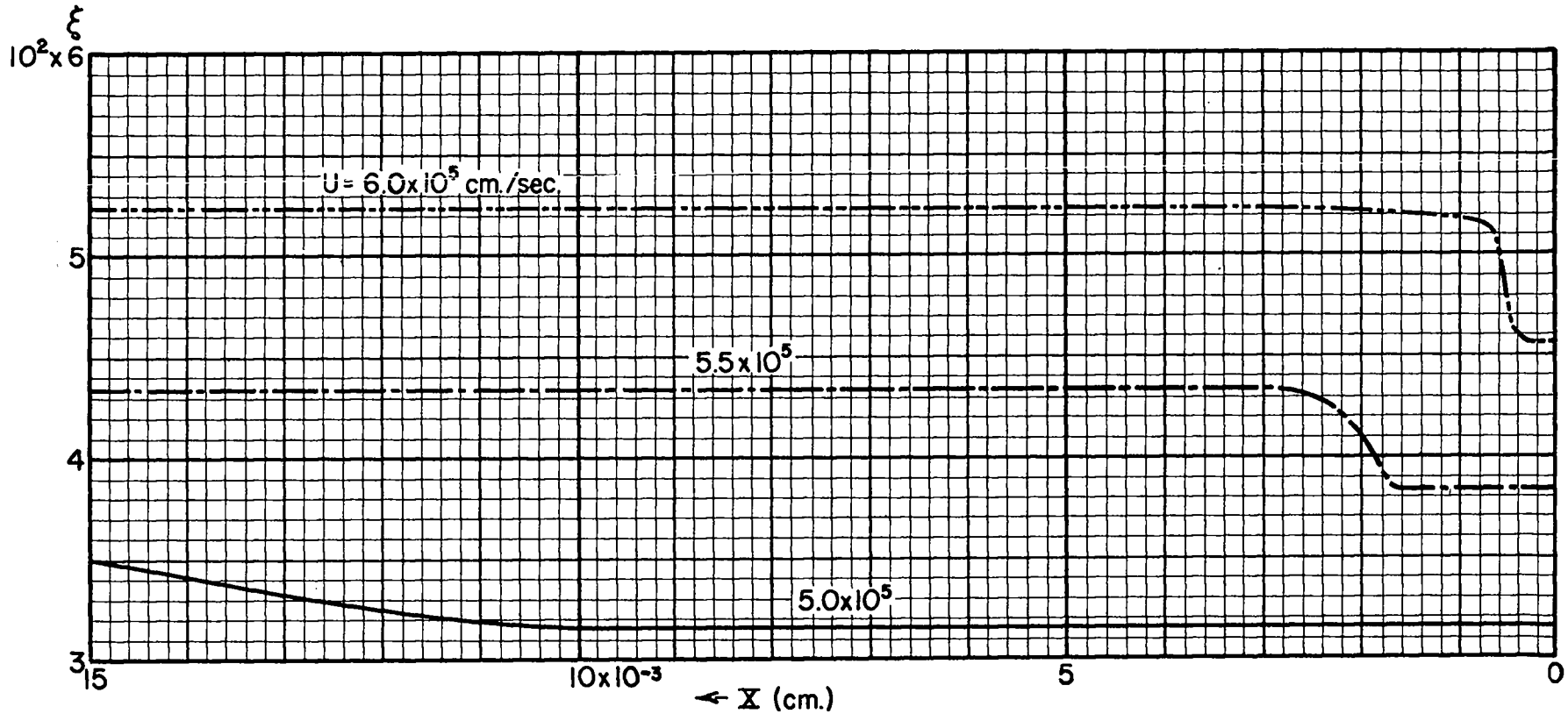


Fig. 14 Pressure ratio vs. (Eulerian) distance behind the shock front for various shock velocities. ($p_1$ = 59.3 cm. Hg.)

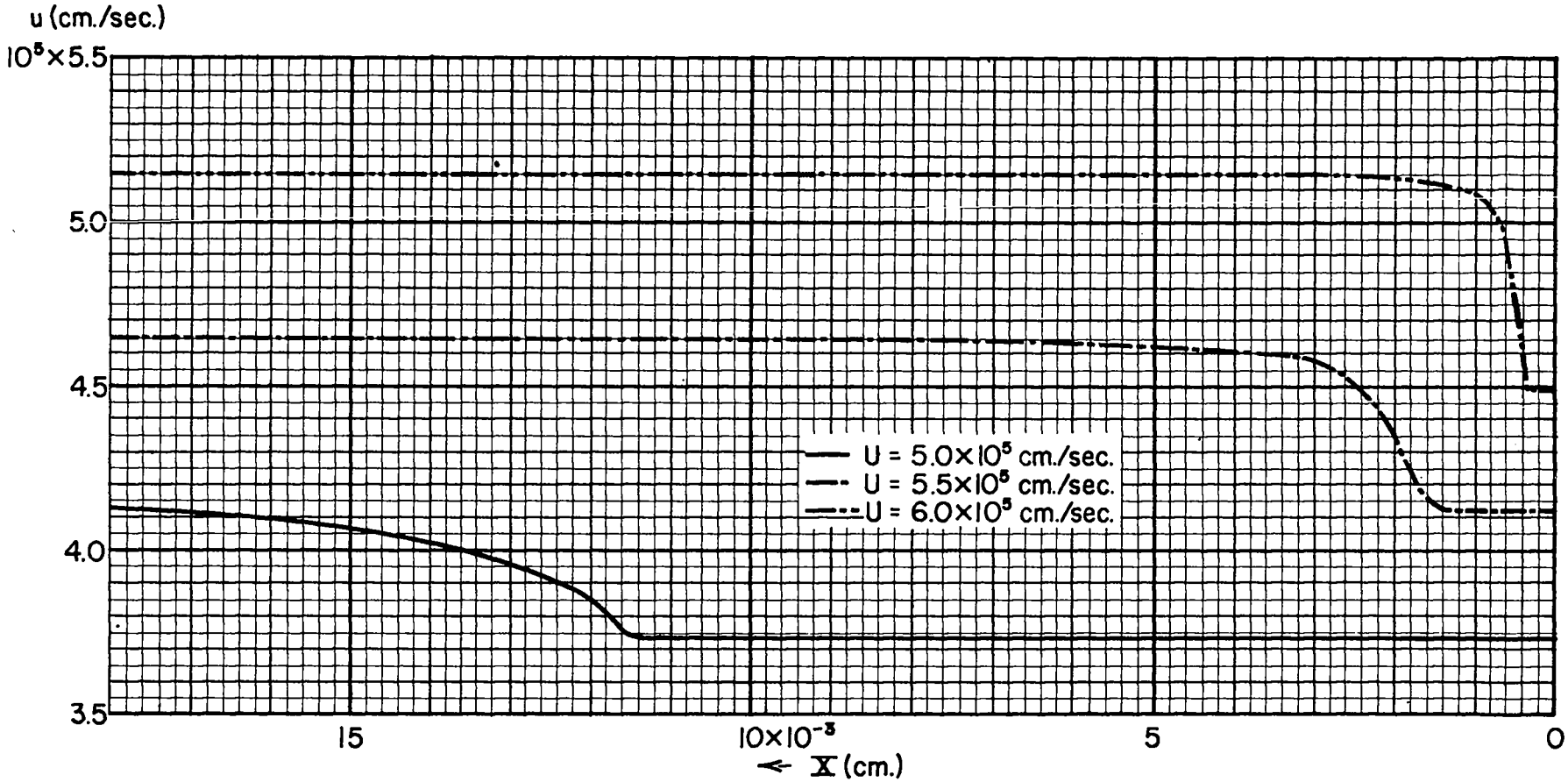


Fig. 15 Material velocity vs. (Eulerian) distance behind the shock front for various shock velocities. ($p_1$ = 59.3 cm. Hg.)

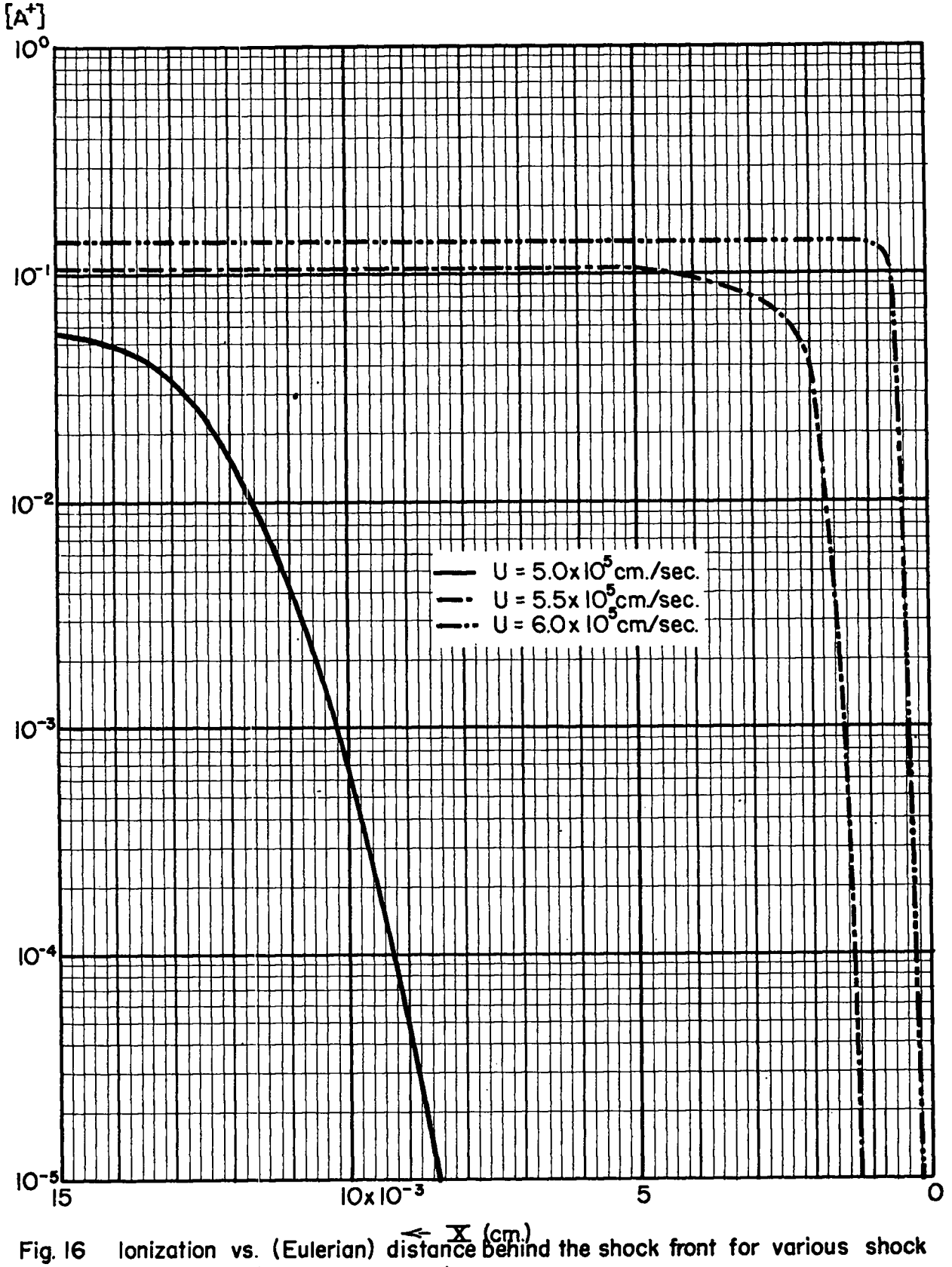


Fig. 16 Ionization vs. (Eulerian) distance behind the shock front for various shock velocities. ($p_1$ = 59.3 cm. Hg.)

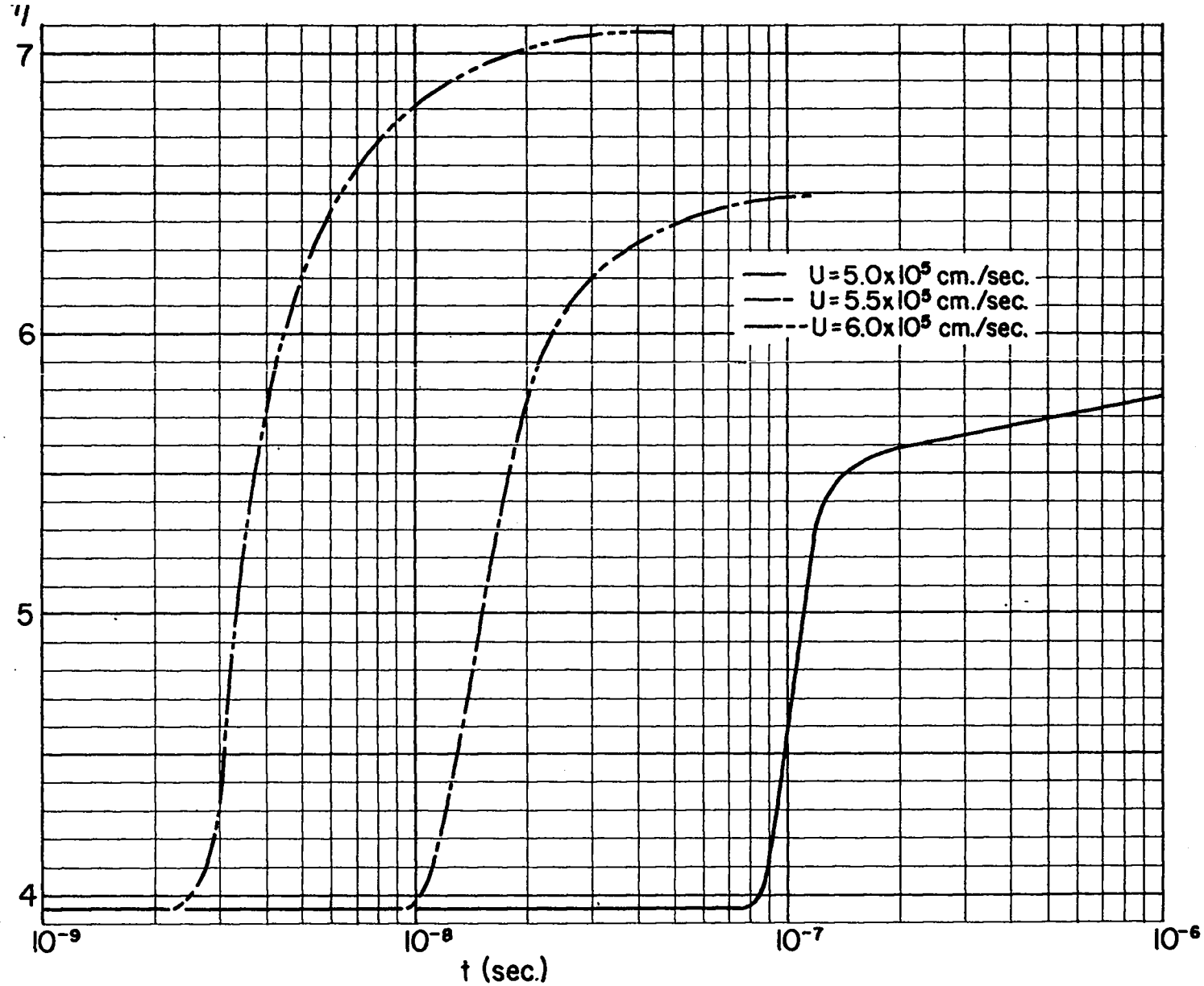


Fig. 17 Compression behind the shock front vs. time ($p_1$=59.3 cm. Hg.)

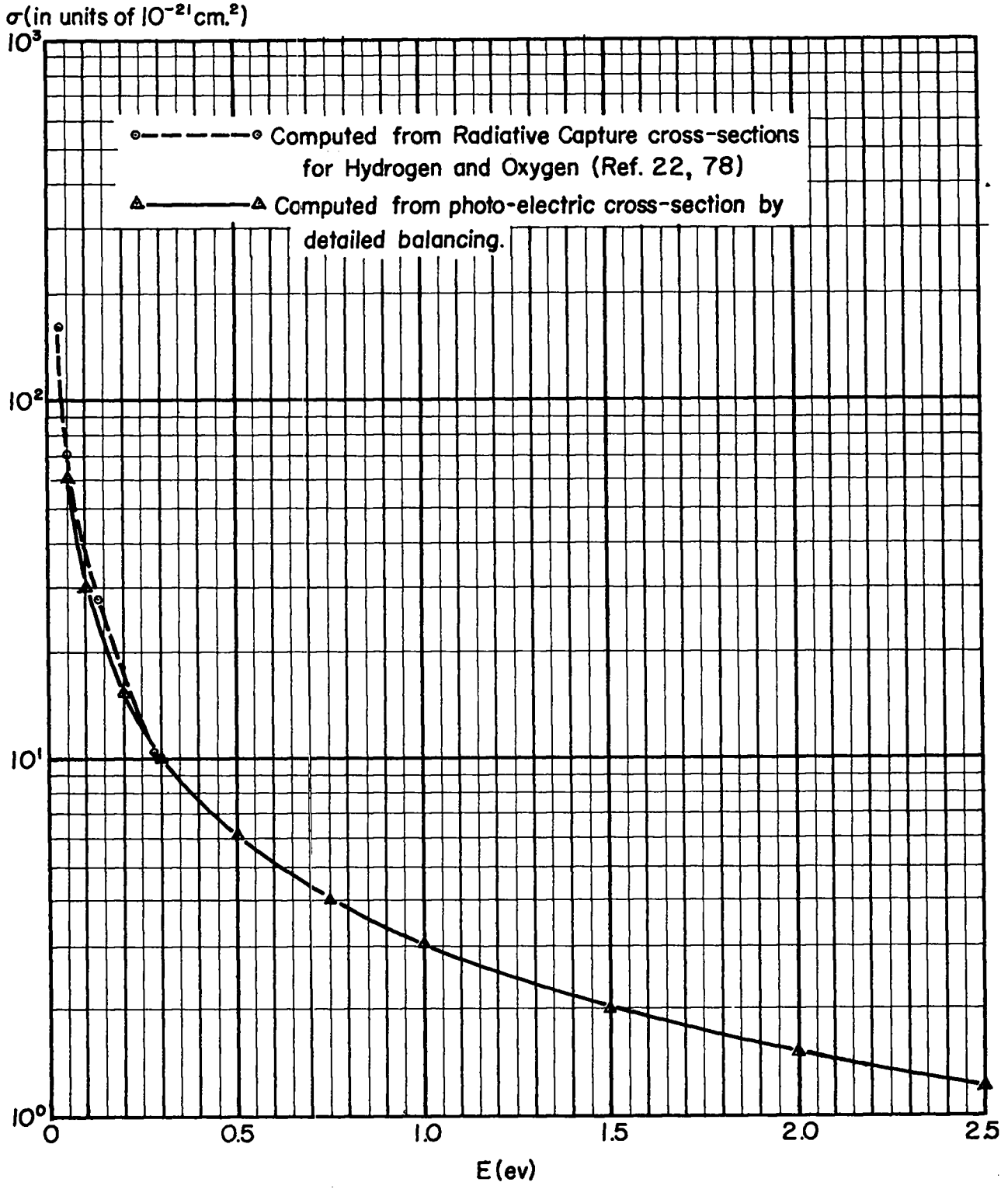


Fig. 18 Radiative Capture cross-section for the reaction $e+A^+ \rightarrow A+h\nu$

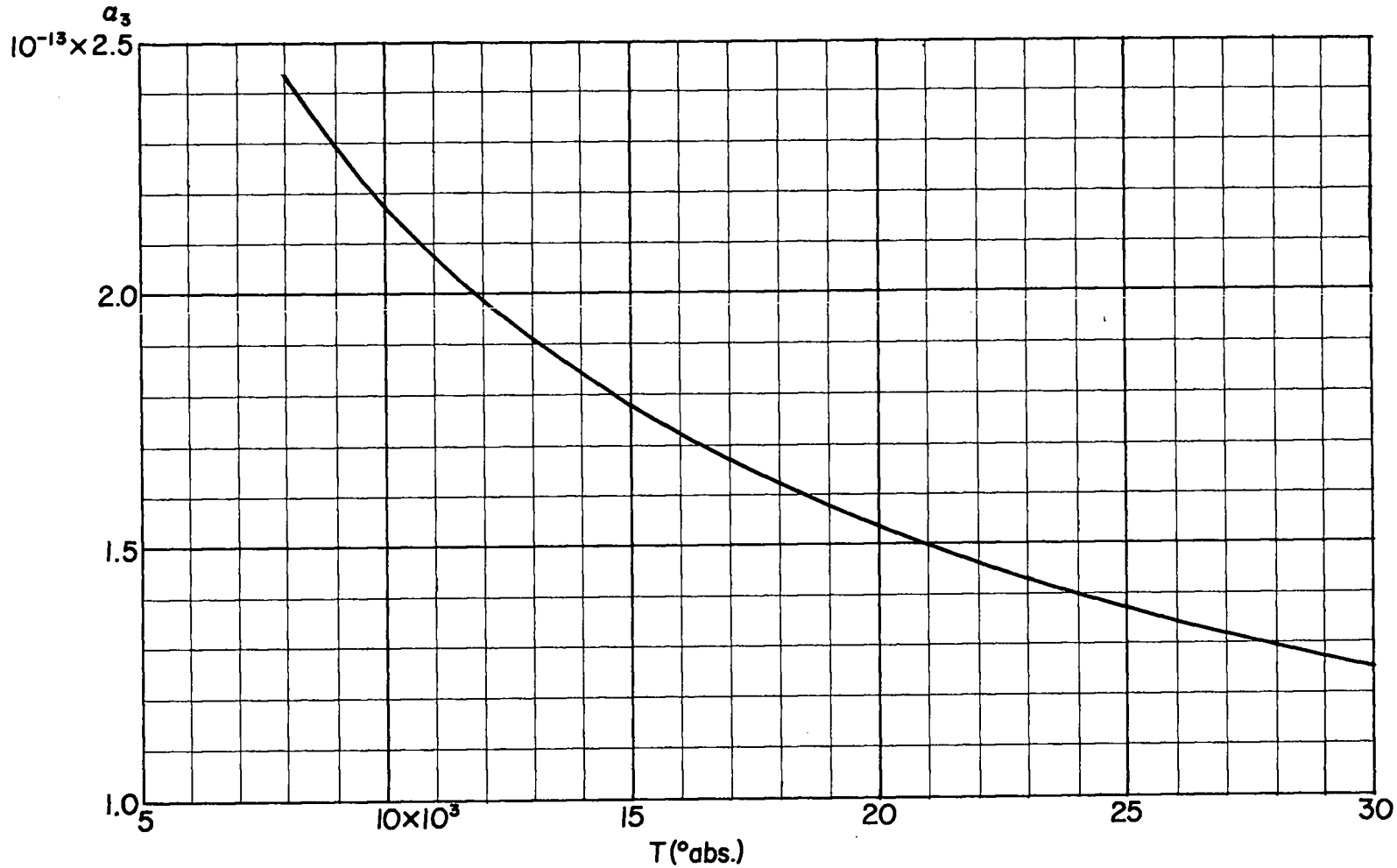


Fig. 19 Radiative recombination coefficient

TABLE I CONSTANTS AND CONVERSION FACTORS

| | | | |
|---|---|---|---|
| Boltzmann's constant | $k$ = | $1.380 \cdot 10^{-16}$ | ergs/degr. |
| Planck's constant | $h$ = | $6.624 \cdot 10^{-27}$ | erg-sec. |
| | = | $4.135 \cdot 10^{-15}$ | ev-sec. |
| | $\hbar$ = | $1.054 \cdot 10^{-27}$ | erg-sec. |
| Charge of electron | $e$ = | $4.803 \cdot 10^{-10}$ | esu |
| Gas constant | $R$ = | $8.3144 \cdot 10^{7}$ | ergs/mole-degr. |
| Avogadro's number | $N_o$ = | $6.023 \cdot 10^{23}$ | per mole. |
| First Bohr radius | $a_o = \frac{\hbar^2}{me^2}$ = | $5.292 \cdot 10^{-9}$ | cm. |
| | $\pi a_o^2$ = | $.8825 \cdot 10^{-16}$ | $cm^2$ |
| Volume of ideal gas (NTP) | $V_o$ = | 22,415 | $cm^3$/mole |
| Classical electron radius | $r_o = \frac{e^2}{mc^2}$ = | $2.8183 \cdot 10^{-13}$ | cm. |
| Mass of electron | $m_e$ = | $9.107 \cdot 10^{-28}$ | gm. |
| Electron volt | 1 ev = | 11,605 degr. = | $1.602 \cdot 10^{-12}$ ergs |
| | $\frac{hc}{k}$ = | 1.44 | degr.-cm. |
| | $R^*$ = | $R/M = 2.0815 \cdot 10^{6}$ | ergs/gm-degr. |
| Mass of argon atom | $m$ = | $6.632 \cdot 10^{-23}$ | gm. |
| Atomic weight of argon | $M$ = | 39.944 gm/mole. | |
| Ionization potential of A I | | 15.76 ev. | |
| Ionization potential of A II | | 27.62 ev. | |
| Total ionization potential of A II | | 43.4 ev. | |
| Atmospheric pressure (Los Alamos) | $p_1$ = | $.7887 \cdot 10^{6}$ | dynes/$cm^2$ |
| Normal temperature (Los Alamos) | $T_1$ = | $285^{\circ}$ | |
| Corresponding density for argon | $\rho_1$ = | $1.3314 \cdot 10^{-3}$ | gm/$cm^3$ |
| Number of argon atoms per $cm^3$ | $n_1$ = | $2.0075 \cdot 10^{19}$ | |

TABLE II ATOMIC CONSTANTS FOR ARGON

| State | $g_n$ | $E_n$ ($cm^{-1}$) | $E_n$ (degrees) |
|---|---|---|---|
| | | Argon atom, A | |
| $3p^6\ {}^1S$ | 1 | 0 | 0 |
| $3p^5$ d | 60 | 113,000 | 162,500 |
| Ionization energy | | 127,110 | 183,000 |
| | | Argon ion, $A^+$ | |
| $3s^2\ 3p^5$ | 4 | 0 | 0 |
| | 2 | 1432 | 2062 |
| $3s\ 3p^6$ | 2 | 108723 | 156560 |
| $3s^2\ 3p^4({}^3P)$ 3d | 8 | 132328 | 190550 |
| | 6 | 132482 | 190770 |
| | 4 | 132632 | 190990 |
| | 2 | 132739 | 191140 |
| $({}^3P)$ 4s | 6 | 134243 | 193310 |
| | 4 | 135087 | 194530 |
| | 2 | 135603 | 195270 |
| $({}^3P)$ 4s | 4 | 138245 | 199070 |
| | 2 | 139259 | 200530 |
| $({}^3P)$ 3d | 10 | 142187 | 204750 |
| | 8 | 142718 | 205510 |
| | 6 | 143109 | 206080 |
| | 4 | 143372 | 206460 |
| $({}^3P)$ 3d | 2 | 144711 | 208380 |
| | 4 | 145670 | 209760 |
| $({}^3P)$ 3d | 2 | 147229 | 212010 |
| | 4 | 147504 | 212410 |
| | 6 | 147877 | 212940 |
| $({}^1D)$ 4s | 4 | 148621 | 214010 |
| | 6 | 148843 | 214330 |
| $({}^3P)$ 3d | 8 | 148180 | 214820 |
| | 6 | 150149 | 216210 |
| $({}^3P)$ 3d | 4 | 150476 | 216690 |
| | 6 | 151088 | 217570 |

TABLE II ATOMIC CONSTANTS FOR ARGON (continued)

| State | $g_n$ | $E_n$ ($cm^{-1}$) | $E_n$ (degrees) |
|---|---|---|---|
| $(^3P)$ 4p | 6 | 155044 | 223260 |
| | 4 | 155352 | 223710 |
| | 2 | 155709 | 224220 |
| $(^3P)$ 4p | 8 | 157235 | 226420 |
| | 6 | 157674 | 227050 |
| | 4 | 158169 | 227760 |
| | 2 | 158429 | 228140 |
| $(^3P)$ 4p | 6 | 158731 | 228570 |
| | 4 | 159394 | 229530 |
| $(^3P)$ 4p | 2 | 159707 | 229980 |
| | 4 | 160240 | 230750 |
| $(^3P)$ 4p | 4 | 161050 | 231910 |
| $(^3P)$ 4p | 2 | 161090 | 231970 |
| $(^1S)$ 4s | 2 | 167309 | 240920 |
| $(^1D)$ 4p | 6 | 170402 | 245380 |
| | 8 | 170531 | 245560 |
| $(^1D)$ 4p | 4 | 172215 | 247990 |
| | 2 | 172817 | 248860 |
| $(^1D)$ 3d | 6 | 172336 | 248160 |
| | 4 | 172831 | 248880 |
| $(^1D)$ 4p | 4 | 173349 | 249620 |
| | 6 | 173394 | 249690 |
| $(^1D)$ 3d | 4 | 174411 | 251150 |
| | 2 | 174822 | 251740 |
| | 4 | 179593 | 258610 |
| | 2 | 179933 | 259100 |
| $(^3P)$ 5s | 6 | 181595 | 261500 |
| | 4 | 182223 | 262400 |
| | 2 | 182952 | 263450 |
| $(^3P)$ 5s | 4 | 183092 | 263650 |
| | 2 | 183916 | 264840 |
| $(^3P)$ 4d | 8 | 183676 | 264490 |
| | 6 | 183798 | 264670 |
| | 4 | 183987 | 264940 |
| | 2 | 184193 | 265240 |

TABLE II ATOMIC CONSTANTS FOR ARGON (continued)

| State | $g_n$ | $E_n$ ($cm^{-1}$) | $E_n$ (degrees) |
|---|---|---|---|
| ($^1$D) 3d | 2 | 184094 | 265100 |
| ($^3$P) 4d | 10 | 185094 | 266530 |
| | 8 | 185625 | 267300 |
| | 6 | 186075 | 267950 |
| | 4 | 186341 | 268330 |
| ($^3$P) 4d | 2 | 186172 | 268090 |
| | 4 | 186471 | 268520 |
| | 6 | 186892 | 269120 |
| ($^1$S) 3d | 6 | 186728 | 268890 |
| | 4 | 186751 | 268920 |
| Ionization energy | | 222820 | 320800 |

TABLE III HIGH EXCITED STATES OF ARGON

| State | $E_{n\ell}$ | $g_{n\ell}$ | Effective statistical weights $g_{n\ell}(\eta)$ | | | | | | | | | | | |
|---|---|---|---|---|---|---|---|---|---|---|---|---|---|---|
| | | | $\eta$ = 1 | 2 | 3 | 4 | 5 | 6 | 7 | 8 | 9 | 10 | 15 | 20 |
| 4s | 48,500 | 2 | 2 | 2 | 2 | 2 | 2 | 2 | 2 | 2 | 2 | 2 | 2 | 1 |
| 4p | 30,400 | 6 | 6 | 6 | 6 | 6 | 6 | 6 | 6 | 6 | 6 | 6 | 6 | 2 |
| 5s | 19,500 | 2 | 2 | 2 | 2 | 2 | 1 | 1 | 0 | 0 | 0 | 0 | 0 | 0 |
| 5p | 14,600 | 6 | 6 | 6 | 6 | 6 | 2 | 2 | 1 | 0 | 0 | 0 | 0 | 0 |
| 4d, 4f | 10,700 | 24 | 24 | 24 | 24 | 24 | 24 | 24 | 24 | 24 | 24 | 24 | 24 | 9 |
| 6s | 10,700 | 2 | 2 | 0 | 0 | 0 | 0 | 0 | 0 | 0 | 0 | 0 | 0 | 0 |
| 6p | 8,500 | 6 | 6 | 1 | 0 | 0 | 0 | 0 | 0 | 0 | 0 | 0 | 0 | 0 |
| 5d, f, g | 6,600 | 42 | 42 | 42 | 42 | 42 | 17 | 11 | 5 | 1 | 0 | 0 | 0 | 0 |
| 7s | 6,700 | 2 | 0 | 0 | 0 | 0 | 0 | 0 | 0 | 0 | 0 | 0 | 0 | 0 |
| 6d, f, g, h | 4,500 | 64 | 64 | 13 | 0 | 0 | 0 | 0 | 0 | 0 | 0 | 0 | 0 | 0 |

TABLE IV PARTITION FUNCTIONS AND EQUILIBRIUM CONSTANT FOR ARGON

| Density Ratio $\eta$ | Temp.($^{o}$abs.) T | $Z_{ion}$ | Z | K/2($p_1$= 59.3 cm. Hg) |
|---|---|---|---|---|
| 2 | 7500 | | 1.0000 | 5.4475 (-9)* |
| 3 | | | | 3.6317 " |
| 4 | | | | 2.7238 " |
| 5 | | | | 2.1790 " |
| 6 | | | | 1.8158 " |
| 7 | | | | 1.5564 " |
| 1 | 8000 | 5.5456 | 1.0000 | 5.5416 (-8) |
| 2 | | | | 2.7708 " |
| 3 | | | | 1.8472 " |
| 4 | | | | 1.3854 " |
| 5 | | | | 1.1083 " |
| 6 | | | | 9.2361 (-9) |
| 7 | | | | 7.9166 " |
| 8 | | | | 6.9270 " |
| 9 | | | | 6.1574 " |
| 10 | | | | 5.5416 " |
| 15 | | | | 3.6944 " |
| 20 | | | | 2.7708 " |
| 2 | 8500 | | 1.0000 | 1.1704 (-7) |
| 3 | | | | 7.8025 (-8) |
| 4 | | | | 5.8519 " |
| 5 | | | | 4.6815 " |
| 6 | | | | 3.9013 " |
| 7 | | | | 3.3439 " |
| 2 | 9000 | | 1.0000 | 4.2332 (-7) |
| 3 | | | | 2.8221 " |
| 4 | | | | 2.1166 " |
| 5 | | | | 1.6933 " |
| 6 | | | | 1.4111 " |
| 7 | | | | 1.2095 " |
| 8 | | | | 1.0583 " |
| 9 | | | | 9.4071 (-8) |
| 10 | | | | 8.4664 " |
| 15 | | | | 5.6443 " |
| 20 | | | | 4.2332 " |
| 2 | 9500 | 5.6098 | 1.0000 | 1.3432 (-6) |
| 3 | | | | 8.9549 (-7) |
| 4 | | | | 6.7162 " |
| 5 | | | | 5.3730 " |
| 6 | | | | 4.4775 " |
| 7 | | | | 3.8378 " |
| 8 | | | | |
| 9 | | | | |
| 10 | | | | |
| 15 | | | | |
| 20 | | | | 1.3433 " |

(continued)

TABLE IV PARTITION FUNCTIONS AND EQUILIBRIUM CONSTANT FOR ARGON

| Density Ratio $\eta$ | Temp.(°abs.) T | $Z_{ion}$ | Z | $K/2(p_1 = 59.3$ cm. Hg) |
|---|---|---|---|---|
| 1 | 10,000 | 5.6273 | 1.0000 | 7.6249 (-6) |
| 2 | | | | 3.8125 " |
| 3 | | | | 2.5417 " |
| 4 | | | | 1.9062 " |
| 5 | | | | 1.5250 " |
| 6 | | | | 1.2708 " |
| 7 | | | | 1.0893 " |
| 8 | | | | 9.5313 (-7) |
| 9 | | | | 8.4723 " |
| 10 | | | | 7.6251 " |
| 15 | | | | 5.0834 " |
| 20 | | | | 3.8126 " |
| 2 | 10,500 | 5.6434 | 1.0001 | 9.8326 (-6) |
| 3 | | | 1.0001 | 6.5551 " |
| 4 | | | 1.0001 | 4.9163 " |
| 5 | | | 1.0001 | 3.9331 " |
| 6 | | | 1.0001 | 3.2776 " |
| 7 | | | 1.0001 | 2.8094 " |
| 8 | | | 1.0001 | 2.4582 " |
| 9 | | | 1.0001 | 2.1850 " |
| 10 | | | 1.0001 | 1.9666 " |
| 15 | | | 1.0001 | 1.3110 " |
| 20 | | | 1.0000 | 9.8331 (-7) |
| 2 | 11,000 | 5.6581 | 1.0002 | 2.3341 (-5) |
| 3 | | | 1.0002 | 1.5561 " |
| 4 | | | 1.0002 | 1.1671 " |
| 5 | | | 1.0001 | 9.3367 (-6) |
| 6 | | | 1.0001 | 7.7806 " |
| 7 | | | 1.0001 | 6.6691 " |
| 8 | | | 1.0001 | 5.8355 " |
| 9 | | | 1.0001 | 5.1867 " |
| 10 | | | 1.0001 | 4.6684 " |
| 15 | | | 1.0001 | 3.1123 " |
| 20 | | | 1.0001 | 2.3343 " |
| 2 | 11,500 | 5.6717 | 1.0003 | 5.1544 (-5) |
| 3 | | | 1.0003 | 3.4364 " |
| 4 | | | 1.0003 | 2.5773 " |
| 5 | | | 1.0003 | 2.0619 " |
| 6 | | | 1.0003 | 1.7183 " |
| 7 | | | 1.0003 | 1.4728 " |
| 8 | | | 1.0002 | 1.2887 " |
| 9 | | | 1.0002 | 1.1454 " |
| 10 | | | 1.0002 | 1.0310 " |
| 15 | | | 1.0002 | 6.8733 (-6) |
| 20 | | | 1.0001 | 5.1555 " |

(continued)

TABLE IV PARTITION FUNCTIONS AND EQUILIBRIUM CONSTANT FOR ARGON

| Density Ratio $\eta$ | Temp.($^{o}$abs.) T | $Z_{ion}$ | Z | K/2($p_1$ = 59.3 cm. Hg) |
|---|---|---|---|---|
| 2 | 12,000 | 5.6842 | 1.0006 | 1.0684 (-4) |
| 3 | | | 1.0005 | 7.1226 (-5) |
| 4 | | | 1.0005 | 5.3419 " |
| 5 | | | 1.0005 | 4.2739 " |
| 6 | | | 1.0004 | 3.5616 " |
| 7 | | | 1.0004 | 3.0529 " |
| 8 | | | 1.0004 | 2.6713 " |
| 9 | | | 1.0004 | 2.3738 " |
| 10 | | | 1.0004 | 2.1371 " |
| 15 | | | 1.0004 | 1.4247 " |
| 20 | | | 1.0002 | 1.0687 " |
| 2 | 13,000 | 5.7067 | 1.0016 | 3.9047 (-4) |
| 3 | | | 1.0015 | 2.6034 " |
| 4 | | | 1.0015 | 1.9525 " |
| 5 | | | 1.0013 | 1.5624 " |
| 6 | | | 1.0012 | 1.3021 " |
| 7 | | | 1.0011 | 1.1161 " |
| 8 | | | 1.0011 | 9.7668 (-5) |
| 9 | | | 1.0011 | 8.6723 " |
| 10 | | | 1.0011 | 7.8134 " |
| 15 | | | 1.0011 | 5.2089 " |
| 20 | | | 1.0006 | 3.9087 " |
| 2 | 14,000 | 5.7262 | 1.0039 | 1.1941 (-3) |
| 3 | | | 1.0036 | 7.9625 (-4) |
| 4 | | | 1.0036 | 5.9719 " |
| 5 | | | 1.0030 | 4.7807 " |
| 6 | | | 1.0029 | 3.9844 " |
| 7 | | | 1.0027 | 3.4159 " |
| 8 | | | 1.0025 | 2.9893 " |
| 9 | | | 1.0025 | 2.6487 " |
| 10 | | | 1.0025 | 2.3914 " |
| 15 | | | 1.0025 | 1.5943 " |
| 20 | | | 1.0013 | 1.1971 " |
| 2 | 15,000 | 5.7434 | 1.0084 | 3.1607 (-3) |
| 3 | | | 1.0079 | 2.1083 " |
| 4 | | | 1.0079 | 1.5812 " |
| 5 | | | 1.0063 | 1.2669 " |
| 6 | | | 1.0060 | 1.0560 " |
| 7 | | | 1.0056 | 9.0559 (-4) |
| 8 | | | 1.0053 | 7.9259 " |
| 9 | | | 1.0053 | 7.0456 " |
| 10 | | | 1.0053 | 6.3410 " |
| 15 | | | 1.0053 | 4.2274 " |
| 20 | | | 1.0028 | 3.1784 " |

(continued)

TABLE IV. PARTITION FUNCTIONS AND EQUILIBRIUM CONSTANT FOR ARGON

| Density Ratio $\eta$ | Temp.($^{o}$abs.) T | $Z_{ion}$ | Z | K/2($p_1$= 59.3 cm. Hg) |
|---|---|---|---|---|
| 2 | 15,500 | 5.7512 | 1.0119 | 4.9106 (-3) |
| 3 | | | 1.0111 | 3.2764 " |
| 4 | | | 1.0111 | 2.4573 " |
| 5 | | | 1.0089 | 1.9702 " |
| 6 | | | 1.0085 | 1.6425 " |
| 7 | | | 1.0078 | 1.4088 " |
| 8 | | | 1.0075 | 1.2331 " |
| 9 | | | 1.0074 | 1.0962 " |
| 10 | | | 1.0074 | 9.8655 (-4) |
| 15 | | | 1.0074 | 6.5770 " |
| 20 | | | 1.0039 | 4.9499 " |
| 2 | 16,000 | 5.7587 | 1.0166 | 7.4237 (-3) |
| 3 | | | 1.0154 | 4.9549 " |
| 4 | | | 1.0154 | 3.7161 " |
| 5 | | | 1.0123 | 2.9822 " |
| 6 | | | 1.0117 | 2.4866 " |
| 7 | | | 1.0108 | 2.1333 " |
| 8 | | | 1.0101 | 1.8678 " |
| 9 | | | 1.0101 | 1.6603 " |
| 2 | 17,000 | 5.7727 | 1.0304 | 1.5758 (-2) |
| 3 | | | 1.0281 | 1.0529 " |
| 4 | | | 1.0281 | 7.8965 (-3) |
| 5 | | | 1.0221 | 6.3545 " |
| 6 | | | 1.0210 | 5.3010 " |
| 7 | | | 1.0193 | 4.5515 " |
| 8 | | | 1.0182 | 3.9865 " |
| 9 | | | 1.0181 | 3.5442 " |
| 10 | | | 1.0181 | 3.1898 " |
| 15 | | | 1.0181 | 2.1265 " |
| 20 | | | 1.0096 | 1.6083 " |
| 2 | 18,000 | 5.7857 | 1.0547 | 3.0571 (-2) |
| 3 | | | 1.0480 | 2.0511 " |
| 4 | | | 1.0480 | 1.5383 " |
| 5 | | | 1.0374 | 1.2433 " |
| 6 | | | 1.0354 | 1.0380 " |
| 7 | | | 1.0324 | 8.9238 (-3) |
| 8 | | | 1.0306 | 7.8219 " |
| 9 | | | 1.0302 | 6.9549 " |
| 10 | | | 1.0302 | 6.2594 " |
| 15 | | | 1.0302 | 4.1730 " |
| 20 | | | 1.0161 | 3.1733 " |

(continued)

TABLE IV PARTITION FUNCTIONS AND EQUILIBRIUM CONSTANT FOR ARGON

| Density Ratio $n$ | Temp.($^{\circ}$abs.) T | $Z_{ion}$ | Z | K/2($p_1$ = 59.3 cm. Hg) |
|---|---|---|---|---|
| 3 | 19,000 | 5.7981 | 1.0777 | 3.7016 (-2) |
| 4 | | | 1.0777 | 2.7762 " |
| 5 | | | 1.0599 | 2.2583 " |
| 6 | | | 1.0567 | 1.8877 " |
| 7 | | | 1.0516 | 1.6259 " |
| 8 | | | 1.0486 | 1.4267 " |
| 9 | | | 1.0480 | 1.2688 " |
| 10 | | | 1.0480 | 1.1419 " |
| 15 | | | 1.0480 | 7.6129 (-3) |
| 20 | | | 1.0256 | 5.8346 " |
| 3 | 20,000 | 5.8106 | 1.1200 | 6.2398 (-2) |
| 4 | | | 1.1200 | 4.6799 " |
| 5 | | | 1.0918 | 3.8407 " |
| 6 | | | 1.0866 | 3.2157 " |
| 7 | | | 1.0786 | 2.7770 " |
| 8 | | | 1.0738 | 2.4405 " |
| 9 | | | 1.0730 | 2.1711 " |
| 10 | | | 1.0730 | 1.9540 " |
| 15 | | | 1.0730 | 1.3026 " |
| 20 | | | 1.0389 | 1.0090 " |
| 3 | 21,000 | 5.8235 | 1.1780 | 9.8903 (-2) |
| 4 | | | 1.1780 | 7.4178 " |
| 5 | | | 1.1352 | 6.1581 " |
| 6 | | | 1.1273 | 5.1675 " |
| 7 | | | 1.1152 | 4.4777 " |
| 8 | | | 1.1080 | 3.9433 " |
| 9 | | | 1.1067 | 3.5093 " |
| 10 | | | 1.1067 | 3.1584 " |
| 15 | | | 1.1067 | 2.1056 " |
| 20 | | | 1.0569 | 1.6536 " |
| 4 | 22,000 | | 1.2551 | 1.1120 (-1) |
| 5 | | | 1.1925 | 9.3632 (-2) |
| 6 | | | 1.1810 | 7.8789 " |
| 7 | | | 1.1632 | 6.8565 " |
| 8 | | | 1.1528 | 6.0538 " |
| 9 | | | 1.1508 | 5.3902 " |
| 10 | | | 1.1508 | 4.8512 " |
| 15 | | | 1.1508 | 3.2341 " |
| 20 | | | 1.0805 | 2.5835 " |

(continued)

TABLE IV PARTITION FUNCTIONS AND EQUILIBRIUM CONSTANT FOR ARGON

| Density Ratio $\eta$ | Temp.(°abs.) T | $Z_{ion}$ | Z | K/2($p_1$ = 59.3 cm. Hg) |
|---|---|---|---|---|
| 4 | 23,000 | 5.8531 | 1.3547 | 1.5854 (-1) |
| 5 | | | 1.2661 | 1.3571 " |
| 6 | | | 1.2497 | 1.1457 " |
| 7 | | | 1.2247 | 1.0021 " |
| 8 | | | 1.2099 | 8.8759 (-2) |
| 9 | | | 1.2072 | 7.9075 " |
| 10 | | | 1.2072 | 7.1168 " |
| 15 | | | 1.2072 | 4.7445 " |
| 20 | | | 1.1105 | 3.8680 " |
| 4 | 24,000 | 5.8712 | 1.4804 | 2.1610 (-1) |
| 5 | | | 1.3585 | 1.8839 " |
| 6 | | | 1.3359 | 1.5965 " |
| 7 | | | 1.3015 | 1.4046 " |
| 8 | | | 1.2812 | 1.2485 " |
| 9 | | | 1.2774 | 1.1131 " |
| 10 | | | 1.2774 | 1.0018 " |
| 15 | | | 1.2774 | 6.6784 (-2) |
| 20 | | | 1.1480 | 5.5736 " |
| 4 | 25,000 | 5.8925 | 1.6357 | 2.8312 (-1) |
| 5 | | | 1.4721 | 2.5165 " |
| 6 | | | 1.4417 | 2.1414 " |
| 7 | | | 1.3957 | 1.8960 " |
| 8 | | | 1.3684 | 1.6921 " |
| 9 | | | 1.3633 | 1.5097 " |
| 10 | | | 1.3633 | 1.3587 " |
| 15 | | | 1.3633 | 9.0582 (-2) |
| 20 | | | 1.1937 | 7.7589 " |
| 4 | 26,000 | 5.9178 | 1.8242 | 3.5831 (-1) |
| 5 | | | 1.6095 | 3.2489 " |
| 6 | | | 1.5693 | 2.7767 " |
| 7 | | | 1.5091 | 2.4751 " |
| 8 | | | 1.4732 | 2.2184 " |
| 9 | | | 1.4665 | 1.9810 " |
| 10 | | | 1.4665 | 1.7829 " |
| 15 | | | 1.4665 | 1.1886 " |
| 20 | | | 1.4665 | 1.0470 " |

* (-9) = $10^{-9}$

TABLE V EQUILIBRIUM CONDITIONS BEHIND THE SHOCK FRONT

| U cm/sec | $\eta$ | T degr. abs. | $\xi$ | u cm/sec | $\sigma$ | $\beta$ | $[A^+]$ | $[A]$ | g |
|---|---|---|---|---|---|---|---|---|---|
| | | | | A. $p_1$ = 59.38 cm. Hg. | | | | | |
| 3.0 $10^5$ | 3.91 | 8322 | 114.07 | 2.2327 $10^5$ | 1.6580 | 2.5198 | .000 | 1.000 | 1.000 |
| 3.5 " | 4.08 | 10918 | 157.11 | 2.6422 " | 1.6285 | 2.5911 | .005 | .995 | 1.005 |
| 4.0 " | 4.55 | 13018 | 211.73 | 3.1209 " | 1.5487 | 2.8225 | .019 | .981 | 1.019 |
| 4.5 " | 5.17 | 14650 | 276.72 | 3.6296 " | 1.4700 | 3.1277 | .041 | .959 | 1.041 |
| 5.0 " | 5.82 | 16023 | 350.51 | 4.1409 " | 1.4069 | 3.4576 | .071 | .929 | 1.071 |
| 5.5 " | 6.483 | 17250 | 432.88 | 4.6516 " | 1.3585 | 3.7894 | .103 | .897 | 1.103 |
| 6.0 " | 7.123 | 18400 | 523.40 | 5.1577 " | 1.3216 | 4.1095 | .138 | .862 | 1.138 |
| 6.5 " | 7.722 | 19480 | 621.86 | 5.6582 " | 1.2934 | 4.4083 | .178 | .822 | 1.178 |
| 7.0 " | 8.264 | 20551 | 728.08 | 6.1530 " | 1.2718 | 4.6792 | .222 | .778 | 1.222 |
| 7.5 " | 8.79 | 21602 | 842.53 | 6.6468 " | 1.2538 | 4.9401 | .265 | .735 | 1.265 |
| 8.0 " | 9.17 | 22777 | 963.57 | 7.1276 " | 1.2422 | 5.1288 | .315 | .685 | 1.315 |
| 8.5 " | 9.59 | 23880 | 1093.48 | 7.6137 " | 1.2306 | 5.3365 | .361 | .639 | 1.361 |
| 9.0 " | 9.925 | 25072 | 1230.60 | 8.0932 " | 1.2221 | 5.5025 | .409 | .591 | 1.409 |
| | | | | B. $p_1$ = 1.0 cm. Hg. | | | | | |
| 3.0 $10^5$ | 3.983 | 8200 | 114.78 | 2.2468 $10^5$ | 1.6416 | 2.5536 | .002 | .998 | 1.002 |
| 3.5 " | 4.491 | 10066 | 161.75 | 2.7207 " | 1.5536 | 2.8064 | .020 | .980 | 1.020 |
| 4.0 " | 5.330 | 11304 | 220.42 | 3.2495 " | 1.4487 | 3.2287 | .043 | .957 | 1.043 |
| 4.5 " | 6.226 | 12250 | 287.94 | 3.7772 " | 1.3731 | 3.6802 | .076 | .924 | 1.076 |
| 5.0 " | 7.20 | 12987 | 364.41 | 4.3056 " | 1.3153 | 4.1716 | .111 | .889 | 1.111 |
| 5.5 " | 8.03 | 13768 | 448.06 | 4.8151 " | 1.2787 | 4.5881 | .155 | .845 | 1.155 |
| 6.0 ' | 8.95 | 14381 | 540.82 | 5.3296 " | 1.2470 | 5.0486 | .198 | .802 | 1.198 |
| 6.5 " | 9.815 | 14989 | 641.56 | 5.8377 " | 1.2231 | 5.4823 | .243 | .757 | 1.243 |
| 7.0 " | 10.57 | 15630 | 749.92 | 6.3377 " | 1.2057 | 5.8614 | .294 | .706 | 1.294 |
| 7.5 " | 11.35 | 16224 | 866.90 | 6.8392 " | 1.1905 | 6.2493 | .342 | .658 | 1.342 |
| 8.0 " | 11.97 | 16802 | 991.13 | 7.3317 " | 1.1799 | 6.5586 | .404 | .596 | 1.404 |
| 8.5 " | 12.63 | 17401 | 1124.09 | 7.8270 " | 1.1699 | 6.8858 | .458 | .542 | 1.458 |
| 9.0 " | 13.05 | 18072 | 1263.59 | 8.3103 " | 1.1641 | 7.0938 | .527 | .473 | 1.527 |

TABLE VI THE NON-EQUILIBRIUM REGION ($p_1$ = 59.38 cm. Hg.)

A. $U = 5.0 \cdot 10^5$ cm./sec.

| $\eta$ | T °abs. | $\xi$ | u cm./sec. | $[A^+]$ | X cm. | t sec. |
|---|---|---|---|---|---|---|
| 3.9532 | 22801 | 316.27 | | 0 | 0 | 0 |
| 3.9532 | 22801 | 316.27 | | 0 | $5.6916 \cdot 10^{-3}$ | $4.50 \cdot 10^{-8}$ |
| 3.9532 | 22800 | 316.27 | $3.7351 \cdot 10^5$ | $2.546 \cdot 10^{-8}$ | 6.0078 " | 4.75 " |
| 3.9532 | 22800 | 316.27 | 3.7351 " | $6.366$ " | 6.3240 " | 5.00 " |
| 3.9532 | 22800 | 316.27 | 3.7351 " | $1.400^{-7}$ | 6.6402 " | 5.25 " |
| 3.9532 | 22800 | 316.27 | 3.7352 " | $3.475^{-6}$ | 7.9049 " | 6.25 " |
| 3.9550 | 22791 | 316.31 | 3.7354 " | $8.539^{-5}$ | 9.1692 " | 7.25 " |
| 3.9925 | 22609 | 317.32 | 3.7425 " | $1.821^{-3}$ | $1.0421^{-2}$ | 8.25 " |
| 4.1572 | 21842 | 321.50 | | $9.052^{-2}$ | 1.1624 " | 9.25 " |
| 4.2686 | 21338 | 324.15 | 3.8155 " | 1.423 " | 1.1917 " | 9.50 " |
| 4.3240 | 21098 | 325.42 | 3.8364 " | 1.657 " | 1.2032 " | 9.60 " |
| 4.3799 | 20859 | 326.67 | 3.8513 " | 1.896 " | 1.2146 " | 9.70 " |
| 4.4366 | 20622 | 327.90 | 3.8659 " | 2.135 " | 1.2259 " | 9.80 " |
| 4.4928 | 20391 | 329.09 | 3.8802 " | 2.369 " | 1.2370 " | 9.90 " |
| 4.5481 | 20169 | 330.23 | 3.8940 " | 2.596 " | 1.2480 " | $1.00^{-7}$ |
| 4.6742 | 19673 | 332.73 | 3.9170 " | 3.118 " | 1.2748 " | 1.025 " |
| 4.7915 | 19233 | 334.94 | 3.9444 " | 3.579 " | 1.3009 " | 1.05 " |
| 4.8963 | 18854 | 336.83 | 3.9682 " | 3.979 " | 1.3264 " | 1.075 " |
| 4.9863 | 18540 | 338.38 | 3.9883 " | 4.313 " | 1.3515 " | 1.10 " |
| 5.0648 | 18273 | 339.69 | 4.0051 " | 4.600 " | 1.3761 " | 1.125 " |
| 5.1334 | 18046 | 340.81 | 4.0193 " | 4.846 " | 1.4005 " | 1.15 " |
| 5.1935 | 17851 | 341.76 | 4.0315 " | 5.058 " | 1.4246 " | 1.175 " |
| 5.3571 | 17332 | 344.24 | 4.0545 " | 5.659 " | 1.5179 " | 1.275 " |
| 5.4742 | 16982 | 345.93 | 4.0775 " | 6.045 " | 1.6092 " | 1.375 " |
| 5.6491 | 16515 | 348.31 | 4.1433 " | 6.398 " | 1.8305 " | 3.875 " |
| 5.7231 | 16294 | 349.28 | 4.1369 " | 6.742 " | 2.0489 " | 6.375 " |
| 5.8200 | 16023 | 350.51 | | .071 | $\infty$ | $\infty$ |

TABLE VI THE NON-EQUILIBRIUM REGION ($p_1$ = 59.38 cm. Hg.)

B. $U = 5.5 \cdot 10^5$

| $\eta$ | T °abs. | $\xi$ | u cm./sec. | $[A^+]$ | X cm. | t sec. |
|---|---|---|---|---|---|---|
| 3.9587 | 27571 | 382.73 | | 0 | 0 | 0 |
| 3.9587 | 27571 | 382.73 | | 0 | $7.6416 \cdot 10^{-4}$ | $5.50 \cdot 10^{-9}$ |
| 3.9612 | 27536 | 382.73 | $4.1054 \cdot 10^5$ | $1.973 \cdot 10^{-7}$ | 9.0298 " | 6.50 " |
| 3.9612 | 27536 | 382.73 | 4.1059 " | 1.254 " | 1.0418 " | 7.50 " |
| 3.9613 | 27535 | 382.74 | 4.1059 " | 7.970 " | 1.1806 " | 8.50 " |
| 3.9621 | 27530 | 382.76 | 4.1061 " | 5.061 " | 1.3194 " | 9.50 " |
| 3.9672 | 27499 | 382.93 | 4.1071 " | 3.183 " | 1.4581 " | 1.05 " |
| 3.9971 | 27319 | 383.89 | 4.1135 " | 1.895 " | 1.5957 " | 1.15 " |
| 4.1266 | 26559 | 387.90 | 4.1462 " | 8.652 " | 1.7289 " | 1.25 " |
| 4.1930 | 26183 | 389.86 | 4.1726 " | 1.201 " | 1.7617 " | 1.275 " |
| 4.2243 | 26009 | 390.76 | 4.1874 " | 1.356 " | 1.7748 " | 1.285 " |
| 4.2571 | 25829 | 391.69 | 4.1973 " | 1.520 " | 1.7877 " | 1.295 " |
| 4.2918 | 25640 | 392.66 | 4.2075 " | 1.693 " | 1.8005 " | 1.305 " |
| 4.3282 | 25444 | 393.66 | 4.2181 " | 1.873 " | 1.8132 " | 1.315 " |
| 4.3660 | 25243 | 394.68 | 4.2290 " | 2.058 " | 1.8258 " | 1.325 " |
| 4.4048 | 25040 | 395.71 | 4.2400 " | 2.247 " | 1.8383 " | 1.335 " |
| 4.4444 | 24835 | 396.75 | 4.2511 " | 2.438 " | 1.8507 " | 1.345 " |
| 4.4844 | 24631 | 397.77 | 4.2621 " | 2.630 " | 1.8629 " | 1.355 " |
| 4.5246 | 24428 | 398.79 | 4.2731 " | 2.821 " | 1.8751 " | 1.365 " |
| 4.5648 | 24229 | 399.78 | 4.2839 " | 3.010 " | 1.8871 " | 1.375 " |
| 4.6047 | 24034 | 400.75 | 4.2944 " | 3.196 " | 1.8991 " | 1.385 " |
| 4.6441 | 23844 | 401.69 | 4.3046 " | 3.379 " | 1.9109 " | 1.395 " |
| 4.6829 | 23659 | 402.60 | 4.3146 " | 3.557 " | 1.9227 " | 1.405 " |
| 4.7731 | 23236 | 404.66 | 4.3311 " | 3.981 " | 1.9515 " | 1.43 " |
| 4.8608 | 22839 | 406.59 | 4.3524 " | 4.373 " | 1.9798 " | 1.455 " |
| 4.9427 | 22480 | 408.33 | 4.3720 " | 4.731 " | 2.0076 " | 1.48 " |
| 5.0187 | 22155 | 409.90 | 4.3896 " | 5.058 " | 2.0350 " | 1.505 " |
| 5.0890 | 21862 | 411.30 | 4.4055 " | 5.355 " | 2.0620 " | 1.53 " |
| 5.1540 | 21597 | 412.57 | 4.4198 " | 5.626 " | 2.0887 " | 1.555 " |
| 5.2141 | 21358 | 413.71 | 4.4327 " | 5.873 " | 2.1150 " | 1.58 " |
| 5.3988 | 20639 | 417.06 | 4.4593 " | 6.668 " | 2.2169 " | 1.68 " |
| 5.5515 | 20085 | 419.66 | 4.4898 " | 7.258 " | 2.3160 " | 1.78 " |
| 5.6740 | 19661 | 421.65 | 4.5138 " | 7.714 " | 2.4129 " | 1.88 " |
| 5.7737 | 19328 | 423.20 | 4.5326 " | 8.076 " | 2.5082 " | 1.98 " |
| 5.8540 | 19067 | 424.41 | 4.5474 " | 8.360 " | 2.6021 " | 2.08 " |
| 5.9935 | 18621 | 426.44 | 4.5655 " | 8.890 " | 2.8315 " | 2.33 " |
| 6.1019 | 18295 | 427.96 | 4.5841 " | 9.253 " | 3.0569 " | 2.58 " |
| 6.1808 | 18064 | 429.03 | 4.5979 " | 9.507 " | 3.2793 " | 2.83 " |
| 6.3262 | 17645 | 430.92 | 4.6161 " | $1.001 \cdot 10^{-1}$ | 4.1487 " | 3.83 " |
| 6.3954 | 17459 | 431.80 | 4.6294 " | 1.021 " | 5.0087 " | 4.83 " |
| 6.483 | 17250 | 432.88 | | .103 | $\infty$ | $\infty$ |

TABLE VI THE NON-EQUILIBRIUM REGION ($p_1$ = 59.38 cm. Hg.)

C. U = $6.0 \cdot 10^5$ cm./sec.

| $\eta$ | T °abs. | $\xi$ | u cm./sec. | $[A^+]$ | X cm. | t sec. |
|---|---|---|---|---|---|---|
| 3.9674 | 32724 | 455.54 | | 0 | 0 | 0 |
| 3.9674 | 32724 | 455.54 | | 0 | $1.3611 \cdot 10^{-4}$ | $9.00 \cdot 10^{-10}$ |
| 3.9674 | 32723 | 455.54 | $4.4876 \cdot 10^5$ | $1.336 \cdot 10^{-7}$ | 1.7391 " | 1.15 $^{-9}$ |
| 3.9674 | 32723 | 455.54 | 4.4876 " | 7.957 " | 2.1172 " | 1.40 " |
| 3.9674 | 32722 | 455.54 | 4.4876 " | 4.723 $^{-6}$ | 2.4953 " | 1.65 " |
| 3.9678 | 32719 | 455.55 | 4.4877 " | 2.804 $^{-5}$ | 2.8733 " | 1.90 " |
| 3.9701 | 32702 | 455.64 | 4.4882 " | 1.658 $^{-4}$ | 3.2512 " | 2.15 " |
| 3.9836 | 32602 | 456.16 | 4.4913 " | 9.612 " | 3.6277 " | 2.40 " |
| 4.0522 | 32102 | 458.74 | 4.5080 " | 4.999 $^{-3}$ | 3.9979 " | 2.65 " |
| 4.2699 | 30591 | 466.39 | 4.5741 " | 1.756 $^{-2}$ | 4.3491 " | 2.90 " |
| 4.4227 | 29597 | 471.30 | 4.6223 " | 2.609 " | 4.4848 " | 3.00 " |
| 4.4687 | 29314 | 472.72 | 4.6503 " | 2.842 " | 4.5184 " | 3.025 " |
| 4.5125 | 29044 | 474.04 | 4.6638 " | 3.078 " | 4.5516 " | 3.05 " |
| 4.5567 | 28775 | 475.35 | 4.6767 " | 3.315 " | 4.5845 " | 3.075 " |
| 4.6014 | 28508 | 476.64 | 4.6896 " | 3.552 " | 4.6171 " | 3.10 " |
| 4.6461 | 28245 | 477.91 | 4.7022 " | 3.787 " | 4.6494 " | 3.125 " |
| 4.6908 | 27986 | 479.16 | 4.7146 " | 4.020 " | 4.6814 " | 3.15 " |
| 4.7351 | 27733 | 480.37 | 4.7267 " | 4.250 " | 4.7131 " | 3.175 " |
| 4.7790 | 27486 | 481.55 | 4.7385 " | 4.475 " | 4.7445 " | 3.20 " |
| 4.8223 | 27246 | 482.69 | 4.7500 " | 4.695 " | 4.7756 " | 3.225 " |
| 4.9787 | 26400 | 486.65 | 4.7768 " | 5.517 " | 4.8961 " | 3.325 " |
| 5.1292 | 25635 | 490.23 | 4.8134 " | 6.251 " | 5.0131 " | 3.425 " |
| 5.2649 | 24980 | 493.28 | 4.8457 " | 6.891 " | 5.1270 " | 3.525 " |
| 5.3857 | 24421 | 495.87 | 4.8732 " | 7.445 " | 5.2384 " | 3.625 " |
| 5.4929 | 23944 | 498.08 | 4.8966 " | 7.925 " | 5.3477 " | 3.725 " |
| 5.5883 | 23533 | 499.96 | 4.9167 " | 8.344 " | 5.4550 " | 3.825 " |
| 5.6735 | 23177 | 501.60 | 4.9340 " | 8.711 " | 5.5608 " | 3.925 " |
| 5.7501 | 22865 | 503.02 | 4.9491 " | 9.036 " | 5.6651 " | 4.025 " |
| 5.8991 | 22268 | 505.69 | 4.9699 " | 9.707 " | 5.9194 " | 4.275 " |
| 6.0297 | 21778 | 507.92 | 4.9937 " | 1.023 $^{-1}$ | 6.1682 " | 4.525 " |
| 6.1379 | 21386 | 509.70 | 5.0133 " | 1.065 " | 6.4125 " | 4.775 " |
| 6.2284 | 21069 | 511.14 | 5.0291 " | 1.100 " | 6.6534 " | 5.025 " |
| 6.3051 | 20807 | 512.33 | 5.0421 " | 1.129 " | 6.8913 " | 5.275 " |
| 6.4941 | 20169 | 515.13 | 5.0630 " | 1.208 " | 7.8152 " | 6.275 " |
| 6.6381 | 19721 | 517.16 | 5.0859 " | 1.258 " | 8.7190 " | 7.275 " |
| 6.7403 | 19415 | 518.55 | 5.1026 " | 1.292 " | 9.6092 " | 8.275 " |
| 6.8678 | 19038 | 520.22 | 5.1182 " | 1.339 " | 1.1793 $^{-3}$ | 1.0775 $^{-8}$ |
| 6.9482 | 18814 | 521.25 | 5.1313 " | 1.363 " | 1.3952 " | 1.3275 " |
| 7.0327 | 18582 | 522.30 | 5.1432 " | 1.389 " | 2.2483 " | 2.3275 " |
| 7.0485 | 18544 | 522.49 | 5.1479 " | 1.391 " | 3.0996 " | 3.3275 " |
| 7.123 | 18400 | 523.40 | | .139 | $\infty$ | $\infty$ |

REFERENCES


1. Rompe, R. and Steenbeck, M., The Plasma State of Gases. Koppers Co. Inc., 1950.
2. Arnot, F. L., Collision Processes in Gases. New York: John Wiley and Sons, Inc., 1950.
3. Goldstein, Herbert, Classical Mechanics. Cambridge, Massachusetts: Addison-Wesley Press, 1950.
4. Grad, Harold, Kinetic Theory and Statistical Mechanics. (Lecture Notes). New York University, 1950.
5. Bates, D. R., Massey, H. S. W. and Stewart, A. L., Proc. Roy. Soc., 216A, 437 (1953).
6. Hartree, D. R., Rep. Progr. Phys., 11, 113 (1946-7).
7. Mott, N. F. and Sneddon, I. N., Wave Mechanics and Its Applications. Oxford: The Clarendon Press, 1948.
8. Hartree, D. R. and Hartree, W., Proc. Roy. Soc., 166A, 450 (1938).
9. Dalgarno, A., Proc. Phys. Soc. (London), 65A, 663-7 (1952).
10. Valentine, J. M., Proc. Roy. Soc., 211A, 75-85 (1952).
11. Kirshner, J. M., and Toffolo, D. S., J. Appl. Phys., 23, 594-8 (1952).
12. Thomson, J. J., Phil. Mag., 47, 337 (1924).
13. Barbiere, D., Phys. Rev., 84, 653-8 (1951).
14. Dalgarno, A., Proc. Phys. Soc. (London), 65A, 663-7 (1952).
15. Knipp, J. K. and Ling, R. C., Phys. Rev., 82, 30-5 (1951).
16. Holtsmark, J., Z. Phys., 55, 437 (1929).
17. Normand, C. E., Phys. Rev., 35, 1217 (1930).
18. Füchtbauer, Chr., Schulz, P. and Brandt, A. F., Z. Phys., 90, 403 (1934).
19. Tsi-Zé, Ny and Shang-Yi, Ch'en, Phys. Rev., 51, 567 (1937).

## REFERENCES


20. Wahlin, H. B., Phys. Rev., 37, 260 (1931).

21. Townsend, J. S., Motion of Electrons in Gases. Oxford: The Clarendon Press, 1925.

22. Massey, H. S. W. and Bates, D. R., Rep. Progr. Phys., 11, 62, (1942).

23. Craggs, J. D. and Hopwood, W., Proc. Phys. Soc., 59, 771 (1947).

24. Biondi, M. A. and Brown, S. C., Phys. Rev., 76, 1697 (1949).

25. Sayers, J., Proc. Roy. Soc., 169A, 83 (1938).

26. Biondi, M. A. and Brown, S. C., Phys. Rev., 75, 1700 (1949).

27. Eddington, A. S., The Internal Constitution of the Stars. London: Cambridge Univ. Press, 1926, p. 224.

28. Morse, P. M. and Stueckelberg, E. C. G., Phys. Rev., 35, 116 (1930).

29. Zanstra, H., Proc. Roy. Soc., 186A, 236 (1946).

30. Biondi, M. A., Phys. Rev., 83, 1078 (1951).

31. Bates, D. R., Phys. Rev., 78, 492 (1950).

32. Loeb, L. B. and Kunkel, W. B., Phys. Rev., 85, 493-4 (1952).

33. Kunkel, W. B., Phys. Rev., 84, 218 (1951).

34. Elevert, G., Z. Naturforsch., 7a, 432-9 (1952).

35. Mohler, F. L., J. Res. Nat. Bur. Stand., 19, 559 (1937).

36. Stueckelberg, E. C. G. and Morse, P.M., Phys. Rev., 36, 16 (1930).

37. Webb, H. W. and Sinclair, D., Phys. Rev., 37, 182 (1931).

38. Seeliger, R., Phys. Zeits., 30, 329 (1929).

39. Compton, K. T. and Langmuir, I., Rev. mod. Phys., 2, 191 (1930).

40. Milne, E. A., Phil. Mag., 47, 209 (1924).

41. Kramers, H. A., Phil. Mag., 46, 836 (1923).

## REFERENCES


42. Oppenheimer, J. R., Z. Phys., 55, 725 (1929).

43. Hartree, D. R. and Hartree, W., Proc. Roy. Soc., 166A, 450 (1938).

44. Thomas, L. H., J. chem. Phys., 12, 449 (1944).

45. Mott-Smith, H. M., Phys. Rev., 82, 885 (1951).

46. Bethe, H. A. and Teller, E., B.R.L. Rep. No. X-117, Aberdeen Proving Ground.

47. Bleakney, W., Phys. Rev., 36, 1303 (1930).

48. Sen, H. K., Phys. Rev., 92, 861 (1953).

49. Rostagni, A., Nuovo Cimento, 13, 389 (1936).

50. Berry, H. W., Phys. Rev., 62, 378 (1942).

51. Batho, H. F., Phys. Rev., 42, 753 (1932).

52. Massey, H. S. W. and Burhop, E. H. S., Electronic and Ionic Impact Phenomena. Oxford: The Clarendon Press, 1952.

53. Bleakney, W., Phys. Rev., 36, 1303 (1930).

54. Stevenson, D. P. and Hipple, J. A., Phys. Rev., 62, 237 (1942).

55. Kenty, C., Phys. Rev., 32, 624 (1928).

56. Thomson, J. J. and Thomson, G. P., Conduction of Electricity Through Gases. Cambridge: The Univ. Press, 1928.

57. Compton, K. T. and Langmuir, I., Rev. mod. Phys., 2, 190 et seq. (1930).

58. Loeb, L. B., Fundamental Processes of Electrical Discharge in Gases. New York: John Wiley and Sons, Inc., 1939.

59. Cobine, J. D., Gaseous Conductors. New York: McGraw-Hill Book Co., Inc., 1941.

60. Becker, R., Z. Phys., 8, 321 (1923).

## REFERENCES


61. Cowan, G. R. and Hornig, D. F., J. chem. Phys., 18, 1008 (1950).

62. Greene, E. F., Cowan, G. R. and Hornig, D. F., J. chem. Phys., 19, 427 (1951).

63. von Mises, R., J. aeronaut. Sci., 17, 551 (1950).

64. Döring, W., Ann. Phys., 5, 133 (1949).

65. Zoller, K., Z. Phys., 130, 1 (1951).

66. Grad, H., Commun. pure appl. Math., 5, 257 (1952).

67. Bethe, H. A., O.S.R.D., 369 (1942).

68. Resler, E. L., Lin, S. C. and Kantrowitz, A., J. appl. Phys., 23, 1390 (1952).

69. Fuchs, K., Kynch, G. J. and Peierls, R., M.S. 61 (1942).

70. Chapman, S. and Cowling, T. G., The Mathematical Theory of Non-Uniform Gases. Cambridge: The Univ. Press, 1939.

71. Eucken, A., Phys. Zeits., 14, 324 (1913).

72. Wayland, H., Phys. Rev., 52, 31 (1937).

73. Varney, R. N., Phys. Rev., 50, 159 (1936).

74. Shreffler, R. G. and Christian, R. H., J. appl. Phys., 25, 324 (1954).

75. Bates, D. R. and Massey, H. S. W., Phil. Mag., 45, 111 (1954).

76. Maier-Leibnitz, H., Z. Phys., 95, 499 (1935).

77. Cowling, T. G., Phil. Mag., 33, 61 (1942).

78. Bates, D. R., Buckingham, R. A., Massey, H. S. W., and Unwin, J. J., Proc. Roy. Soc., 170A, 322 (1939).

79. Mott, N. F. and Massey, H. S. W., The Theory of Atomic Collisions. Oxford: The Clarendon Press, 1949.

## REFERENCES


80. Menzel, D. H. and Pekeris, C. L., M.N.R.A.S., 96, 77 (1935).

81. Mayer, H., Los Alamos report, 647 (declassified).

82. Blatt, J. M. and Weisskopf, V. F., Theoretical Nuclear Physics. New York: John Wiley and Sons, 1952.

83. Heitler, W., The Quantum Theory of Radiation. Oxford University Press (1950).

84. Hamilton, R. L., Jensen, J. W. and Koski, W. S., Los Alamos report, 621 (declassified).